Theses and Dissertations   Theses and Dissertations

12-14-2013

The Mechanism by Which Oximes Reactivate Cholinesterases Inhibited by Organophosphates

Manikanthan Hari Naga Venkata Bhavaraju

Follow this and additional works at: https://scholarsjunction.msstate.edu/td

The mechanism by which oximes reactivate cholinesterases inhibited by

organophosphates

By

Manikanthan Hari Naga Venkata Bhavaraju

A Dissertation
Submitted to the Faculty of
Mississippi State University
in Partial Fulfillment of the Requirements
for the Doctor of Philosophy
in Chemistry
in the Department of Chemistry

Mississippi State, Mississippi

December 2013

The mechanism by which oximes reactivate cholinesterases inhibited by

organophosphates

By

Manikanthan Hari Naga Venkata Bhavaraju

Approved:

_____
Steven R. Gwaltney
(Director of Dissertation)

_____
Edwin A. Lewis
(Committee Member)

_____
Svein Saebø
(Committee Member)

_____
Stephen C. Foster
(Committee Member/Graduate Coordinator)

_____
Mark A. Novotny
(Committee Member)

_____
R. Gregory Dunaway
Professor and Dean
College of Arts & Sciences

Name: Manikanthan Hari Naga Venkata Bhavaraju

Date of Degree: December 14, 2013

Institution: Mississippi State University

Major Field: Chemistry

Major Professor: Dr. Steven R. Gwaltney

Title of Study: The mechanism by which oximes reactivate cholinesterases inhibited by organophosphates

Pages in Study: 131

Candidate for Degree of Doctor of Philosophy

The enzymes acetylcholinesterase (AChE) and butyrylcholinesterase (BChE) are inhibited by nerve agents such as sarin and tabun. In general, the inhibited enzymes are reactivated by bisquaternary ammonium compounds (oximes). The binding free energies of the oximes; 2-PAM, MMB-4, HI-6, and obidoxime bound to human AChE (hAChE) and human BChE (hBChE) inhibited by sarin and tabun and also to the uninhibited enzymes were calculated using various computational methods.

Using thermodynamic integration, the binding free energies of all the inhibited and uninhibited systems of MMB-4 and obidoxime were evaluated. The standard binding free energies (dA) were more negative than the experimental values due to limitations of the ff99 forcefield. The RMS error of dA for the inhibited systems of MMB-4 was 2.1 kcal/mol, and for obidoxime systems it was 4.8 kcal/mol with respect to the experimental free energies.

The binding enthalpies calculated using MM-GBSA and MM-PBSA methods for 2-PAM, MMB-4, HI-6, and obidoxime systems were negative, except for hBChE-sarin-MMB-4 and hBChE-sarin-obidoxime. For all the systems the TdS values calculated

using normal mode analysis were equal to or lower in magnitude than their corresponding binding enthalpies. As a result, the estimated free energies were positive for most of the systems. Clearly, the present algorithms cannot effectively estimate the binding entropies for a protein-ligand system. Met81 has commonly shown favorable interactions, and lysine or arginine exhibited unfavorable interactions with the reactivator in all the systems.

Second, the interactions between chloropyrifos-oxon (Cpo) and experimentally tested neutral and monopyridinium oximes bound to the Q192 or R192 polymorphs of human paraoxonase1 (hPON1) were studied. The equilibrated Q192 and R192 hPON1 were structurally different than the crystal structure of recombinant PON1. The neutral oximes have shown more favorable interactions with Cpo in Q192 hPON1 + Cpo system compared to R192 hPON1 + Cpo. Whereas the monopyridinium oximes interacted more affectively with Cpo in R192 hPON1 than Q192 hPON1. The relative deprotonation energy of the monopyridinium oxime was lower than the neutral oxime. Hence, the monopyridinium oxime can hydrolyze an organophosphate at a higher rate than a neutral oxime.

DEDICATION

I would like to dedicate this research work to Lord Ayyappa, my mother Venkata Durga Nagalakshmi Bhavaraju, and my wife Srilalita Neti.

ACKNOWLEDGEMENTS

TABLE OF CONTENTS

LIST OF TABLES

LIST OF FIGURES

x

LIST OF ABBREVATIONS

ΔA	Change in the Helmholtz free energy
ΔE	Change in the internal energy
ΔG_{sol}	Free energy of solvation
ΔH	Change in enthalpy
ΔS	Change in entropy
2-PAM	2-pyridine aldoxime methyl chloride
A	observable property of a system
a	acceleration
ACh	acetylcholine
AChE	acetylcholinesterase
Ala	alanine
apo-A1	apolipoprotein-A1
Asn	asparagine
Asp	aspartic acid
BChE	butyrylcholinesterase
Cpo	chloropyrifos-oxon
e	charge of a species
F	force acting on a particle
FEP	Free energy perturbation

FFT	Fast Fourier Transform
fs	femtosecond
FT	Fourier Transform
g_k	gradient
gaff	general atomic forcefield
Glu	glutamate
H	Hamiltonian
h	Planck constant
hAChE	human acetylcholinesterase
hBChE	human butyrylcholinesterase
HDL	high density lipoprotein
HF	Hartree fock
HI-6	1-(2-hydroxyiminomethyl-1-pyridinio)-3-(4-carbamoyl-1-pyridinio)-2-oxapropane dichloride
His	histidine
HLö7	1-(((4-(aminocarbonyl)pyridinio)methoxy)methyl)-2,4-bis((hydroxyamino)methyl) pyridinium diiodide
hPON1	human paraoxonase1
I	ionic strength of the solution
Ile	isoleucine
k_B	Boltzmann constant
K_d	Dissociation constant
L_x	dimension of the central box along x-axis
L_y	dimension of the central box along y-axis

L_z	dimension of the central box along z-axis
M	Molarity
m	mass
MC	Monte Carlo
MD	Molecular dynamic simulations
Met	methionine
MMB-4	1, 1'-methylene-bis(4-(hydroxyimino)methyl) pyridinium dibromide
MM-GBSA	Molecular mechanics Generalized Born Surface area
MM-PBSA	Molecular mechanics Poisson Boltzmann Surface area
NEMP	4-nitrophenyl ethyl methylphosphonate
NIMP	4-nitrophenyl isopropyl methylphosphonate
NPT	Isothermal-Isobaric ensemble
ns	nanosecond
NVE	Microcanonical ensemble
NVT	Canonical ensemble
Obidoxime	1, 1'-(oxydimethylene)bis(pyridinium-4-carbaldoxime) dichloride
OP	organophosphate
p	momentum
PBC	periodic boundary conditions
PDB	protein data bank
PME	particle mesh ewald
PON	paraoxonase

ps	picosecond
Q	partition coefficient
R	ideal gas constant
r	position
rePON1	recombinant paraoxonase 1
RMSd	root mean square deviation
Sarin	Propan-2-yl methylphosphonofluoridate
SASA	solvent accessible surface area
Ser	serine
Soman	3, 3-dimethyl butan-2-yl-methylphosphonofluoridate
T	kinetic energy or temperature
Tabun	Ethyl N, N-dimethylphosphoramidocyanidate
tAChE	*torpedo californica* acetylcholinesterase
TEMP	3, 5, 6-trichloro-2-pyridinyl ethyl methylphosphonate
Thr	threonine
TI	thermodynamic integration
TIMP	3, 5, 6-trichloro-2-pyrindinyl isopropyl methylphosphonate
TMB-4	1, 1'-propylene-bis(4-(hydroxyimino)methyl) pyridinium dichloride
Trp	tryptophan
Tyr	tyrosine
V	potential energy
V_n	rotational barrier height

v	velocity
VX	Ethyl ({2-[bis(propan-2-yl)amino]ethyl}sulfanyl) (methyl)phosphinate
γ	phase factor or collision frequency
$\varepsilon(r)$	dielectric constant
κ	isothermal compressibility
λ	perturbing parameter
μVT	Grandcanonical ensemble
ξ	frictional coefficient
$\rho(r)$	probability density
τ	coupling parameter
ω	torsional angle
κ	Debye-Hückel inverse length

CHAPTER I

INTRODUCTION

1.1   Introduction

The enzymes acetylcholinesterase (AChE, EC 3.1.1.7) and butyrylcholinesterase (BChE, EC 3.1.1.8) belong to the family of cholinesterases.[1] Both AChE and BChE are inhibited by the organophosphates (OP's) such as nerve agents, *i.e*. sarin, tabun, soman, *etc*.[2-4] Nerve agents can harm human beings and other living species.[5-7] For 50 years, pyridinium oximes have been used to treat inhibited cholinesterases for OP exposure.[8-9] In order to understand the inhibition process and to validate the reactivation efficiency of various oximes, the tertiary structural information of AChE and BChE must be known.

Many crystal structures of AChE such as *torpedo californica,* mouse, human, *etc*. have been reported in the literature.[10-14] However, only a handful of BChE structures are known (34 crystal structures were found in the protein data bank as of 2013). The enzymes AChE and BChE are structurally similar.[15-16] The existence and function of AChE was first proposed by Dale in 1914.[17] AChE mainly hydrolyzes the neurotransmitter acetylcholine (ACh) into acetic acid and choline in the postsynaptic vesicle.[18] On the other hand, BChE also hydrolyzes ACh and other molecules such as butyrylcholine.[19] It hydrolyzes a wide range of toxic esters: cocaine, heroin, and pesticides.[19-21]

1.2   Acetylcholinesterase

The crystal structure of AChE derived from *torpedo californica* (tAChE) has provided a wealth of information regarding the important regions of the enzyme.[11] The active site is located at the bottom of a 20 Å deep gorge. The gorge contains 14 aromatic residues, which provide extra stability to the incoming ligands through electrostatic and van der Waals interactions.[10,22-25] The active site contains a catalytic triad Glu-His-Ser.[10] Furthermore, the oxyanion hole[26] and the peripheral anionic site[27-28] influence the incoming ligand and its interaction with the catalytic serine. The ligand often interacts with the residues of the peripheral anionic site (present at the entrance of the gorge) and hence partially blocks the gorge entrance.[18,29] Sussman *et al.*[10] have suggested that certain bulky aromatic compounds cannot fit into the gorge and thereby interact with the peripheral anionic site residues. But OP's and monoquaternary and bisquaternary pyridinium compounds can enter and interact with the catalytic serine.

As mentioned earlier, the main function of AChE is to hydrolyze ACh. The breakdown of ACh occurs in two steps: acylation and deacylation.[30-34] The mechanism involving acylation and deacylation are shown in Figure 1.1. There exists a strong hydrogen bond between the H atom of the active site serine-OH and N at the ϵ position of the catalytic His, which leads to the deprotonation of the serine. Simultaneously, Ser-O$^-$ attacks the carbonyl carbon of the choline ester. Hence, choline gets liberated. A hydrogen bond between H of the δN on histidine and an O of COO$^-$ on the glumate also exists (both His and Glu are catalytic residues). During the acylation process, the carbonyl O of the ACh forms hydrogen bonds with the oxyanion residues. Then, in the

second step a water molecule attacks the acylated enzyme, restoring the enzyme activity by liberating acetic acid.
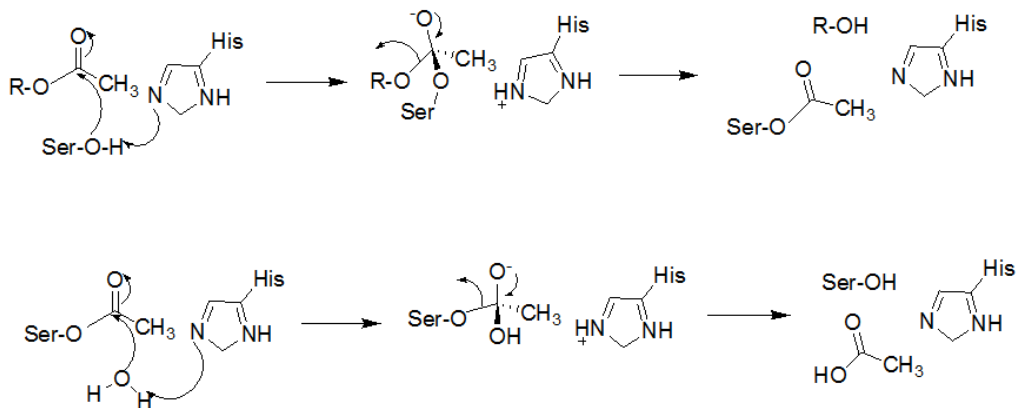
Figure 1.1   Hydrolysis process of ACh

The acylation and deacylation steps of the ACh hydrolysis process are catalyzed by AChE.

1.3   Organophosphates

Organophosphates are phosphorous-containing organic compounds and are generally used as pesticides and nerve agents.[4,35-37] Immediately previous to and during World War II, Germany developed nerve agents to target humans.[38,39] The first nerve agent, tabun (1935),[40,41] was synthesized by Schrader's group, followed by sarin in 1938,[41] upon the insistence of the Nazi government. Soman (1944)[40] was synthesized by Richard Kuhn in Germany. Later, VX [42] was synthesized by Tammelin (1957) in the United Kingdom. The structures of soman, sarin, tabun, and VX are shown in Figure 1.2. Iraq used nerve agents to kill its own Kurdish population, and Iranian soliders during the Iran-Iraq war (1980's).[43,44] Nerve agents were also used during the terrorist attacks in Japan (1995).[45]

3
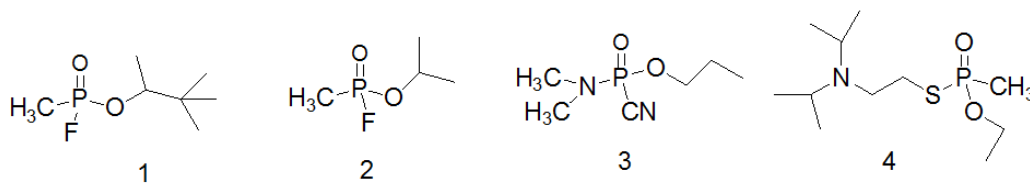
Figure 1.2   The nerve agents 1) soman, 2) sarin, 3) tabun, and 4) VX

Nerve agents inactivate AChE by phosphonylating the active site serine.[3,46] As a result, the breakdown of ACh is prevented.   Thus, ACh accumulates in the neuronal synapses and neuromuscular junctions, causing paralysis, seizures, and other cholinergic syndromes.[47-49]

1.4   Mechanism of inhibition

The nerve agents are electrophilic in nature. During the phosphonylation process, a covalent bond is formed between the nerve agent and the active site serine.[50-52] The inhibition process is a two-step mechanism and is shown in Figure 1.3. Initially, Ser-O⁻ attacks the P atom of the nerve agent. Then, an OP-serine pentacoordinated intermediate is formed. In the second step, the leaving group gets detached from the OP-serine complex.
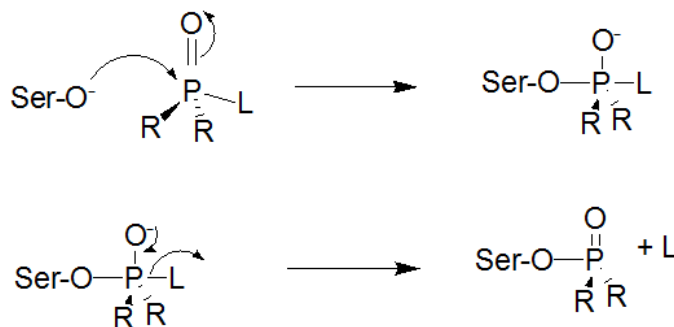
Figure 1.3   Reaction pathway of a nerve agent inhibiting the active site serine of AChE where L = the leaving group

1.5   Oximes as reactivators

The inhibited OP-serine complex undergoes aging or reactivation. Aging is an irreversible process, wherein the activity of the enzyme is permanently lost.[53,54] As shown in Figure 1.2, the nerve agents has a P-O-R moiety. During the aging process, the O-R bond gets dissociated in the presence of a water molecule as shown in Figure 1.4. Due to the cleavage of the O-R bond, a negative charge is formed on the OP-serine adduct. The enzyme cannot be reactivated because the negative charge inhibits the nucleophilic attack. Therefore, before the enzyme undergoes aging it has to be reactivated. Generally, a reactivator, *i.e.* a bispyridinium quaternary ammonium salt (oxime), is introduced into the active site.[55,56] The oxime breaks the OP-serine bond and removes the nerve agent from the active site.
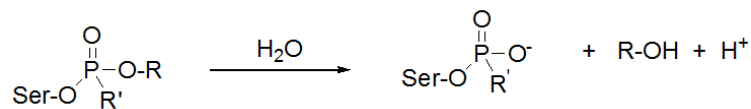
Figure 1.4   The aging process of AChE in the presence of a water molecule

Eberhard Gross experimentally showed that atropine can be used for treatment of nerve agent exposure.[42] However, it was observed that atropine is only a good antimuscarnic agent but not a reactivating agent.[36,57,58] In 1951, Wilson showed that hydroxylamine reactivates AChE phosphanylated with tetraethylpyrophosphate.[59] Later, a new class of antidotes, molecules containing quaternary ammonium groups, was developed, which can reactivate AChE against OP exposure. 2-PAM was proven to be a better reactivator than hydroxylamine.[47,60,61] Some of the *in vitro* experiments have shown that 2-PAM cannot efficiently reactivate cholinesterases against sarin, cyclosarin, tabun, paraoxon, and VX exposure.[62-65] So, newer oximes (TMB-4,[66] obidoxime,[47,67] HI-6,[68,69] HLö7,[70] and MMB-4[71]) were synthesized. The structures of 2-PAM, TMB-4, obidoxime, HI-6, HLö7, and MMB-4 are shown in Figure 1.5.
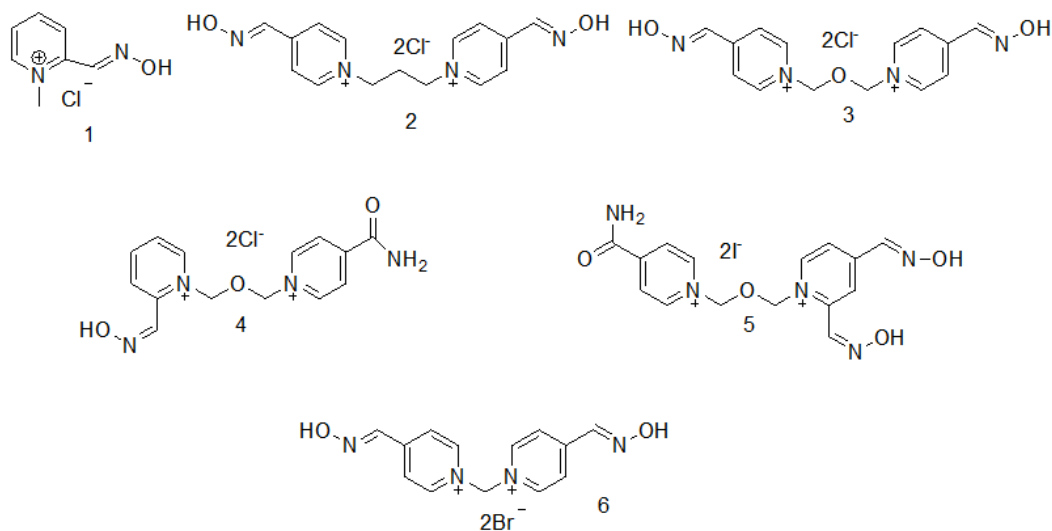
Figure 1.5   Structures of monoquaternary and bisquaternary ammonium compounds 1) 2-PAM, 2) TMB-4, 3) obidoxime, 4) HI-6, 5) HLö7, and 6) MMB-4

6

The current standard treatment for nerve agent exposure is giving the patient atropine and an oxime (2-PAM or obidoxime).[72,73] Atropine blocks the overstimulation caused by the excess ACh at the peripheral muscarinic receptors, whereas the oxime restores the activity of the enzyme.[58,74] The oxime reactivation mechanism is not well understood. The most widely accepted mechanism for oxime reactivation is similar to inhibition process and is shown in Figure 1.6.[36,75,76]
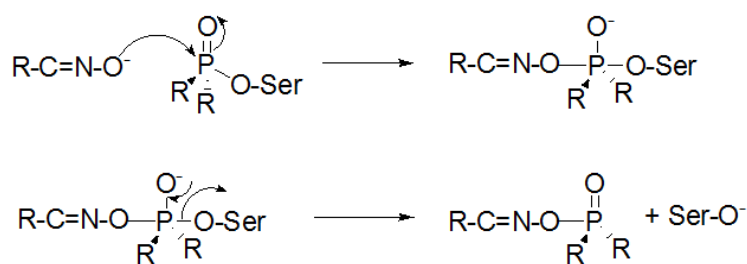
Figure 1.6   Oxime reactivation mechanism

Several *in vitro* and *in vivo* rat models and *in vivo* guinea pigs models were studied to analyze the effectiveness of newer oximes against various nerve agent exposures.[58,77-81] The efficacy of the oximes against nerve agents cannot be tested on humans due to ethical issues. Therefore, only a few human erythrocyte *in vitro* models are currently available.[56,82,83] Unfortunately, no universal antidote is available for all nerve agent exposures.

Worek *et al.* showed that HI-6 cannot reactivate AChE effectively against tabun exposure.[84] In fact, tabun-inhibited AChE and BChE are highly resistant towards reactivation.[85-87] The reactivation of tabun-inhibited AChE or BChE takes longer than sarin or VX-inhibited cholinesterases.[88] It has been suggested that the lone pair of

electrons present on the amide group of tabun inhibits the nucleophilic attack of the oxime.[87] However, HI-6 can effectively reactivate AChE inhibited by sarin and soman.[69,88] One of the limitations of HI-6 is its poor stability in an aqueous medium.[89,90] Therefore, some countries, like Canada, are using a powdered form of HI-6 in an auto-injector. Obidoxime can efficiently reactivate AChE and BChE against sarin and tabun.[56,62,63,88] MMB-4 has shown promising results in reactivating inhibited cholinesterases.[52,77,91,92] In some of the *in vitro* models, MMB-4 has shown higher reactivation efficiency than 2-PAM and HI-6 while reactivating AChE inhibited by sarin, cyclosarin, tabun, and VX.[83,93-95]

In order to efficiently reactivate the inhibited cholinesterases, oximes should meet certain structural requirements. Using an *in vitro* model (rat brain), Kuca *et al*. tested the efficiency of 2-PAM, obidoxime, HI-6, MMB-4, TMB-4, and HLö7 on AChE inhibited by soman, tabun, cyclosarin, sarin, and VX.[57] Based on their analysis, they have suggested that the oxime reactivating efficiency depends on the following criteria:

a) Presence of quaternary nitrogen in the reactivator

The quaternary nitrogen increases the reactivation efficiency of the oxime. Binding affinities of bisquaternary ammonium salts (HI-6, MMB-4, *etc*.) to cholinesterases inhibited by nerve agents are higher compared to mono-quaternary compounds, *i.e.,* 2-PAM.[80, 96-98]

8

b) Rigidity of the linker

The linker attaches two pyridinium rings of a reactivator. The reactivation efficiency of an oxime decreases if the linker is not flexible, since a rigid molecule cannot orient properly in the active site, in order to break the OP-serine bond.[57]

c) Oxime group

The oxime group is a strong nucleophile and has the ability to break the OP-serine bond. As a result, the OP gets detached from the active site, and the activity of the protein gets restored.

d) Position of oxime group on the pyridinium ring

The position of the oxime group attached to the quaternary pyridinium ring plays an important role in the reactivation process. An oxime group present at a *para* or *ortho* position relative to the quaternary nitrogen exhibits a higher reactivation rate compared to an oxime at a *meta* position.[62,94,99,100]

e) Number of oxime groups in the reactivators

There is no generalized rule for the number of oxime groups. The reactivator should have at least one oxime group.[57]

Numerous *in vivo* and *in vitro* studies and a very few clinical trials have been carried out for analyzing the reactivation efficiency of various oximes. None of the presently available oximes can effectively reactivate inhibited AChE or BChE against all nerve agent exposures. A lot of time and money are involved in testing the efficiency of oximes in trials. Therefore, computational tools can be used to verify the reactivation efficiency of oximes. The efficiency of various oximes can be explored by calculating

the free energy of binding and comparing them against each other. These analyses will also provide new insights about various oxime conformations, their interactions, and their spatial orientations in the active site.

An alternative route to address nerve agent exposure is to increase the rate of nerve agent detoxification. This can prevent the inhibition of AChE or BChE upon nerve agent exposure to some extent. A detailed description of this process is discussed below.

1.6   Paraoxonase 1

The mammalian enzyme paraoxonase (PON) exists in three isoforms: PON1, PON2, and PON3.[101,102] Both PON1 and PON3 are mainly found in the liver, whereas PON2 is located in many tissues.[103,104] PON1 is extensively studied, as it hydrolyzes a wide variety of molecules.[105-107] PON1 is synthesized in the liver and gets secreted into the blood stream.[103] It further gets attached to a high density lipoprotein (HDL) particle containing apolipoprotein A1 (apo-A1).[108-110] Apo-A1 increases the stability and the hydrolysis process of PON1.[111,112] PON1 bound to HDL particles decreases the risk of atherosclerosis.[113-116]

PON1 was characterized by Aldridge in 1953 as an "A" esterase enzyme, which can hydrolyze paraoxon. On the other hand, "B" esterases, i.e. cholinesterases, are inhibited by paraoxon.[117,118] Uriel in 1961 detected the activity of PON1 in an immuno-precipitate of HDL particles.[119] The main function of PON1 is to hydrolyze lactones produced during lipid oxidation.[120,121] Additionally, it can also hydrolyze organophosphates, *i.e.* paraoxon, chlorpyrifos-oxon (active metabolites of parathion and chloropyrifos), *etc.*, and nerve agents such as sarin, soman, and VX.[104-107,122] Therefore,

PON1 plays an important role in lowering the toxicity of nerve agents. The structures of paraoxon and chlorpyrifos-oxon are shown in Figure 1.7.
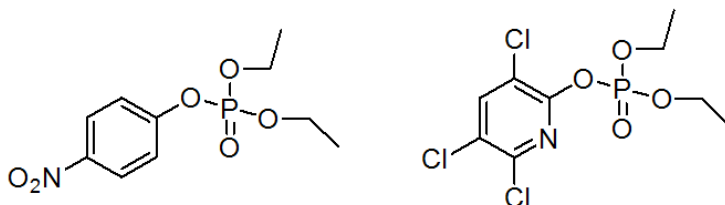
Figure 1.7   Structures of paraoxon and chlorpyrisfos-oxon

1.7   Structure of PON1

The crystal structure of pure human PON1 has not yet been determined. Human PON1 is unstable and insoluble, and it aggregates in the absence of detergents.[104,123] In general, human PON1 exhibits a R192Q polymorphism, influencing the catalytic properties of the protein.[124,125] The R192 form of PON1 hydrolyzes both paraoxon and chlorpyrifos-oxon more efficiently than Q192.[107,126,127]

Harel *et al.* (PDB ID: 1V04) reported the crystal structure of a recombinant PON1 (rePON1).[104] It was obtained by shuffling the PON1 genes of rabbit, human, rat, and mouse. The primary sequence identity between rePON1 and wild-type rabbit was about 91%. Similarly, wild-type human and rabbit PON1 sequences are also closely related to each other (86%).[103] The active site and catalytic activity of rePON1 were similar to wild-type rabbit and human enzymes. In order to increase the solubility, mutations were made in the exterior regions of rePON1 that did not affect its enzymatic activity. The 1V04 structure was determined at pH 4.5, where the enzyme is biologically inactive. In

2012, David *et al*. determined two crystal structures of rePON1 at pH 6.5 (active).[128] The first structure (PDB ID: 3SRE) contains a phosphate ion in the active site, whereas the second one (PDB ID: 3SRG) contains 2-hydroxyquinoline, which is considered to be a strong inhibitor of PON1, along with a phosphate ion.

PON1 is a six-bladed β-propeller containing two Ca^{2+} ions in the central tunnel as shown in the Figure 1.8. The catalytic Ca^{2+} ion lies in the bottom of the active site. The Ca^{2+} ions maintain the structural stability and play a major role in the catalytic mechanism of the protein.[104,128,129] The N-terminus (H1 loop, residues 1-18) is highly hydrophobic and is anchored into the HDL particle.[103,104,130] Similarly, the H2 loop (residues 182-196) is in contact with the membrane layer. It was observed that residue Y71 was facing towards (inwards) the active site in the presence of a ligand and outwards in its absence. The surface loop (72-79) and Y71 influence the entrance of the ligand into the active site.[128] The protein exhibits closed and open conformations depending upon the movement of the flexible surface loop. In a ligand-bound protein, the surface loop is structured and acts as a lid to the active site (closed conformation). As a result, the active site becomes narrow. In the absence of a ligand, the loop is disordered, and the protein exists in an open conformation. In all three crystals of rePON1, the anchored loop (H1 loop) was not resolved. The conformation of the surface loop was properly described only in the 3SRG structure.
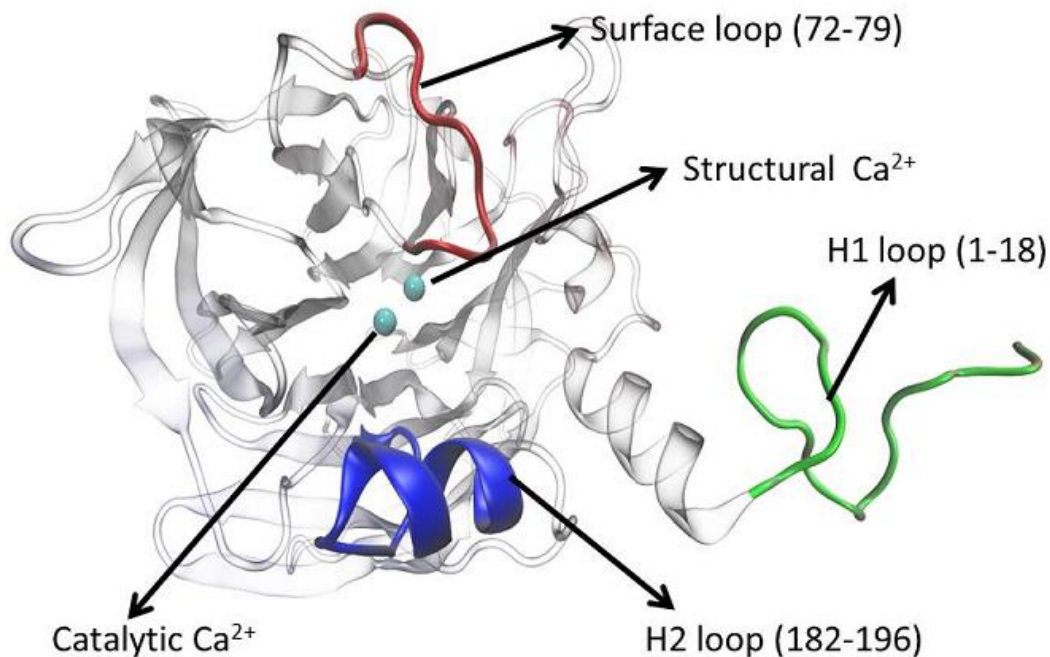
Figure 1.8   Structure of Q192 human PON1

1.8   Hydrolysis mechanism

Harel *et al.* showed that the hydrolysis of lactones, arylesters, and organophosphates occurs by a nucleophilic attack of a hydroxide ion (formed from a water molecule) in the active site.[104] During this process, the O atom of C=O of lactones or P=O of organophosphates must be close to the catalytic Ca^{2+}. The catalytic Ca^{2+} ion pulls the electron density present on the O of C=O or P=O towards it. The deprotonation of water in the active site is poorly understood. The hydroxide ion is a moderately strong nucleophile. Therefore, the hydrolysis rates of paraoxon, chlorpyrisfos-oxon, and nerve agents are rather slow.[107,131,132] David *et al.* have shown that the His115/His134 dyad deprotonates the water molecule during the hydrolysis of lactones or arylesters.[128] The

13

general mechanisms for the hydrolysis of lactones and esters are shown in Figure 1.9 a) and 1.9 b).
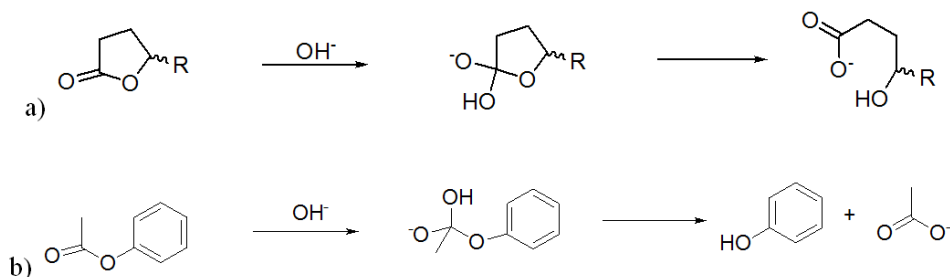
Figure 1.9   Hydrolysis mechanism of a) lactones and b) esters

In the case of organophosphate hydrolysis, the deprotonation step is still not clear. One suggested mechanism is that D269 of PON1 acts as a nucleophile and forms a covalent bond with the organophosphate, followed by a nucleophilic attack of a hydroxide ion.[133-135] This mechanism is similar to the inhibition and reactivation processes of cholinesterases. However, unlike cholinesterase, PON1 does not undergo aging.[136] Hence, this mechanism is not widely accepted. Some computational studies have shown that E53 or D269 or both may be involved in the deprotonation of water.[123,137] The hydrolysis of organophosphates involves the formation of a pentacoordinated intermediate, as compared to the tetracoordinated intermediate in lactones and arylesters shown in Figure 1.3.

Since PON1 is a promiscuous protein, understanding and analyzing organophosphate hydrolysis is essential. Further, to enhance the hydrolysis process, new ligands can be computationally tested and experimentally verified.

1.9   Research Goals

This research project consists of two major parts. The main goals of the two parts are described below.

The goals of the first part are to determining the oxime free energy of binding in human AChE and BChE inhibited by nerve agents using thermodynamic integration (TI); to explore alternative methods for calculating free energy of binding; to compare the oxime free energy of binding calculated using TI with the alternative methods and also with available experimental values; and to identify important active site residues which participate in the reactivation process. The goals of the second part are to construct a model of the 3D structures of Q192 and R192 human PON1 (hPON1) using homology modeling; to perform docking studies to analyze the orientation and the binding interactions of chlorpyrifos-oxon (Cpo) with the active site residues of hPON1; and to dock a variety of neutral and monopyridinium oximes into the active site of the complex (hPON1+ Cpo). This novel study will be useful to computationally identify a few oximes which show favorable interactions with the complex.

Basic background information about MD simulations, various methods for calculating protein-ligand free energy of binding, and a brief description of docking studies are discussed in Chapter 2. The results and discussion of oximes' free energies of binding are explained in Chapters 3 and 4. Similarly, the outcomes of human PON1+ Cpo docking studies are explained in Chapter 5. Finally, the overall conclusions of the research are discussed in Chapter 6.

CHAPTER II

METHODS

This chapter is broadly divided into three sections: introduction to molecular dynamics simulations, free energy methods, and docking studies.

2.1 Introduction to molecular dynamics simulations

The role of computational simulations is significantly increasing in various fields, for example, pharmacology, drug design, materials science, interstellar chemistry, *etc.*[138-141] For the last few decades computer storage capacity and processor speed have tremendously increased.[142,143] As a result, high performance computing centers equipped with thousands of processors and data storage capacity on the order of terabytes or petabytes are being established all over the world.[142] So, scientists belonging to various fields are designing algorithms and software for solving challenging and interesting scientific problems.[144-146]

A variety of theoretical/computational methods and models have been developed to explain, cross check, and illustrate various theories and experimental results.[146-150] Molecular modeling is one such computational technique. It is categorized into quantum mechanics and molecular mechanics. Quantum mechanics are used to calculate bond dissociation energies, conformational analysis, geometry optimization, transition state, etc. for molecules containing less than 500 atoms using different theoretical methods.[151]

Similarly, molecular mechanics are used to analyze thermodynamic and kinetic properties of macromolecules (proteins and nucleic acids) based on Newton's second law of motion.[152,153] Two important branches of molecular mechanics are Molecular Dynamics (MD) and Monte Carlo (MC) simulations.

2.1.1 Molecular dynamics

Molecular dynamics calculations are widely used to study thermal stability and folding or unfolding of proteins, to analyze the interactions between proteins and membranes, to determine protein-ligand and protein-nucleic acid binding energies, and to estimate various thermodynamic properties of macromolecules.[154-159] In the 1950's for the first time Alder and Wainwright used the concept of MD to study the vibration of atoms.[160,161] McCammon *et al.* (1977) performed the first protein simulation.[162]

As mentioned earlier, MD depends on Newton's second law of motion. The force is calculated by taking a gradient of the potential energy (*V*). The potential energy is determined using an appropriate forcefield

$$F = -\nabla V. \tag{2.1}$$

By combining Newton's second law of motion and Eq. 2.1, we obtain

$$\frac{dV}{dr} = m\frac{d^2r}{dt^2}. \tag{2.2}$$

In an MD simulation, the initial velocities of all the atoms of a system are randomly assigned to a Maxwell-Boltzmann distribution at a given temperature as given in Eq. 2.3. Then, the corresponding accelerations, velocities, and positions at any time t can be calculated by

$$P(v) = \sqrt{\frac{m_i}{2\pi k_B T}} \exp\left(-\frac{1}{2}\frac{mv^2}{k_B T}\right), \quad (2.3)$$

where, m = mass, v = velocity, k_B = Boltzmann constant, T = temperature, and $P(v)$ = probability of an atom with a velocity v.

2.1.2   Bonding and non-bonding terms

The potential energy is calculated using bonding and non-bonding terms for a system. The bonding terms include bond length, bond angle, and torsions. Van der Waals and electrostatic terms are considered as non-bonded interactions. The net potential can be represented as

$$V_{net} = V_{bond\ length} + V_{bond\ angle} + V_{torsion} + V_{non-bonded}, \quad (2.4)$$

$$V_{net} = \Sigma_{bonds}\frac{k}{2}(l - l_i)^2 + \Sigma_{angles}\frac{k}{2}(\theta - \theta_i)^2 + \Sigma_{torsion}\frac{V_n}{2}\left(1 + Cos(n\omega - \gamma)\right) +$$

$$\Sigma_{van\ der\ Waals}\ 4\varepsilon_{ij}\left[\left(\frac{\sigma_{ij}}{r_{ij}}\right)^m - \left(\frac{\sigma_{ij}}{r_{ij}}\right)^n\right] + \Sigma_{electrostatic}\frac{q_i q_j}{4\pi\varepsilon_o r_{ij}}. \quad (2.5)$$

The first term ($V_{bond\ length}$) is calculated by taking the square of the difference between the bond length and its reference value. The second term ($V_{bond\ angle}$) is determined by squaring the difference between the bond angle and its equilibrium value. In the torsion expression ($V_{torsion}$), ω is the torsional angle, V_n is the rotational barrier height, n is the number of minimum points when the bond is rotated by 360°, and γ is the phase factor which determines where the torsional angle passes through its minimum value. The van der Waals term consists of attractive (r^{-n}) and repulsive (r^{-m}) terms, wherein a variety of n-m terms are available (6-12, 10-12, 6-9, etc.).[163,164] The most commonly used term is a Lennard Jones 6-12 potential.[165] Finally, the coulombic term

18

calculates the electrostatic interaction between two charged species separated by a

distance of r_{ij}.

2.1.3   Minimization methods

The initial conformation of a biological system may not be in a local minimum.

Hence, the system must be minimized before it is equilibrated or sampled using MD

simulations. The most commonly used minimization techniques are steepest descent,[166]

conjugate gradient,[167] and Newton-Raphson methods.[168] In this study we have used

steepest descent and conjugate gradient. During the process, the coordinates of the atoms

are gradually changed. In the end the system reaches a minimum on its potential energy

surface (PES) after several iterations.

2.1.3.1   The steepest descent method

In the steepest descent method the initial configuration of a system is provided by

the user and is represented by a vector x_i. At each step the gradient (g_k) will be

calculated. This method is very effective if the system is located far away from a

minimum. But the convergence criterion becomes slow as the system approaches its

minimum. Therefore, often the initial iterations (user defined) will be performed using

the steepest descent algorithm followed by conjugate gradient to quickly locate minima.

2.1.3.2   The conjugate gradient method

The conjugate gradient method performs very efficiently in a narrow valley. The

gradients of successive steps are orthogonal to each other, and the directions are

conjugate. At any particular iteration, when the system moves in the direction N_k from a

point X_k, the direction is calculated using the gradient of that point and the direction of

the previous move.

$$N_k = -g_k + \gamma_k N_{k-1}, \qquad (2.6)$$

where γ_k is a constant.

2.1.4   Periodic boundary conditions

In some of the MD simulations, a macromolecule of interest will be placed inside

a box containing dimensions L_x, L_y, and L_z. Then, solvent molecules and counter ions (to

neutralize the charge of the system) will be added. The different types of simulation

boxes are cubic, truncated octahedron, hexagonal prism, rhombic dodecahedron, and

elongated dodecahedron.[169] Depending upon the nature and size of a system, an

appropriate box must be chosen. In this study we have used cubic and truncated

octahedron boxes. By applying Periodic Boundary Conditions (PBC) and using a

minimum number of particles, one can efficiently sample the phase space and calculate

various properties of a system. Under PBC, the box will be replicated in all 3N

directions. The 2D arrangement of this replication is shown in Figure 2.1.
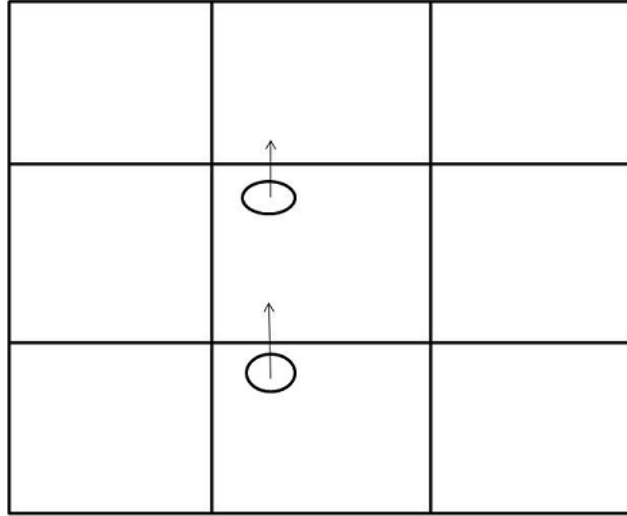
Figure 2.1   Reimagining of a particle

Under periodic boundary conditions, when a particle drifts out of a particular box, its image will replace it

     If a particle drifts out of the central box, its image will replace it as shown in

Figure 2.1. In other words, the particle will be translated or reimaged back into the box.

This ensures that the simulation is performed with a constant number of particles. The

most expensive part of an MD simulation is calculating the non-bonded interactions

between the particles of the system. The total number of non-bonded interactions is

equal to the square of the total number of particles in a system. In priniciple, the non-

bonded interactions between every pair of atoms must be calculated. However, in

practice, a *non-bonded cutoff* or *minimum image convention* is applied.[170-172]

     In a *minimum image convention*, each particle sees at least one image of all other

particles of a system, and the interaction is calculated with the nearest atom or image.

When a *non-bonded cutoff* is applied, the non-bonded interactions between all pairs of

atoms are calculated within the cutoff region. The interactions outside the cutoff region

are set to zero. In general, a cutoff value of 8-10 Å is recommended for calculating all non-bonded interactions.[173]

2.1.5 Particle Mesh Ewald

Typically, electrostatic interactions are calculated using an Ewald summation.[169] In an Ewald summation, each particle in the central box interacts with all other particles within the box and also with the images located in all the image boxes. The location of each image box can be linked to the central box using a vector. The vector components are an integral multiple of the dimensions of the central box, *i.e.* $\pm iL_x$, $\pm iL_y$, $\pm iL_z$. The interactions between all pairs of atoms within the central box and the interactions of each atom (central box) with the images situated in the image boxes can be written as

$$V = \frac{1}{2}\sum'_{|n|=0}\sum_{i=1}^{N}\sum_{j=1}^{N}\frac{q_i q_j}{4\pi\varepsilon_o |r_{ij}+n|}. \tag{2.7}$$

The prime on the first summation in Eq. 2.7 implies that the series will not include the interaction $i = j$ for $n = 0$. The summation shown in Eq. 2.7 converges slowly. To speed up the convergence, the summation is divided into real space and reciprocal space. The Ewald sum in the reciprocal space was initially calculated using a Fourier transform (FT). To perform the FT, each point charge was engulfed by a Gaussian charge distribution of an equal magnitude using the following functional form:

$$\rho(r) = \frac{q_i \alpha^3}{\pi^{\frac{3}{2}}}\exp(-\alpha^2 r^2). \tag{2.8}$$

Using FT, the calculated function of the reciprocal space was not smooth enough. Further, computing the Ewald summation is very expensive, as the algorithm scales as N^2. Therefore, Particle Mesh Ewald was introduced, where the charge density on an

atom is distributed onto surrounding grid points.[174,175] Instead of an FT, the reciprocal space is computed using a Fast Fourier transform (FFT) to obtain a smooth function. Due to the usage of FFT, the overall scaling of the algorithm now becomes N×lnN.

2.1.6   Ensembles

The experiments are generally performed under constant temperature, pressure, volume, *etc.*, and the experimental values are determined at the macroscopic level. However, the interactions between atoms or molecules takes place at the microscopic level. These two levels can be connected using a statistical ensemble. An ensemble is defined as a collection of points in a phase space, representing a particular thermodynamic state of a system.[169] To mimic the experimental conditions, the MD simulations are performed using a particular ensemble, and thereby various properties of a system are calculated. In an MD simulation different points are generated in the phase space as a function of time under a constant ensemble, which corresponds to various conformations of a biological system. The different kinds of ensembles are described below:

- *Microcanonical ensemble* (NVE): This ensemble contains a fixed number of particles, constant volume, and constant energy.
- *Canonical ensemble* (NVT): This thermodynamic state is defined by a fixed number of particles and constant volume and temperature.
- *Isothermal-Isobaric ensemble* (NPT): This collection is characterized by a fixed number of particles and constant pressure and temperature.

23

- *Grand canonical ensemble* (μVT): This is defined by a constant chemical potential, volume, and temperature.

In our studies, all the MD simulations were performed under NVT or NPT conditions. Other conditions are also possible but are not generally used.

2.1.7   Ensemble average

To determine experimental values such as pressure or heat capacity, one requires details about the position (r) and momentum (p) of every particle in a system. Any measured value is averaged over a particular duration of time. Therefore, an average value of a property, determined over a period of time for an N particle system can be written as:

$$A_{avg} = \iint dp^N dr^N A(p^N, r^N),$$ (2.9)

where A = observable property of a system.

In order to calculate the property of a system, an average value is replaced by an ensemble average, wherein, numerous replicas of a system are simultaneously considered. Hence the property can be represented as

$$< A > = \iint dp^N dr^N A(p^N, r^N) \rho(p^N, r^N),$$ (2.10)

where ρ = probability density of a system.

According to the *Ergodic* hypothesis, the ensemble average is equal to the time average[169]

$$A_{avg} = < A >.$$ (2.11)

Under NVT conditions the probability density can be defined as

24

$$\rho(p^N, r^N) = \frac{exp\left[-\frac{H(p^N, r^N)}{k_BT}\right]}{Q}, \qquad (2.12)$$

where $\mathcal{H}$ = Hamiltonian, k_B = Boltzmann constant, and Q = partition function.

The partition function under the canonical ensemble can be written as

$$Q_{NVT} = \frac{1}{N!}\frac{1}{h^{3N}} \iint dp^N \, dr^N \exp\left[-\frac{\mathcal{H}(p^N, r^N)}{k_BT}\right]. \qquad (2.13)$$

2.1.8 Integrating algorithms

In MD simulations, the time propagation of physical quantities such as positions, velocities, accelerations, *etc.* are approximated using Taylor series expansions.

$$r(t + \delta t) = r(t) + \delta t v(t) + \frac{1}{2}\delta t^2 a(t) + \cdots, \qquad (2.14)$$

$$v(t + \delta t) = v(t) + \delta t a(t) + \frac{1}{2}\delta t^2 b(t) + \cdots, \qquad (2.15)$$

$$a(t + \delta t) = a(t) + \delta t b(t) + \cdots, \qquad (2.16)$$

where r = position, v = velocity, a = acceleration, and b = third derivative of position with respect to time.

These quantities are calculated using procedures such as Verlet,[176] Leap-frog,[177] Velocity-Verlet,[178] or Beeman's algorithm.[179]

2.1.8.1 Verlet algorithm

The Verlet algorithm uses the positions and accelerations at time t and the positions of previous step r $(t - \delta t)$ to calculate the new positions at $t + \delta t$.

$$r(t + \delta t) = r(t) + \delta t v(t) + \frac{1}{2}\delta t^2 a(t) + \cdots, \qquad (2.17)$$

$$r(t - \delta t) = r(t) - \delta t v(t) + \frac{1}{2}\delta t^2 a(t) - \cdots. \qquad (2.18)$$

25

Adding Eq.'s 2.17 and 2.18 we obtain

$$r(t + \delta t) = 2r(t) - r(t - \delta t) + \delta t^2 a(t). \tag{2.19}$$

The velocity term does not appear in this algorithm. The velocity is calculated using

$$v\left(t + \frac{1}{2}\delta t\right) = \frac{[r(t+\delta t)-r(t)]}{\delta t}, \tag{2.20}$$

$$v(t) = \frac{[r(t+\delta t)-r(t-\delta t)]}{2\delta t}. \tag{2.21}$$

The implementation of the Verlet algorithm is straightforward, and the storage requirements are modest. Some of the limitations of this algorithm are as follows:

a) The positions at *r (t + δt)* are obtained by adding a small term $\delta t^2 a(t)$ to the difference of two large terms *(2r(t) – r(t - δt))*. As a result the precision of the positions may be lost.

b) There is no explicit term to calculate the velocities.

2.1.8.2   Leap-frog algorithm

In the leap-frog algorithm, the positions and velocities are calculated using the following equations

$$r(t + \delta t) = r(t) + \delta t v\left(t + \frac{1}{2}\delta t\right), \tag{2.22}$$

$$v\left(t + \frac{1}{2}\delta t\right) = v\left(t - \frac{1}{2}\delta t\right) + \delta t a(t). \tag{2.23}$$

The velocities at *t+1/2δt* are initially calculated. Then, the positions at *t + δt* are determined in the next step. In this way, the velocities leap over the positions to give new positions. Similarly, the positions leap over the velocities to determine new values

of velocities. Unlike the Verlet algorithm, the leap-frog algorithm has a velocity term.

However, the velocity and the position cannot be calculated simultaneously at a particular

time t. The velocities at time t are calculated using

$$v(t) = \frac{1}{2}\left[v\left(t + \frac{1}{2}\delta t\right) + v\left(t - \frac{1}{2}\delta t\right)\right]. \tag{2.24}$$

2.1.8.3   Velocity-Verlet algorithm

In a Velocity-Verlet algorithm the positions, velocities, and accelerations are

calculated at the same time. Initially, the positions at $t + \delta t$ are calculated using

$$r(t + \delta t) = r(t) + \delta t v(t) + \frac{1}{2}\delta t^2 a(t). \tag{2.25}$$

The new forces are determined using current positions and then the accelerations

at $t + \delta t$ are calculated. Finally, the velocities at $t + \delta t$ are calculated using accerelations

at t and $t + \delta t$ as shown below:

$$v(t + \delta t) = v(t) + \frac{1}{2}\delta t a(t) + \frac{1}{2}\delta t a(t + \delta t). \tag{2.26}$$

Similar to the Leap-frog algorithm, Velocity-Verlet also has an explicit term to

calculate velocities. This method is numerically stable and therefore is most widely used

in MD simulations. In this study we have used the Velocity-Verlet algorithm. A detailed

explanation of Beeman's algorithm is provided elsewhere.[169]

2.1.9   Time step

There is no standard rule for choosing a time step in MD simulations. The time

step δt should be selected in such a way that it should not affect the overall dynamics of a

system. Generally, the time step should be approximately $1/10^{th}$ of the shortest period of

motion of a system. In a chemical system the bond stretches involving hydrogen will have the highest frequencies, and the time period for C-H, O-H, and N-H bond stretches are about 10 fs. Therefore, the most commonly used time step in MD is 1 fs.

2.1.10   Thermostat

In MD simulations various properties of a biological system are evaluated at constant temperature. Hence, a hypothetical thermostat is used to maintain a constant temperature throughout the simulation. The temperature of a system depends on the average kinetic energy.

$$< K >_{NVT} = \frac{3}{2} N k_B T. \qquad (2.27)$$

Some of the commonly used thermostats are

a) Berendsen thermostat

b) Langevin thermostat

c) Nosé Hoover thermostat.

2.1.10.1   Berendsen thermostat

The system is coupled to an external bath at a desired temperature.[180] Then, the velocities of all atoms of a system are scaled for a specified number of steps using a scaling factor λ.

$$\lambda^2 = 1 + \frac{\delta t}{\tau} \left(\frac{T_{bath}}{T(t)} - 1 \right), \qquad (2.28)$$

where $T(t)$ is the temperature of the system, and τ is a coupling parameter whose value determines how loosely or tightly the system and the bath are coupled together. For a 1 fs time step, the suggested value of the coupling parameter is about 0.4 ps. The system

28

can be made to fluctuate around a desired temperature using this thermostat. The

velocity scaling may cause a few artifacts. Sometimes, the temperature of the entire

system may be constant, but the temperature of the solvent might be higher than the

temperature of the solute. This leads to an unequal distribution of energy within the

system. One of the ways to overcome this problem is to implement stochastic dynamics.

These dynamics are based on a Langevin equation of motion.

2.1.10.2   Langevin thermostat

For a Langevin thermostat, each particle behaves as if it is immersed in a bath of

viscous medium.[181] The Langevin equation of motion is used instead of Newton's

second law of motion. The Langevin equation of motion for a particle is given as

$$m\frac{d^2x(t)}{dt^2} = F - \gamma\frac{dx(t)}{dt}m + R(t). \tag{2.29}$$

The term F is the force acting on a particle, and the second term is the motion of a

particle in the solvent medium, generally known as frictional drag due to the solvent.

The frictional force on a particle is given by

$$F_{frictional} = -\xi v, \tag{2.30}$$

where ξ is the frictional coefficient, which is directly related to the collision frequency γ,

and $\gamma = \xi/m$ (m = mass of the particle). The third term represents the random fluctuations

caused by the interaction of a particle with the solvent molecules. $R(t)$ is proportional to

$(2k_B(T*m))^{1/2}$. $R(t)$ and γ are adjusted to maintain the desired temperature.

The advantages of the Langevin thermostat are 1) the canonical ensemble can be

effectively sampled. 2) Each particle will be in contact with a local bath. 3) Due to the

presence of *R(t)*, it is possible to take larger time steps. In this study, we have used the Langevin thermostat. A detailed explanation of the Nosé Hoover thermostat is described elsewhere.[182]

2.1.11 Barostat

The simulations can also be performed under constant pressure. The system will be maintained under constant pressure by varying the volume of the simulation box. The volume fluctuation depends on the isothermal compressibility.

$$\kappa = -\frac{1}{V}\left(\frac{\partial V}{\partial P}\right)_T.$$ (2.31)

The volume of a simulation box is scaled by a factor of λ, which is equivalent to scaling the atomic coordinates by $\lambda^{1/3}$.

$$\lambda = 1 - \kappa\frac{\delta t}{\tau_p}(P - P_{bath}),$$ (2.32)

where δt = time step, τ_p = coupling constant, P = pressure of the system, and P_{bath} = pressure of the bath. The new positions are given as

$$r_i' = \lambda^{1/3}r_i,$$ (2.33)

where r_i' are the new positions and r_i are the current positions.

2.2   Free energy calculations

Among all the thermodynamic properties, the most important is the change in free energy. When a system is simulated under the canonical ensemble, the Helmholtz free energy can be determined. Under NPT conditions, the Gibbs free energy can be calculated. Traditional MD or MC simulations do not efficiently sample the whole phase

space of a system. Hence, the free energy values derived using these methods will have large errors.

Usually, the system of interest will be initially sampled using MC or MD simulations. Then, free energy perturbation (FEP) or thermodynamic integration (TI) methods are used to calculate free energy changes.[183,184] We have used thermodynamic integration to determine protein-ligand free energy of binding. A detailed description of FEP is provided elsewhere.[169]

2.2.1   Thermodynamic integration

Thermodynamic integration (TI) is one of the most accurate methods for calculating the free energy of binding. The change in free energy is determined by

$$\Delta A = \int_{\lambda=0}^{\lambda=1} \langle \frac{\partial V}{\partial \lambda} \rangle_\lambda \ d\lambda. \tag{2.34}$$

ΔA is determined by calculating an ensemble average of the derivative of potential energy with respect to λ, where λ is a perturbing parameter. At $\lambda=0$, the receptor and ligand will have 100% interaction, and at $\lambda=1$ they will have no interaction. The ΔA value is calculated by considering a series of λ values between 0 and 1. At each λ value the system must be properly equilibrated. The integral value given in Eq. 2.34 is calculated numerically. The derivation of the above expression is shown below.

The Helmholtz free energy at any λ value is represented as

$$A(\lambda) = -k_B T ln Q(\lambda). \tag{2.35}$$

If λ is varied from 0 and 1, then the change in free energy is given by

$$\Delta A = - \int_0^1 \frac{k_B T}{Q(\lambda)} \frac{\partial Q(\lambda)}{\partial \lambda} \ d\lambda. \tag{2.36}$$

The partition coefficient Q under NVT conditions is

$$Q_{NVT} = \frac{1}{N!} \frac{1}{h^{3N}} \iint dp^N \, dr^N \exp\left[-\frac{\mathcal{H}\left(p^N, r^N\right)}{k_B T}\right]. \tag{2.37}$$

Therefore, $\partial Q/\partial \lambda$ can be written as

$$\frac{\partial Q}{\partial \lambda} = -\frac{1}{N!} \frac{1}{h^{3N}} \frac{1}{k_B T} \iint dp^N \, dr^N \frac{\partial \mathcal{H}(p^N, r^N)}{\partial \lambda} \exp\left[-\frac{\mathcal{H}\left(p^N, r^N\right)}{k_B T}\right]. \tag{2.38}$$

Substituting Eq. 2.37 and Eq.2.38 into Eq. 2.36 gives

$$\Delta A = \int_0^1 \frac{\iint dp^N dr^N \frac{\partial \mathcal{H}\left(p^N, r^N\right)}{\partial \lambda} \exp\left(\frac{-\mathcal{H}\left(p^N, r^N\right)}{k_B T}\right)}{\iint dp^N dr^N \exp\left(\frac{-\mathcal{H}\left(p^N, r^N\right)}{k_B T}\right)} \, d\lambda. \tag{2.39}$$

By applying the *Ergodic* hypothesis, Eq. 2.39 becomes

$$\Delta A = \int_0^1 \langle \frac{\partial H}{\partial \lambda} \rangle_\lambda \, d\lambda, \tag{2.40}$$

where $<\,>_\lambda$ is an ensemble average with respect to λ. The Hamiltonian can be written as

$$\mathcal{H}(\lambda) = T + V(\lambda). \tag{2.41}$$

Under NVT conditions the ensemble average of the kinetic energy is constant and can be ignored. Therefore, the ensemble average of the Hamiltonian is equal to the ensemble average of the potential energy, and hence Eq. 2.40 becomes

$$\Delta A = \int_0^1 \langle \frac{\partial V}{\partial \lambda} \rangle_\lambda \, d\lambda. \tag{2.42}$$

The integrand of the above expression is determined using numerical integration. Thus, ΔA can also be written as

$$\Delta A = \sum_i w_i \left\langle \frac{\partial V}{\partial \lambda} \right\rangle_i, \tag{2.43}$$

where the w_i's are the weights.

The potential energy is calculated using a mixed potential function as shown below

$$V(\lambda) = (1-\lambda)^k V_0 + [1-(1-\lambda)]^k V_1, \tag{2.44}$$

where V_0 is the potential of the unperturbed Hamiltonian, V_1 is the potential of the perturbed Hamiltonian, and k is a value between 1 and 6.

In a TI calculation, the electrostatic interactions and then the van der Waals interactions of a ligand with the active site residues of a protein are eliminated by varying λ between 0 and 1. The partial atomic charges of the atoms of a ligand are made to zero to eliminate the electrostatic interactions, and in a separate calculation the ε (interaction strength) term in the Lennard-Jones potential becomes zero to remove the van der Waals interactions. When a linear-mixing potential function is used, i.e. $k = 1$, the integrand in Eq. 2.42 diverges at $\lambda = 1$ when removing the van der Waals interactions.[185] At $\lambda = 1$, ε becomes zero, and hence the van der Waals potential also becomes zero. However, near $\lambda = 1$, ε is close to zero, but not exactly zero. Then, if the distance between two atoms approaches zero, the van der Waals term in the potential energy of the system approaches infinity. Hence, when a linear-mixing potential function is used, special numerical integration methods must be applied in order to achieve a better estimate of the integral. As long as $k \geq 4$, the integral becomes finite as $\lambda \to 1$, but a better estimate of the free energy is obtained by using $k = 6$.[185]

2.2.2   Implicit solvent models

The free energy of binding determined using FEP or TI is time consuming and expensive.[186] Typically, both these methods estimate the free energy changes using an explicit solvent simulation. In an explicit solvent model, the solute will be surrounded by thousands of solvent molecules. Hence, most of the computational time is spent in calculating solvent-solvent and solute-solvent interactions. However, if the explicit solvent molecules can be replaced by an infinite solvent continuum medium with a specific dielectric constant, then more time can be dedicated to sample the solute particles. The solvent continuum model is commonly known as the implicit solvent model.

The free energy of binding for a protein-ligand system can be expressed as

$$\Delta G_{bind} = \Delta E_{forcefield} + \Delta G_{sol} - T\Delta S, \qquad (2.45)$$

where $\Delta E_{forcefield}$ is the internal energy of a system in the gas phase.

$$\Delta E = \Delta E_{bonding} + \Delta E_{non-bonded}. \qquad (2.46)$$

Similarly, ΔG_{sol} is calculated using the following relationship

$$\Delta G_{sol} = \Delta G_{elec} + \Delta G_{vdw} + \Delta G_{cavity}. \qquad (2.47)$$

ΔG_{elec} is an electrostatic term and the last two terms are non-polar contributions. The solvent molecules have to reorganize and create a cavity when a solute is added to a pure solvent. Therefore, the entropy of the solvent decreases, and the term ΔG_{cavity} will be positive. Various methods have been proposed for calculating ΔG_{elec}. The most widely used methods are Poisson-Boltzmann and Generalized Born. The $T\Delta S$ values were calculated by performing normal mode analyses.

2.2.2.1 Poisson-Boltzmann

The linearized form of the Poisson-Boltzmann equation can be written as[187]

$$\nabla[\varepsilon(r)\nabla\phi(r)] - \kappa'^2 \sin h[\phi(r)] = -4\pi\rho(r), \qquad (2.48)$$

where $\phi(r)$ is the electrostatic potential, $\rho(r)$ is the charge density, and $\varepsilon(r)$ is the dielectric constant of the medium, and κ'^2 can be calculated using the Debye-Hückel inverse length κ and is given by

$$\kappa^2 = \frac{\kappa'^2}{\varepsilon} = \frac{8\pi N_A e^2 I}{1000\varepsilon k_B T}, \qquad (2.49)$$

where e = charge, I = ionic strength of the solution, and N_A = Avogadro's number.

The Poisson-Boltzmann equation is solved numerically using a finite-difference method.[188,189] The electrostatic interactions are calculated using grid points. The solute is assigned a dielectric constant of 1, 2, or 4, and the solvent, usually water, is assigned a dielectric constant of 80. The grid points belonging to the solute and the solvent can be distinguished by estimating the solvent accessible surface area. Thus, a unique dielectric constant will be allocated to the grid points belonging to solute or solvent areas.

2.2.2.2 Generalized Born

Solving the Poisson-Boltzmann equation using numerical integration is time consuming, memory intensive, and computationally expensive.[190] Therefore, an alternative approach for calculating ΔG_{elec} is using the Generalized Born equation.[191,192] The Generalized Born model is computationally inexpensive and can be calculated much faster than the Poisson-Boltzmann method.

In a Generalized Born equation, each atom of a system is represented by a sphere of radius r_i and charge q_i. The spherical particle is assumed to be filled with uniform matter and has a dielectric constant ranging from 1-4, and the surrounding solvent medium contains a dielectric constant of 80.[193] The interactions between each pair of atoms is calculated, and the net electrostatic interactions of a system is defined as

$$\Delta G_{elec} \approx \Delta G_{gb} = -\frac{1}{2}\left(1 - \frac{1}{\epsilon}\right)\sum_{i=1}^{N}\sum_{j=1}^{N}\frac{q_i q_j}{f(r_{ij}, a_{ij})}. \tag{2.50}$$

The function f depends on r_{ij} and the Born radii a_{ij} and is given by

$$f(r_{ij}, a_{ij}) = \sqrt{(r^2_{ij} + a^2_{ij}\, e^{-D})}, \tag{2.51}$$

where r_{ij} is the distance between the atoms i and j, $a_{ij} = (a_i a_j)^{1/2}$, a_i and a_j are known as effective Born radii, and $D = r^2_{ij}/(2a_{ij})^2$.

2.2.2.3   Non polar contribution

Apart from the electrostatic contribution, ΔG_{sol} also depends on the van der Waals and cavity terms as shown below

$$\Delta G_{vdw} + \Delta G_{cavity} = \gamma SASA + b, \tag{2.52}$$

where γ and b are constants and $SASA$ is the solvent accessible surface area.

During cavity formation the solvent molecules in the first solvation shell are affected the most. Similarly, the van der Waals interactions between the solute and solvent molecules mainly occur in the first solvation shell, too. Therefore, the van der Waals and cavity terms are combined.[194,195] Usually, a probe of radius 1.4 Å will be made to roll along the van der Waals surface of the solute to calculate the $SASA$.[196,197]

2.2.2.4　Normal mode analysis

Biological systems (*i.e.* proteins) may exist in more than one conformation.[198,199] The tertiary structure of a protein will change during a conformational change. Similarly, the protein will undergo structural changes upon the binding of small, drug-like molecules.[200] These changes occur on the order of micro or milliseconds.[201] Therefore, longer MD simulations must be performed for observing such changes. However, carrying out such simulations is computationally expensive and time consuming.[201,202] Alternatively, these changes can be analyzed by conducting a normal mode analysis.[203]

The potential energy of a system is calculated using a defined forcefield. Then, the system will be minimized to a local minimum. Later, a 3N×3N Hessian matrix is constructed. Further, the Hessian matrix will be converted into a force constant matrix using the following relationship.

$$F = M^{-1/2}V''M^{-1/2}, \tag{2.53}$$

where *M* is a diagonal matrix and contains the masses of the atoms and *V''* is the Hessian matrix.

The *F* matrix is diagonalized, determining its eigenvalues and eigenvectors. Finally, the frequencies corresponding to each normal mode are calculated using the eigenvalues.

$$\nu_k = \frac{\sqrt{\lambda_k}}{2\pi}. \tag{2.54}$$

Thermodynamic properties such as internal energy, enthalpy, and entropy can be calculated using a normal mode analysis. The net entropy can be represented as

$$\Delta S_{net} = \Delta S_{translational} + \Delta S_{rotational} + \Delta S_{vibrational}. \qquad (2.55)$$

The vibrational entropy term plays an important role when determining the free energy of binding. The vibrational entropy is given by

$$S_{vib} = R \sum_{i=1}^{3N-6} \left[\frac{h\nu_i}{k_B T \left(e^{\frac{h\nu_i}{k_B T}} - 1 \right)} - ln\left(1 - e^{-\frac{h\nu_i}{k_B T}} \right) \right], \qquad (2.56)$$

where ν_i is the frequency.

The low frequency modes are important as they correspond to large scale motions of proteins.[204,205] Therefore, the contribution of vibrational entropy from these modes will influence the net entropy of a system.

2.3 Docking studies

Docking studies are mainly used for analyzing protein-protein, protein-ligand, and protein-nucleotide binding interactions.[206-208] In protein-ligand molecular docking, the orientation and conformation of a ligand in the active site are determined.[209] Similarly, the interactions between the ligand and the active site residues are analyzed, and their corresponding binding energies are calculated.[210,211] Another important part of docking studies is virtual screening. Using a virtual screening process, thousands of small molecules are screened to identify a set of ligands which can effectively bind to a protein of interest.[212,213] This technique helps to engineer new lead molecules in the drug-design field. Over the last decade the computational accuracy, performance, and speed of many docking programs have increased tremendously.[214-216] The predicted protein-ligand binding modes and affinities values can be within experimental errors.[216,217]

Sampling and scoring are the two major steps in docking studies. In the sampling section, ligand sampling and protein flexibility plays a major role.[218] During the docking studies, hundreds or thousands of ligand poses will be generated. The orientation, interaction, and binding of each pose in the active site will be examined. Using a scoring function, all conformers will be ranked based on their binding energies in order to identify a best conformer.[210,219] Therefore, a scoring function is a crucial component in identifying the lowest energy conformer and binding mode of a ligand. There exists a variety of sampling techniques and scoring functions, some of which are briefly explained in the following section.

2.3.1 Sampling techniques

When a ligand binds to a protein, the active site residues will often rearrange to accommodate the ligand. As a result, the conformation of the entire protein or the side-chain conformation of an amino acid may change.[218,220] During protein-ligand docking studies, the protein can be made flexible. However, from a computational stand point, the entire protein cannot be made flexible due to the size of a protein and its numerous degrees of freedom. Therefore, various approaches have been proposed to tackle protein flexibility. Some of them are discussed below.

2.3.1.1 Soft docking

In this method the protein and ligand structures are allowed to change only to some extent. Both structures are represented as smooth molecular surfaces.[221,222] The molecular surface of the ligand is translated and rotated in different ways to align with the active site surface. The overlapped volume during the interactions is subtracted to

avoid van der Waals repulsions. However, various ligand conformations are not completely explored. This method is simple and computationally efficient, but the binding modes and affinities are not accurate and reliable.

2.3.1.2   Rigid docking

In this approach, the backbone and the side chains of the protein are made rigid. The analysis is done using a single conformation of the protein.[223,224] During the process, the ligand is made flexible, and various conformers of the ligand are considered. Finally, an optimal binding pose and a lowest energy conformer of a ligand will be detected. This method is computationally fast and inexpensive. Due to the rigidity of the protein, when a ligand binds to the active site, it may overlap or sterically clash with the active site residues. In order to obtain reliable binding poses, the system can be minimized.

2.3.1.3   Side-chain flexibility

In this approach, the side chains of a protein are made flexible, and the backbone atoms are made rigid. The conformation of side chains are changed using a rotamer library.[225,226] A rotamer library mainly consists of experimentally observed side-chain conformers of various amino acids.[225] Depending upon the interaction between a ligand and the active site residues, the side-chain conformation of an amino acid located in the active site or in any other site will be changed. This treatment allows for the exploration of the conformational phase space of a protein in the presence of a ligand. One of the advantages of this method is that a lower energy conformer of a protein can be obtained when compared to the methods discussed above.

2.3.1.4   Multiple protein structure docking

The most efficient way to incorporate protein flexibility is to consider an ensemble of various protein structures.[227-229] A few similar regions from a selected set of proteins structures will be identified to construct the flexible binding site of a protein of interest.[230] The similar regions are merged together, and the dissimilar regions are used to create new conformers of a protein. In another approach the protein of interest is divided into a rigid part and several flexible parts according to the protein structures present in the ensemble.[231] Depending upon the displacement or orientation of the ligand, for each flexible part a particular conformer will be selected. Then, all the selected conformers will be attached to the rigid part of the protein. This procedure helps to construct a protein-ligand structure. This method scales linearly and efficiently predicts the protein-ligand binding modes and affinities.

Another way to attain protein flexibility is to consider an experimentally determined protein structure and run a short MD simulation. Then, generate a few snapshots of the protein from the last few nanoseconds of the sampling process. The ligand will then be docked to all generated snapshots. In this way, we can dock the ligand to different conformers of the protein. Finally, the interactions between the ligand and the active site residues in all snapshots will be analyzed, and the best binding mode and affinity will be selected.

2.3.2   Ligand sampling

The most important aspect of molecular docking is ligand sampling. The following methods are commonly used.

2.3.2.1 Systematic search

This method explores all possible binding poses and also all degrees of freedom of a ligand in the active site. The basic approach is to systematically rotate each rotatable bond in order to analyze various conformers of a ligand.[232] In a given system, as the number of rotatable bonds increases, the complexity of the algorithm increases exponentially. However, this method can be applicable if the molecule has a small number of rotatable bonds.

2.3.2.2 Random search

Random search algorithms are also known as stochastic algorithms, wherein the orientation and conformation of a ligand are randomly changed to explore the ligand's conformational phase space. The most commonly used algorithms are Monte Carlo[233,234] and genetic algorithms.[235,236]

2.3.2.2.1 Monte Carlo

In a Monte Carlo algorithm the following are the steps involved:

a) Using a random number generator, the current conformation of a ligand will be randomly changed, and a new conformer will be produced.

b) The energy of the new conformer will be determined.

c) If the energy of the new conformer is less than the energy of the previous one, then the new conformer will be taken as the current conformer for the next iteration.

d) If the energy of the new conformer is higher than the energy of the previous conformer, then a Boltzmann factor based on the energy difference will be

calculated. A random number between 0 and 1 will be generated, and if the Boltzmann factor is greater than the random number, then the new conformer will be accepted.

Various conformations of a ligand are randomly generated and are accepted based on the above procedure. This process is repeated for several hundreds to thousands of iterations (user defined). Further, a few of the lowest energy conformers are selected. The corresponding binding affinities are calculated and ranked according to their energy values.

2.3.2.2.2 Genetic algorithm

An initial population of various conformers of a ligand must be generated. The generated conformers will be categorized into different groups, depending upon their orientation and interactions with the active site. Within the same group, the bond lengths, bond angles, and dihedral angles are randomly changed, which is commonly known as a mutation. Further, a side chain or a part of a ligand is exchanged among any two selected conformers, *i.e.* crossover.

Additionally, a complete conformer or a part of a conformer will be exchanged among various groups, which is known as a migration. In each group, each conformer will be translated and rotated. At the end of every iteration, the favorable conformers are selected, optimized, and ranked using a scoring function. Then, the lowest energy conformer is chosen and taken as an initial structure for next iteration. Based on the results of the previous iteration, the mutations, crossovers, and migration processes are adjusted in the present iteration to obtain a better structure than the previous step. In this

way, a rigorous ligand search will be performed for user defined iterations, and the selected ligands will be ranked based on a scoring function. This is an efficient method for identifying a suitable conformer of a ligand when it binds into the active site of a protein.

2.3.3   Scoring function

The scoring function is an important step in molecular docking studies. An efficient scoring function should be capable of calculating the energies of various conformers of a ligand, rank them, and select a best conformer. Most of the docking programs use simple scoring functions that are computationally fast and effective. Some of the docking programs are missing the entropic effects when a ligand binds into the active site of a protein.[237] A number of scoring functions have been developed, which are mainly divided into the following categories.

2.3.3.1   Forcefield scoring function

The binding energy of a ligand can be calculated using molecular mechanics forcefields.[238,239] The internal terms of the ligands (bond lengths, bond angles, and torsions) and the non-bonded terms are calculated. The van der Waals interactions are calculated using a Lennard-Jones potential, and the electrostatic interactions are calculated using Coulombs law. To decrease the computational cost, the solvent effects are included using solvent continuum models with a constant dielectric constant. Determining the entropic contribution to the binding energy is a major challenge in this field.

44

2.3.3.2 Empirical scoring function

The binding energy of various ligand conformers is calculated as sum of van der Waals, electrostatics, hydrogen bonding, desolvation, and hydrophobicity and is represented as

$$\Delta G = \sum w_i \Delta G_i. \tag{2.57}$$

The coefficients, w_i, are determined by performing a regression analysis on a training set containing a variety of experimentally known protein-ligand binding energies.[240] The empirical scoring function is much simpler than forcefield scoring. However, the validity of the weighing terms and the regression analysis primarily depends upon the training set.

2.3.3.3 Knowledge-based scoring function

The crystal structures of relatively similar protein-ligand systems will be considered as a training set.[241-243] This scoring function mainly relies on the structural information of the training set, rather than binding energies. In each protein-ligand system, the atomic pair interaction potential is calculated using an empirical method[244] and is given as

$$w(r) = -k_B T ln \left[\frac{\rho(r)}{\rho(r)^*} \right], \tag{2.58}$$

where $\rho(r)$ is the density of the protein-ligand atom pair at the distance r and $\rho(r)^*$ is a reference state. In the reference state, two atoms of an atomic pair do not interact with each other. The ligand binding energy is calculated by combining the interaction potential of all protein-ligand systems of the training set. The ligand binding potential is calculated using a large set of experimentally known protein-ligand structures.

Therefore, this scoring function can be more accurate than forcefield and empirical

scoring functions.

CHAPTER III

BINDING FREE ENERGIES OF OXIMES CALCULATED USING

THERMODYNAMIC INTEGRATION

The main aim of this study was to calculate the oxime free energy of binding in

human AChE (hAChE) and human BChE (hBChE) inhibited by nerve agents. We were

also interested to calculate the oxime free energy of binding in uninhibited hAChE and

hBChE. The nerve agents sarin and tabun and the reactivators 2-PAM, MMB-4, HI-6,

and obidoxime were considered. In this chapter the interactions of oximes with various

active site residues in all inhibited and uninhibited systems of hAChE and hBChE are

discussed. The outcomes of TI calculations and a comparison with available

experimental values are also reported.

3.1   Computational methods

3.1.1   Cholinesterases models

The crystal structures of hAChE (PDB code: 1F8U)[245] and hBChE (PDB code:

1P0I)[246] were imported from the PDB server.[247] The enzymes hAChE and hBChE

consists of 539 and 529 residues respectively. The missing residues of hAChE (1-12)

and hBChE (1-3, 378, 379, and 455) were modeled and placed in their respective

locations using Spartan'06. In both enzymes the cysteine residues were connected

through S-S bonds. Using *xleap*, the S-S bonds between the residues 65 and 92, 253 and

268, and 405 and 525 in hAChE and between 65 and 92, 252 and 263, and 400 and 519 in hBChE were connected. Then, the modified protein structures were simulated using an implicit solvent model. The systems were initially minimized for 1000 steps, heated (10-300K) for 100 ps, and then equilibrated for 1 ns using Amber8[248] and the ff99 forcefield[249] with a 16 Å cutoff. The equilibrated structures were submitted to the H++ server,[250,251] to obtain the protonation states of the titratable residues and the total charge of the protein.

3.1.2   Modeling of inhibited cholinesterases and reactivators

The sarin-serine and tabun-serine models were built using Spartan'06. The leaving groups, –F and –CN in sarin and tabun were removed from the models. Conformational analysis was done using AM1,[252] and the lowest energy conformer was chosen. A geometry optimization was done with Hartree-Fock (HF) and the 6-31G* basis set using Q-Chem 3.2.[151] In the ff99 forcefield, the partial atomic charges of the amino acids atoms are derived using HF/6-31G*. Hence, to maintain consistency with the forcefield, the optimization was done using HF/6-31G*. Further, the partial atomic charges for sarin-serine and tabun-serine were derived using the restrained electrostatic potential approach.[253]

The active serine in hAChE (S199) and hBChE (S198) were removed and replaced with the optimized sarin-serine and tabun-serine (OP-serine) structures. In this way, four different inhibited enzymes, hAChE-sarin, hAChE-tabun, hBChE-sarin, and hBChE-tabun were constructed. Then, all the inhibited systems were equilibrated using a similar procedure as mentioned above.

The oximes 2-PAM, MMB-4, HI-6, and obidoxime were also built using Spartan'06. Their conformational analyses, geometry optimization, and partial atomic charges were calculated using a similar procedure to that described earlier.

3.1.3   Docking studies

All the docking studies were performed with the Lamarckian genetic algorithm[236] using Autodock4.[254] 2-PAM, MMB-4, HI-6, and obidoxime were individually docked to all inhibited and uninhibited systems. In the inhibited systems, the OP-serine complex was made flexible, while the remaining part of the protein was treated as rigid. Similarly, the active site serine was considered as flexible in the uninhibited enzymes. Various conformers of the reactivator were visualized using VMD.[255] In the inhibited systems a particular conformer of the reactivator was selected based on the following criteria. The O-H (on the oxime group) of the reactivator and P of the OP-serine should align along the same axis. Secondly, a conformer of the reactivator with the shortest distance between O-H of the reactivator and P of the OP-serine was selected. In case of uninhibited systems, a conformer of the reactivator which was closest to the active site serine was chosen. The interactions of the selected conformers of the reactivators with all inhibited and uninhibited systems were verified by performing MD simulations.

3.1.4   Molecular dynamics simulations

Explicit solvent MD simulations were performed using Amber 8 and the ff99 forcefield. Amber's general atomic forcefield (*gaff*)[256] was used for the reactivators (ligands). Using *xleap*, the inhibited and uninhibited systems were taken in a truncated octahedron box and solvated with TIP3P[257] water molecules. The inhibited and the

49

uninhibited hAChE systems were neutralized with 5 Na^+ ions. hBChE was neutralized with 2 Cl^- ions. The minimization, heating, equilibration, and sampling were performed using the *sander* module of Amber8. Initial minimization was done for 1000 steps with a force constant restraint of 500 kcal/mol/Å^2 on the enzyme and the reactivator. Then, the whole system was minimized for 2500 steps. The system was heated for 100 ps from 10 K to 300 K under NVT conditions with a restraint of 10 kcal/mol/Å^2 on the protein and the reactivator. Next, it was equilibrated for 900 ps at 300 K under NPT conditions. Under NVT conditions, the system was sampled for 10 ns. During the equilibration and sampling process, the hydrogens were constrained using the SHAKE algorithm,[258,259] and a constant temperature was maintained using Langevin dynamics with a collision frequency of 1.0 ps^{-1}.[181] The electrostatic interactions were handled using Particle Mesh Ewald (PME)[260-262] under periodic boundary conditions with an 8 Å cutoff. All the dynamics were performed with a time step of 2 fs.

3.1.5   Thermodynamic integration

The TI calculations were performed using eight different λ values (0.02544, 0.12923, 0.29707, 0.5, 0.70292, 0.87076, 0.97455, 1.0), $k = 6$, and NVT conditions. The simulations were performed using a 1 fs time step. Each system was sampled on an average of 10-20 ns for each λ value. The coordinates and the velocities at the end of the explicit solvent sampling process were used as initial inputs.

The free energy of binding was calculated in two steps. Initially, the electrostatic and later the van der Waals interactions between protein and ligand were removed. These interactions are gradually eliminated by perturbing the system using the λ

parameter, which controls the interaction between the receptor and the ligand. The electrostatic and van der Waals calculations were separately simulated.

The chemical process between an inhibited or uninhibited system and an oxime during the TI calculations can be represented as

$$enzyme\ (aq) + oxime\ (aq) \rightarrow complex\ (aq) \qquad\qquad \Delta A_{TI}, \qquad (3.1)$$
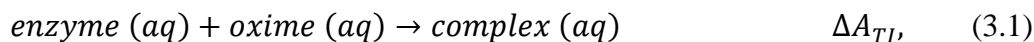
where *enzyme (aq)* = inhibited/uninhibited system, *oxime (aq)* = oxime, *complex (aq)* = inhibited/uninhibited system + oxime, and ΔA_{TI} = binding free energy.

The above process takes place in two steps:

$$complex\ (aq) \rightarrow enzyme\ (aq) + oxime\ (g) \quad \Delta A_{complex,TI}\ (step\ 1), \qquad (3.2)$$

$$oxime\ (aq) \rightarrow oxime\ (g) \qquad\qquad\qquad \Delta A_{oxime,TI}\ (step\ 2). \qquad (3.3)$$
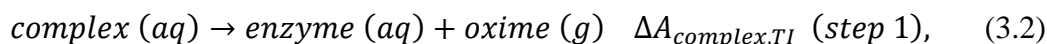
In the first step the complex gets dissociated into *enzyme (aq)* and *oxime (g)*. During this process the interactions between the oxime and the active site residues gradually decrease and the aqueous phase oxime vanishes from the active site and appears in the gas phase. In order to complete the thermodynamic cycle, the reactivator has to reappear in solution somewhere else. Therefore, the oxime was separately taken in a truncated octahedron box along with explicit water molecules (step 2). They were minimized, heated, equilibrated, and sampled for 10 ns using a similar procedure as mentioned earlier. Later, the TI simulations for the oxime by itself were performed. The net free energy of binding from step 1 and step 2 can be written as

$$\Delta A_{TI} = \Delta A_{oxime,TI} - \Delta A_{complex,TI}. \qquad (3.4)$$

3.2   Results and discussion

3.2.1   Explicit solvent simulations

The protein-ligand interactions are largely influenced by the solvent. In MD simulations, the solute-solvent and solvent-solvent interactions can be considered by performing explicit solvent simulations. All the inhibited and uninhibited systems were sampled for 10 ns. The stability of the systems was verified by plotting RMSd vs. time graphs. The RMSd vs. time plot of all the inhibited and uninhibited systems of 2-PAM, MMB-4, HI-6, and obidoxime are shown in Figures 3.1, 3.2, 3.3, and 3.4.
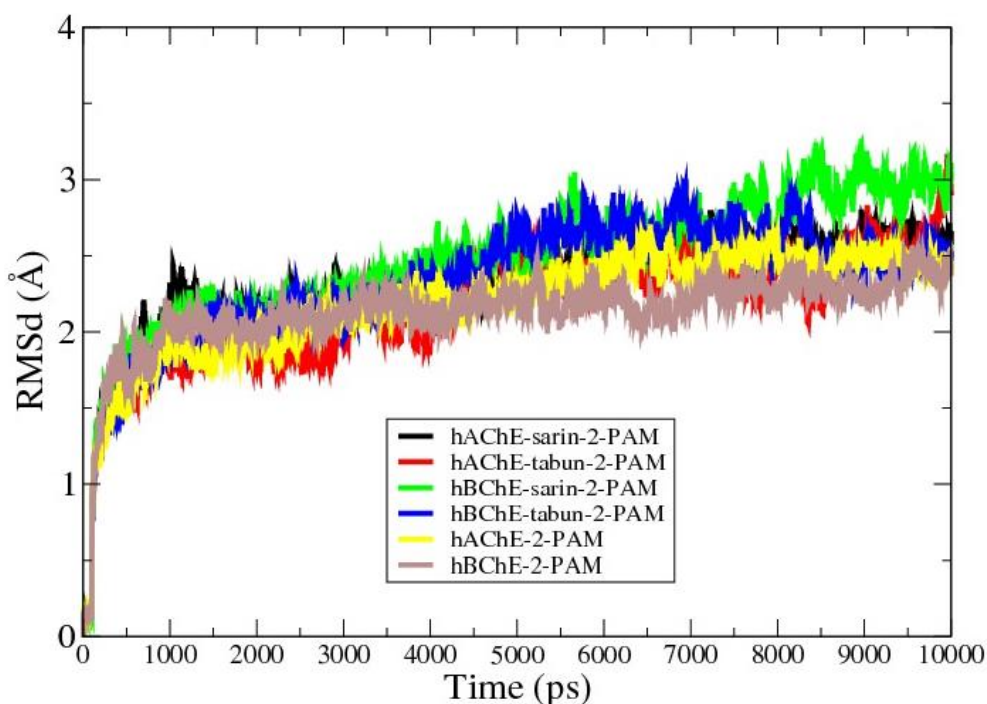
Figure 3.1   RMSd vs. time plots of inhibited and uninhibited systems with 2-PAM
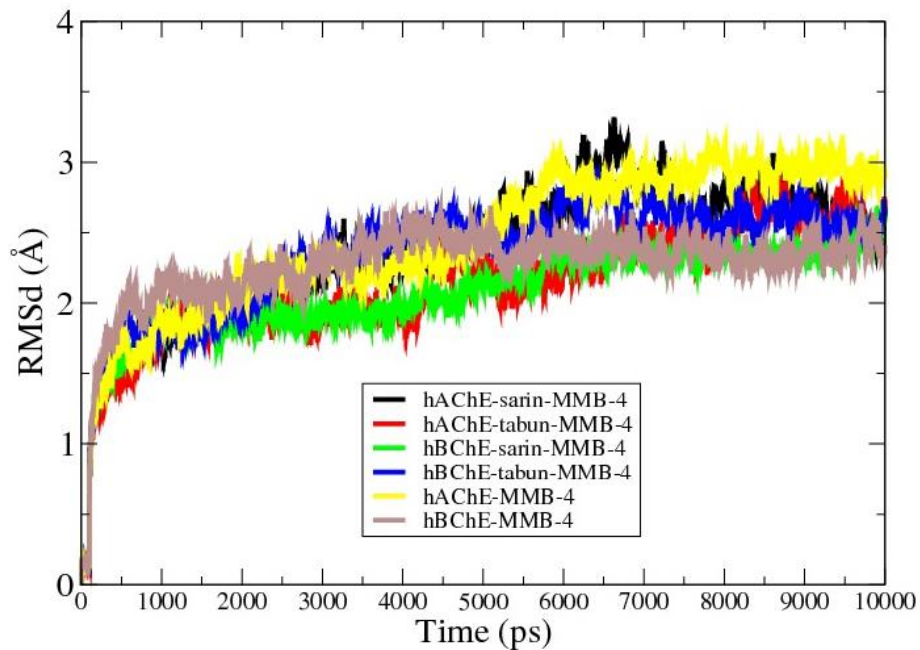
Figure 3.2   RMSd vs. time plots of inhibited and uninhibited systems with MMB-4
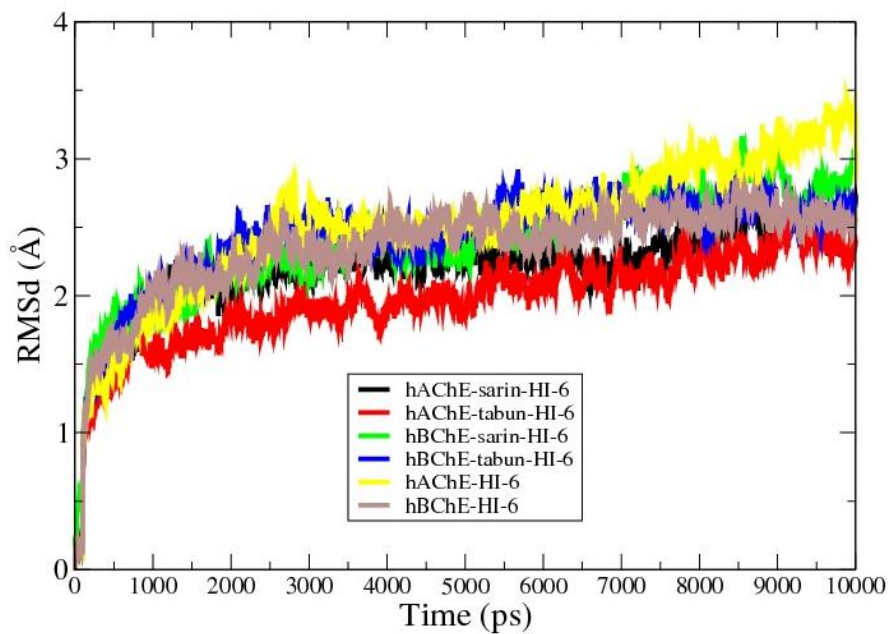
Figure 3.3   RMSd vs. time plots of inhibited and uninhibited systems with HI-6
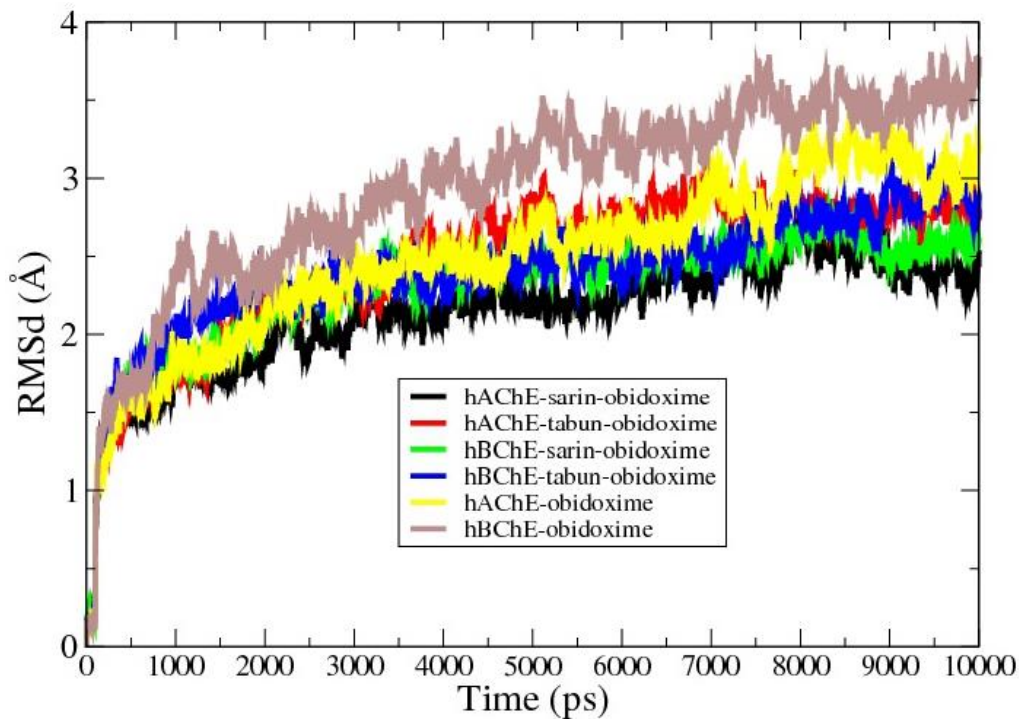
Figure 3.4   RMSd vs. time plots of inhibited and uninhibited systems with obidoxime

During the explicit solvent simulations, the reactivator was expected to exhibit hydrogen bonding, electrostatic interactions, or π-π stacking with the active site residues. Using *ptraj*, hydrogen bonds between the reactivator and the active site residues were analyzed. For this process, the last 5 ns of the sampling process were considered. The hydrogen bond analysis of 2-PAM, MMB-4, HI-6, and obidoxime are shown in Table 3.1. The atom labels on MMB-4, HI-6, and obidoxime as tabulated in Table 3.1 are shown in Figure 3.5.

Table 3.1 Hydrogen bonding analysis of inhibited and uninhibited systems of 2-PAM, MMB-4, HI-6, and obidoxime.

System	Donor	Acceptor H	Acceptor	Occupation (%)
hAChE-tabun-2-PAM	ASP70@OD	2-PAM@H	2-PAM@O	9.08
hAChE-2-PAM	GLU448@OE	2-PAM@H	2-PAM@O	91.19
hBChE-sarin-2-PAM	GLU325@O	2-PAM@H	2-PAM@O	4.38
hBChE-tabun-2-PAM	ALA328@O	2-PAM@H	2-PAM@O	41.20
hBChE-2-PAM	GLU441@OE	2-PAM@H	2-PAM@O	30.10
hAChE-sarin-MMB-4	GLU198@OE	MMB-4@H'	MMB-4@O'	80.78
	GLU80@OE	MMB-4@H"	MMB-4@O"	79.96
hAChE-tabun-MMB-4	GLU448@OE	MMB-4@H'	MMB-4@O'	58.92
hAChE-MMB-4	GLU448@OE	MMB-4@H'	MMB-4@O'	34.66
hBChE-MMB-4	GLU80@OE	MMB-4@H"	MMB-4@O"	63.90
	MMB4@O'	GLY115@H	GLY115@N	13.06
hAChE-sarin-HI-6	ASP127@OD	HI-6@N'H"	HI-6@N'	5.00
hAChE-tabun-HI-6	GLU80@OE	HI-6@N'H"	HI-6@N'	11.40
hBChE-sarin-HI-6	HIS438@O	HI-6@N'H'	HI-6@N'	31.64
hBChE-tabun-HI-6	HI6@O'	HIS126@HE	HIS126@NE2	4.08
hBChE-HI-6	GLU80@OE	HI-6@N'H"	HI-6@N'	46.81
hAChE-tabun-obidoxime	GLU448@OE	OBD@H'	OBD@O'	100
hAChE-obidoxime	GLU80@OE	OBD@H'	OBD@O'	36.14
hBChE-tabun-obidoxime	GLU443@OE	OBD@H"	OBD@O"	100
hBChE-obidoxime	OBD@O'	GLY117@H	GLY117@N	98.64
	GLU197@OE	OBD@H'	OBD@O'	75.96
	GLU443@OE	OBD@H"	OBD@O"	50.92

Where OD = oxygen at δ position, OE = oxygen at ε position, HE = hydrogen at ε position, and OBD = obidoxime.
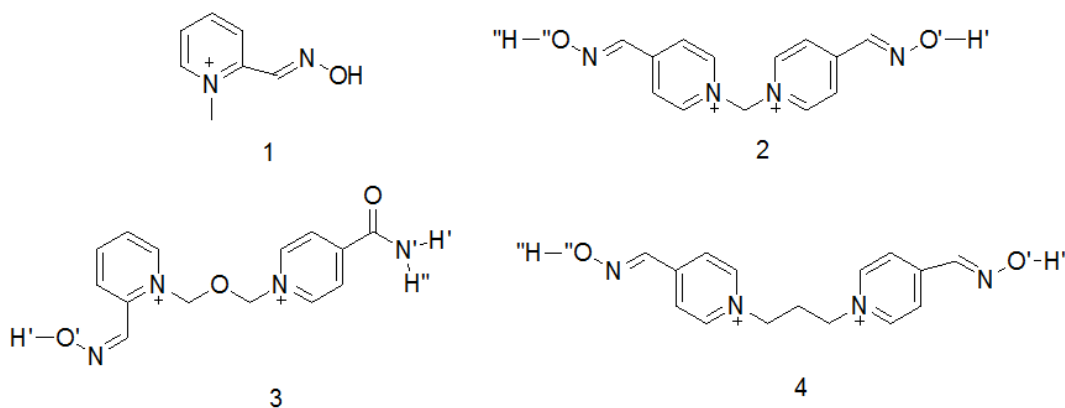
Figure 3.5 Structures of 1) 2-PAM, 2) MMB-4, 3) HI-6, and 4) obidoxime

2-PAM displayed highest percentage of hydrogen bond interaction with Glu448 in hAChE-2-PAM among all the inhibited and uninhibited systems of 2-PAM, a moderate percentage of interactions with Glu441 in hBChE-2-PAM, and with Ala328 in hBChE-tabun-2PAM. In addition, 2-PAM has exhibited a low percentage of interaction with Asp70 in hAChE-tabun-2-PAM and with Glu325 in hBChE-sarin-2-PAM systems. 2-PAM did not display hydrogen bond interactions in hAChE-sarin-2-PAM.

MMB-4 did not exhibit hydrogen bonding in hBChE-sarin-MMB-4 and hBChE-tabun-MMB-4. Similarly, obidoxime did not display hydrogen bonding with the active site residues in hAChE-sarin-obidoxime and hBChE-sarin-obidoxime systems. However, MMB-4 has shown interactions with Glu80 and Glu198 in hAChE-sarin-MMB-4 and with Glu80 in hBChE-MMB-4 system. Among all the reactivators, only obidoxime has shown a 100% hydrogen bond interaction throughout the 5 ns of simulation with Glu448 in hAChE-tabun-obidoxime and with Glu443 in hBChE-tabun-obidoxime.

HI-6 exhibited hydrogen bonding in hAChE-sarin-HI-6, hAChE-tabun-HI-6, and hBChE-tabun-HI-6, and no hydrogen bond formation in hAChE-HI-6. MMB-4 and obidoxime have shown higher percentages of hydrogen bond interaction with various active site residues compared to 2-PAM and HI-6. Glu80 was a common residue which has shown hydrogen bonding interactions with MMB-4, HI-6, and obidoxime.

The reactivators have also displayed π-π interactions with various active site residues. 2-PAM exhibited π-π interactions with Tyr333 and Tyr73 in hAChE-sarin-2-PAM, as shown in Figure 3.6, and with Trp282 in hAChE-tabun-2-PAM. In hAChE-tabun-MMB-4, MMB-4 displayed a π-π interaction with Tyr333 as shown in Figure 3.7. Similarly, MMB-4 also exhibited π-π interactions with Tyr332 in hBChE-sarin-MMB-4

and with Tyr129 in hAChE-MMB-4. HI-6 displayed π-π interactions with Tyr332 and

Tyr440 in hBChE-sarin-HI-6 as shown in Figure 3.8. Obidoxime did not show any π-π

interactions.
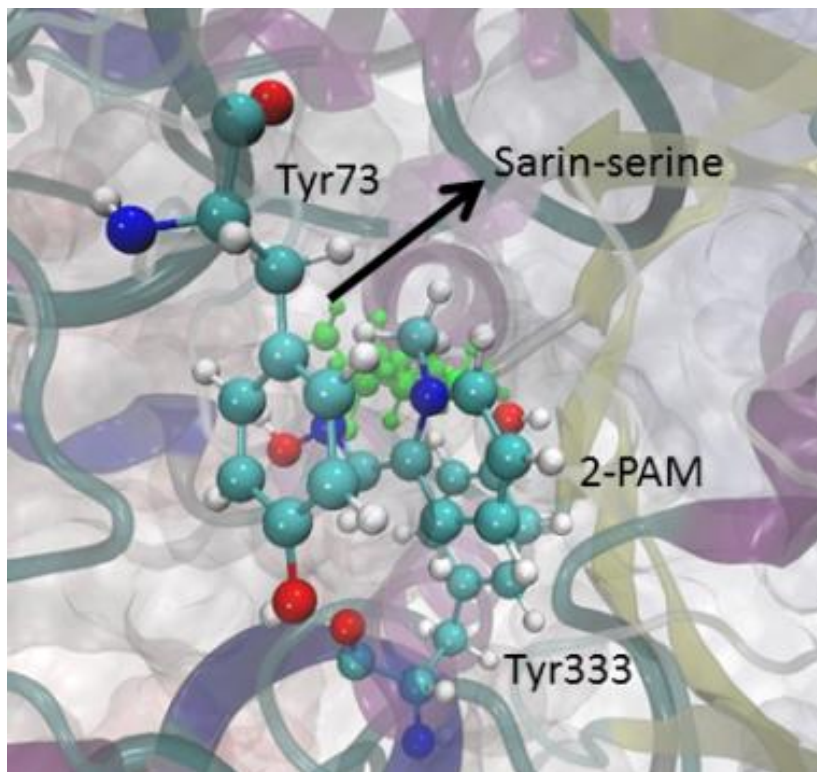
Figure 3.6   2-PAM displaying π-π stacking with Tyr73 and Tyr333 in hAChE-sarin-2-
PAM
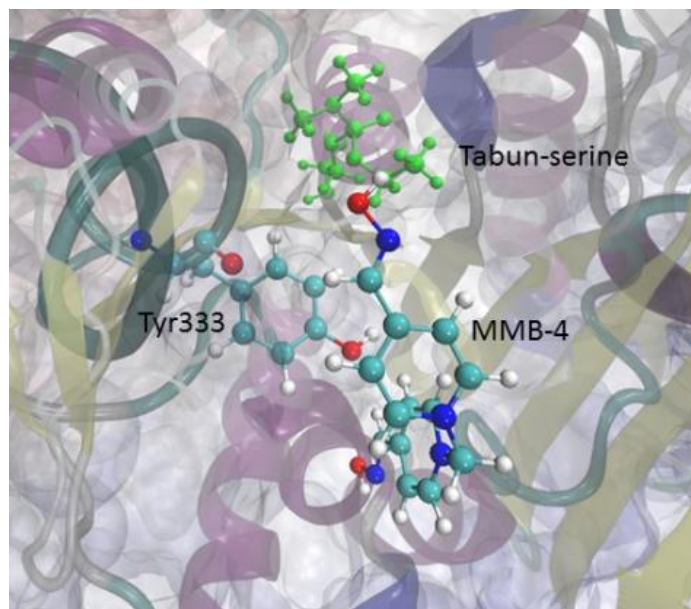
Figure 3.7   MMB-4 displaying π-π stacking with Tyr333 in hAChE-tabun-MMB-4
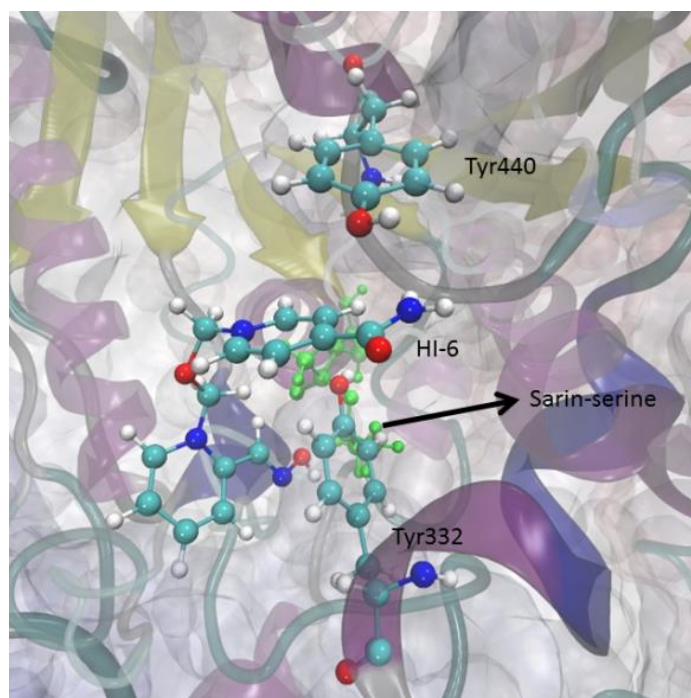
Figure 3.8   HI-6 displaying π- π stacking with Tyr332 and Tyr440 in hBChE-sarin-HI-6

3.2.2   Thermodynamic integration

TI calculations were performed for all the inhibited and uninhibited systems of MMB-4 and obidoxime. For each λ value, the simulation was run until it converged. ΔA was obtained by multiplying the $dV/d\lambda$ term for each λ value with the standard weights provided in the Amber manual. A detailed explanation for calculating ΔA is provided in the Amber tutorial.[263] To verify convergence, $dV/d\lambda$ vs. λ graphs were plotted.   The $dV/d\lambda$ vs. λ plots of the electrostatic and van der Waals simulations for all MMB-4 systems are shown in Figures 3.9 and 3.10. Similarly, the corresponding plots of all obidoxime systems are shown in Figures 3.11 and 3.12. The systems simulated with 0.02544, 0.12923, 0.29707, 0.5, 0.70292, and 0.87076 λ values on average took 20 ns for convergence, whereas for $\lambda = 0.9707$ and 1 they took 8-10 ns to converge. The individual electrostatic and van der Waals contribution and their combined energy values for all MMB-4 and obidoxime systems are tabulated in Table 3.2. The free energy of binding was calculated using Eq. 3.4.
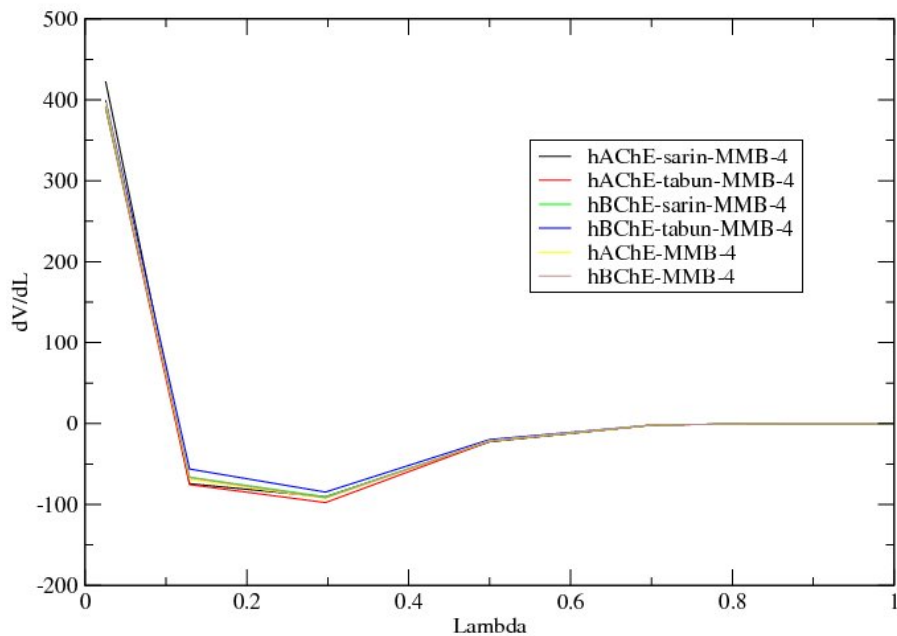
Figure 3.9   dV/dλ vs. λ plot for the electrostatic simulation of the inhibited and uninhibited systems of MMB-4
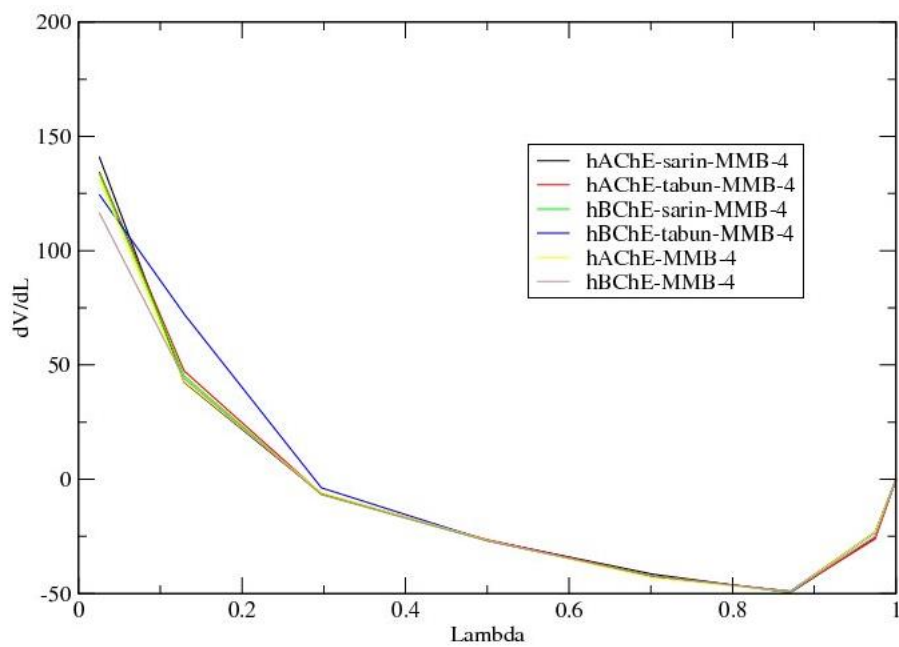
Figure 3.10   dV/dλ vs. λ plot for the van der Waals simulation of the inhibited and uninhibited systems of MMB-4
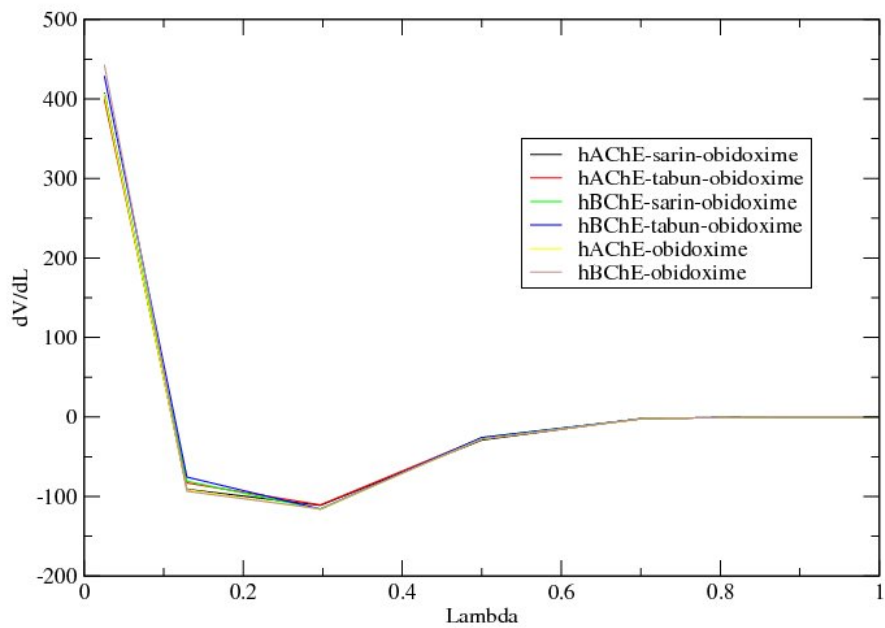
Figure 3.11   dV/dλ vs. λ plot for the electrostatic simulation of the inhibited and
uninhibited systems of obidoxime
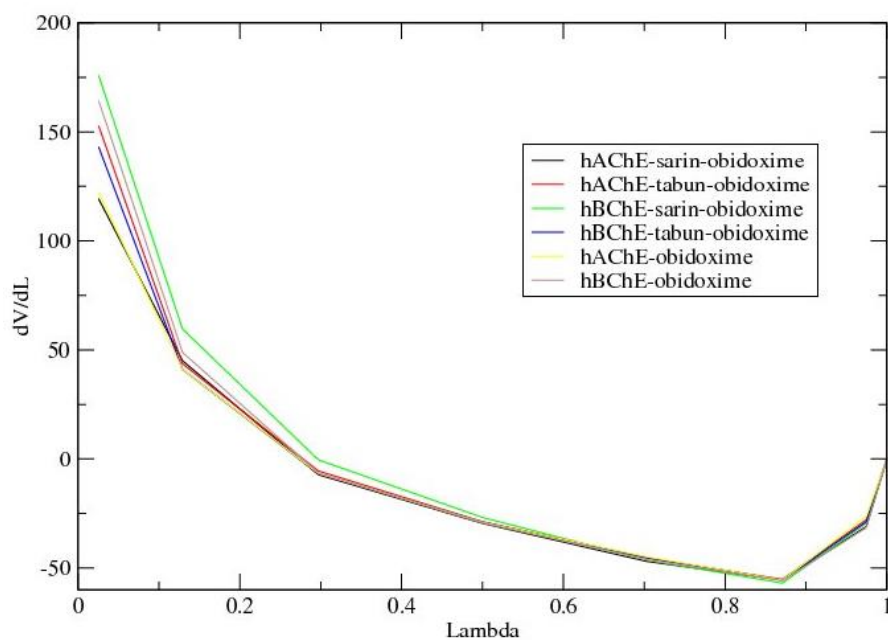
Figure 3.12   dV/dλ vs. λ plot for the van der Waals simulation for the inhibited and
uninhibited systems of obidoxime

61

Table 3.2   Electrostatic, van der Waals, and total energies of inhibited and uninhibited systems of MMB-4 and obidoxime (kcal/mol).

System	Electrostatics	Van der Waals	Total
hAChE-sarin-MMB-4	-5.3	-8.2	-13.5
hAChE-tabun-MMB-4	-9.0	-8.0	-17.0
hAChE-MMB-4	-6.4	-8.8	-15.2
hBChE-sarin-MMB-4	-6.1	-8.4	-14.5
hBChE-tabun-MMB-4	-2.6	-4.7	-7.3
hBChE-MMB-4	-6.2	-9.6	-15.8
hAChE-sarin-obidoxime	-13.9	-12.3	-26.2
hAChE-tabun-obidoxime	-12.8	-9.3	-22.1
hAChE-obidoxime	-14.8	-11.7	-26.5
hBChE-sarin-obidoxime	-13.0	-4.7	-17.7
hBChE-tabun-obidoxime	-10.7	-10.6	-21.3
hBChE-obidoxime	-12.6	-8.6	-21.2
MMB-4	-10.2	-12.6	-22.8
Obidoxime	-18.4	-13.3	-31.7

The calculated binding free energy values were compared with the available experiments. The dissociation constant values (K_d) of oxime reactivation for all the inhibited systems of MMB-4 and obidoxime (except hBChE-tabun-MMB-4) were obtained from the literature.[264-267] While comparing the computational values with the experimental free energies, both must be converted to standard free energies. The experimental K_d values are usually expressed in μM concentration, even though equilibrium constants are unitless. Therefore, the experimental K_d (in μM) values were made unitless, and ΔG^0 (dissociation) was calculated using $-RTln(K_d)$. The binding ΔG^0_{exp} value was obtained by taking $-\Delta G^0$ of dissociation.

In an MD calculation the effective concentration is not 1 M. Therefore, in case of the TI results, while converting the free energy value to a standard free energy, an extra term must be added to Eq. 3.4. If the simulation box sizes of complex, receptor, and

ligand were the same size during the TI calculation, then the following correction is valid.[268,269]

$$\Delta A^o = \Delta A_{TI} - RT ln \left(\frac{V}{V_o} \right), \tag{3.5}$$

where V is the volume of the simulated complex box and V_o is the volume occupied by one ligand (1661 Å^3) at a concentration of 1 M.

During the TI calculations a larger box was used for the complex and receptor than for the oxime (the complex and receptor box sizes are equal). Since the free energy is path independent, we have assumed that the complex and receptor will transform from large boxes to standard boxes containing a volume of V_o, and the oxime from a small box to a standard box, too. The following correction was derived in order to obtain the standard free energy term by modifying the chemical steps 3.2 and 3.3:

$$compex^L (aq) \rightarrow enzyme^L (aq) + oxime (g), \tag{3.6}$$
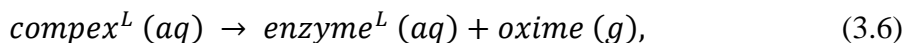
$$\Delta A^o_{complex} = \Delta A_{complex,TI} - RT ln \left(\frac{V_o}{V_c} \right) + RT ln \left(\frac{V_o}{V_r} \right). \tag{3.7}$$

Since the volume of the complex and receptor solvated boxes are equal, i.e. $V_c = V_r$; therefore

$$\Delta A^o_{complex} = \Delta A_{complex,TI} . \tag{3.8}$$

Similarly,

$$oxime^S (aq) \rightarrow oxime (g), \tag{3.9}$$

$$\Delta A^o_{oxime} = \Delta A_{oxime,TI} - RT ln \left(\frac{V_o}{V_s} \right), \tag{3.10}$$

where V_s is the volume of the reactivator solvated box.

Combining Eq.'s 3.8 and 3.10, the standard free energy of binding can be written as

$$\Delta A^o = \Delta A^o{}_{oxime} - \Delta A^o{}_{complex}. \tag{3.11}$$

Therefore,

$$\Delta A^o = \Delta A_{oxime,TI} - \Delta A_{complex,TI} - RTln\left(\frac{V_o}{V_s}\right). \tag{3.12}$$

According to Eq. 3.4, $\Delta A_{TI} = \Delta A_{oxime,\ TI} - \Delta A_{complex,\ TI}$, and hence Eq. 3.12 can be written as

$$\Delta A^o = \Delta A_{TI} - RTln\left(\frac{V_o}{V_s}\right). \tag{3.13}$$

ΔA_{TI}, $RTln(V_o/V_s)$, ΔA^o, $\Delta G^0{}_{exp}$, and the difference between ΔA^0 and $\Delta G^0{}_{exp}$ values for all

inhibited and uninhibited systems of MMB-4 and obidoxime are tabulated in Table 3.3.

Table 3.3 A comparison of calculated free energies (kcal/mol) with experimental values (kcal/mol) for MMB-4 and obidoxime inhibited and uninhibited systems.

System	ΔA_{TI}	$RTln(V_o/V_s)$	ΔA^0	$\Delta G^0{}_{exp}$	$\Delta A^0 - \Delta G^0{}_{exp}$
hAChE-sarin-MMB-4	-9.2	-2.2	-7.0	-3.9[a]	-3.1
hAChE-tabun-MMB-4	-5.8	-2.2	-3.6	-3.6[a]	0
hAChE-MMB-4	-7.6	-2.2	-5.4	--	--
hBChE-sarin-MMB-4	-8.3	-2.2	-6.1	-4.2[b]	-1.9
hBChE-tabun-MMB-4	-15.5	-2.2	-13.3	--	--
hBChE-MMB-4	-6.8	-2.2	-4.6	--	--
hAChE-sarin-obidoxime	-5.4	-2.2	-3.2	-6.2[c]	3.0
hAChE-tabun-obidoxime	-9.6	-2.2	-7.4	-5.1[d]	-2.3
hAChE-obidoxime	-5.1	-2.2	-2.9	--	--
hBChE-sarin-obidoxime	-14.0	-2.2	-11.8	-4.1[b]	-7.7
hBChE-tabun-obidoxime	-10.3	-2.2	-8.1	-4.0[b]	-4.1
hBChE-obidoxime	-10.4	-2.2	-8.2	--	--

a = Ref. 266, b = Ref. 265, c = Ref. 264, and d = Ref. 267

Except for hAChE-tabun-MMB-4, the ΔA^0 values of all the inhibited systems with

MMB-4 were lower than hAChE-MMB-4 and hBChE-MMB-4. The ΔA^o values of all

the inhibited systems with obidoxime were lower than hAChE-obidoxime. Similarly,

among all the inhibited systems of obidoxime, only the ΔA^o value of hBChE-tabun-obidoxime was lower than hBChE-obidoxime. Based on the ΔA^o values, MMB-4 binds more efficiently than obidoxime to hAChE-sarin and hBChE-tabun systems. The obidoxime binds more effectively to hAChE-tabun and hBChE-sarin systems compared to MMB-4. In case of uninhibited systems, MMB-4 displayed the lowest binding energy for hAChE and obidoxime for hBChE.

The computational and experimental standard free energy values of hAChE-tabun-MMB-4 are equal. The differences between the calculated and experimental free energies for hAChE-sarin-MMB-4, hBChE-sarin-MMB-4, hAChE-tabun-obidoxime, and hBChE-tabun-obidoxime are within 4.2 kcal/mol. For hAChE-sarin-obidoxime, the experimental value was lower than TI's value by 3 kcal/mol. The accuracy of the estimated ΔA^o values for all the inhibited systems of MMB-4 and obidoxime can be considered to be at the ff99 forcefield limit. Usually, the binding free energies calculated using TI or FEP will be closer to the experimental values (within 1-2 kcal/mol).[270-273] However, in our studies, most of the calculated ΔA^o values lie outside that range.

This can be a forcefield issue, as there are some known problems with the ff99 forcefield. During longer simulations (some 10's of ns), the ff99 forcefield over-stabilizes the conformations of *alpha*-helical regions, and hence, it may structurally or energtically affect the secondary structure of a protein.[274] These issues were later addressed by introducing the ff99SB forcefield.[274] Therefore, we have chosen the ff99SB forcefield for the PON1 studies discussed later. Out of all the inhibited systems of MMB-4 and obidoxime, a large energy difference (-7.7 kcal/mol) was observed only in hBChE-sarin-obidoxime. Apart from the forcefield limitation, this difference may also

arise due to the errors in the experiment. Therefore, we suggest that the related experiments for hBChE-sarin-obidoxime system be reconsidered.

The free energy of binding calculated using TI or FEP methods are incredibly expensive and time consuming. For each system (inhibited or uninhibited systems of MMB-4 or obidoxime), the electrostatic and van der Waals contributions were individually calculated using a seven point numerical integration, and for each numerical integration point a 10 to 20 ns simulation was performed. A total of 7×2 numerical integration points (electrostatic + van der Waals) was performed for each individual system. All the TI calculations were performed at the High Performance Computing Collaboratory at Mississippi State University. We had an access to a total of 60 processors.

For a given numerical point, it took one day to perform a 1 ns simulation using 4 processors. So, ideally it takes 20 days to perform a 20 ns simulation for each numerical integral of a system. By running parallel jobs (*i.e.* using 4 processors, a 1 ns simulation was performed for each numerical point, and hence a total of 56 processors were used to achieve a 1 ns simulation for 14 numerical points of a system in 1 day) a 20 ns simulation for all numerical integration points of a system can be achieved in 20 days. The TI calculations were performed for 12 different systems (4 inhibited and 2 inhibited systems of MMB-4 and obidoxime), and thereby it takes 240 days of wall clock time to complete all the calculations. However, it took two years to successfully finish all the desired simulations.

CHAPTER IV

BINDING FREE ENERGIES OF OXIMES CALCULATED USING SOLVENT

CONTINUUM MODELS AND NORMAL MODE ANALYSES

As mentioned earlier, the protein-ligand binding free energies calculated using

FEP or TI methods are computationally expensive and time consuming. Therefore, we

could not perform TI calculations for inhibited and uninhibited systems of 2-PAM and

HI-6. Hence, the continuum solvent models were explored, which are computationally

much less expensive than TI. The binding enthalpies (ΔH) were calculated using

Molecular Mechanics Generalized Born Surface Area (MM-GBSA) and Molecular

Mechanics Poisson-Boltzmann Surface Area (MM-PBSA) methods, and the $T\Delta S$

contributions were evaluated using normal mode analyses. The binding free energies

were estimated using the above mentioned methods for inhibited and uninhibited systems

with 2-PAM, MMB-4, HI-6, and obidoxime. Finally, the calculated binding free energy

values for all MMB-4 and obidoxime systems were compared with the TI results.

4.1   Computational methods

The ΔH values and normal mode analyses were calculated with the *MMPBSA.py*

script using AmberTools1.5[275] and the ff99 forcefield.[249] For the solvation energy the

electrostatic and hydrophobic interactions were calculated separately. The electrostatic

interactions are estimated by using Poisson-Boltzmann or Generalized Born equations,

and the hydrophobic interactions are calculated using solvent-accessible-surface-area-dependent terms.[276]

For each system, the last 5 ns of the explicit solvent sampling process was considered, and a total of 250 snapshots were generated, *i.e.*, one snapshot for every 20 ps. The *MMPBSA.py* script automatically identifies the corresponding residues of complex, receptor, and ligand within a given complex system. An individual enthalpy value was calculated for each of them (complex, receptor, and ligand). Finally, ΔH is determined using the following equation.

$$\Delta H = H_{complex} - H_{receptor} - H_{ligand}. \qquad (4.1)$$

The ΔH calculated using the *MMPBSA.py* script is a sum of the internal energy ($\Delta E_{forcefield}$) and the free energy of solvation ($\Delta G_{solv} = \Delta G_{elec} + \Delta G_{vdw} + \Delta G_{cavity}$), as shown in Eq.'s 2.45-2.47. Since the calculated value includes entropic terms such as cavity formation and hydrophobic effects observed during solute-solvent interactions, the obtained value (ΔH) is not exactly a binding enthalpy. In the computational community the sum of $\Delta E_{forcefield}$ and ΔG_{solv} is commonly referred as ΔH. The calculated ΔH values cannot be compared with the experimental binding enthalpies, measured using isothermal calorimetric titrations. The ΔS of $T\Delta S$ term calculated using normal mode analysis specifically refers to only the change in the entropy of the substrate and receptor as they bind. The majority of the protein-ligand binding entropic effects are included in the ΔH term.

The normal mode analysis is memory intensive and time consuming. Hence, initially, the $T\Delta S$ values were calculated using 10, 15, 20, and 25 snapshots for various

68

systems. In the tested systems, the calculated $T\Delta S$ values using 15, 20, and 25 snapshots were within ±1 kcal/mol of the value obtained using 10 snapshots. So, given the number of systems, we decided to use 10 snapshots for each system. Again, the last 5 ns of the explicit solvent sampling process were considered for the analysis. During the entropy evaluation ($T\Delta S$), all systems were initially minimized until the root mean square of the gradient vector was less than 0.0009 kcal/mol/Å. Finally, the average $T\Delta S$ value was calculated using all generated snapshots.

4.2   Results and discussions

4.2.1   Binding enthalpy calculations

The binding enthalpies values (ΔH_{GBSA} and ΔH_{PBSA}) and free energy values (ΔG_{GBSA} and ΔG_{GBSA}) for the inhibited and uninhibited systems of 2-PAM, MMB-4, HI-6, and obidoxime are tabulated in Table 4.1. ΔH_{GBSA} values of all the inhibited systems of 2-PAM (except hAChE-tabun-2-PAM) were lower than the corresponding values for the uninhibited systems, whereas only the ΔH_{PBSA} values of hAChE-sarin-2-PAM and hBChE-sarin-2-PAM were lower than hAChE-2-PAM and hBChE-2-PAM.

Table 4.1   Binding enthalpies (kcal/mol), $T\Delta S$ values (kcal/mol), and calculated free energies (kcal/mol) of 2-PAM, MMB-4, HI-6, and obidoxime systems.

System	ΔH_{GBSA}	ΔH_{PBSA}	$T\Delta S$	ΔG_{GBSA}	ΔG_{PBSA}
hAChE-sarin-2-PAM	-14.1 ± 1.6	-13.5 ± 2.3	-13.9 ± 5.3	-0.2	0.4
hAChE-tabun-2-PAM	-2.8 ± 1.7	-4.3 ± 2.0	-13.2 ± 1.4	10.4	8.9
hAChE-2-PAM	-8.4 ± 1.6	-10.1 ± 2.2	-20.1 ± 7.7	11.7	10.0
hBChE-sarin-2-PAM	-17.5 ± 2.7	-13.7 ± 5.1	-13.3 ± 5.1	-4.2	-0.4
hBChE-tabun-2-PAM	-8.7 ± 1.6	-5.4 ± 3.4	-14.3 ± 3.5	5.6	8.9
hBChE-2-PAM	-8.4 ± 2.2	-10.6 ± 3.3	-13.3 ± 6.6	4.9	2.7
hAChE-sarin-MMB-4	-11.8 ± 2.3	-19.3 ± 3.1	-19.6 ± 4.2	7.7	0.3
hAChE-tabun-MMB-4	-14.7 ± 2.5	-11.5 ± 4.0	-20.4 ± 5.5	5.7	8.9
hAChE-MMB-4	-14.1 ± 2.0	-8.6 ± 4.8	-18.4 ± 4.1	4.3	9.9
hBChE-sarin-MMB-4	254.7 ± 6.7	5.4 ± 7.4	-19.5 ± 7.2	274.1	24.9
hBChE-tabun-MMB-4	-21.2 ± 2.6	-14.7 ± 3.9	-21.2 ± 2.7	0.0	6.6
hBChE-MMB-4	-11.7 ± 1.8	-19.5 ± 2.6	-22.4 ± 5.0	10.7	2.9
hAChE-sarin-HI-6	-11.2 ± 1.8	-15.4 ± 2.3	-10.6 ± 6.8	-0.6	-4.8
hAChE-tabun-HI-6	-9.5 ± 3.1	-13.9 ± 4.1	-17.8 ± 7.2	8.3	3.9
hAChE-HI-6	-22.3 ± 3.3	-24.2 ± 3.7	-25.4 ± 6.4	3.1	1.2
hBChE-sarin-HI-6	-18.0 ± 2.3	-20.9 ± 3.5	-23.8 ± 4.5	5.7	2.9
hBChE-tabun-HI-6	-15.3 ± 4.1	-13.5 ± 4.5	-25.9 ± 7.4	10.7	12.4
hBChE-HI-6	-15.4 ± 3.6	-14.8 ± 5.6	-18.1 ± 10.5	2.7	3.3
hAChE-sarin-obidoxime	-19.9 ± 2.2	-19.8 ± 4.3	-19.9 ± 6.1	0.0	0.1
hAChE-tabun-obidoxime	-15.4 ± 2.4	-20.5 ± 2.9	-18.9 ± 5.9	3.5	-1.6
hAChE-obidoxime	-3.5 ± 2.1	-9.8 ± 3.4	-18.7 ± 7.4	15.2	8.9
hBChE-sarin-obidoxime	266.7 ± 85.7	14.8 ± 8.9	-21.2 ± 9.5	287.9	36.0
hBChE-tabun-obidoxime	-23.2 ± 2.9	-24.9 ± 4.5	-25.5 ± 5.6	2.4	0.6
hBChE-obidoxime	-20.6 ± 2.5	-25.3 ± 3.9	-13.5 ± 9.1	-7.1	-11.8

The ΔH_{GBSA} values of hAChE-sarin-MMB-4, hAChE-tabun-MMB-4, and hBChE-tabun-MMB-4 were lower than hBChE-MMB-4. Similarly, the ΔH_{PBSA} values of all the inhibited systems of MMB-4 (except hBChE-sarin-MMB-4) were lower than hAChE-MMB-4. However, the ΔH_{PBSA} of all inhibited systems of MMB-4 were higher than the hBChE-MMB-4 value.

In the case of HI-6, only the hBChE-sarin-HI-6 system's ΔH_{GBSA} value was lower than the hBChE-HI-6 value. The ΔH_{PBSA} values of hAChE-sarin-HI-6 and hBChE-sarin-HI-6 were lower than hBChE-HI-6. Both ΔH_{GBSA} and ΔH_{PBSA} values of hAChE-HI-6 were lower compared to all inhibited systems of HI-6. The ΔH_{GBSA} and ΔH_{PBSA} values of hAChE-sarin-obidoxime, hAChE-tabun-obidoxime, and hBChE-tabun-obidoxime were

lower than hAChE-obidoxime. A common trend was not observed among the inhibited and uninhibited systems of the reactivators.

The ΔH values of inhibited and uninhibited systems of MMB-4 and obidoxime were lower than the corresponding TI ΔA^0 values. Overall, the ΔH values were negative except for hBChE-sarin-MMB-4 and hBChE-sarin-obidoxime. To check the accuracy of the simulations, the ΔH values for these systems were also calculated using a three trajectory method. Initially, the hBChE-sarin (receptor) was minimized, heated, equilibrated, and sampled for 10 ns using an explicit solvent simulation as described earlier. Later, the receptor's enthalpy was calculated using MM-GBSA and MM-PBSA with 250 snapshots (using last 5 ns of the sampling process). Similarly, ΔH for hBChE-sarin-MMB-4, hBChE-sarin-obidoxime, MMB-4, and obidoxime were individually calculated. Using Eq. 4.1, the ΔH values were calculated for hBChE-sarin-MMB-4 and hBChE-sarin-obidoxime. The binding enthalpies values were again positive. Hence, these two systems appear to be problem cases for GBSA and PBSA calculations.

4.2.2   Normal mode analysis

The free energies of binding were calculated using

$$\Delta G_{GBSA/PBSA} = \Delta H_{GBSA/PBSA} - T\Delta S. \qquad (4.2)$$

The $T\Delta S$ values were mostly equal to or lower than the respective ΔH_{GBSA} and ΔH_{PBSA} values. As a result, the calculated free energies of binding, *i.e.,* ΔG_{GBSA} and ΔG_{PBSA}, were positive, except for hBChE-sarin-2-PAM, hAChE-sarin-HI-6, and hBChE-obidoxime, as shown in Table 4.1. Similarly, ΔG_{GBSA} for hAChE-sarin-2-PAM and ΔG_{PBSA} for hAChE-tabun-obidoxime were also negative.   The ΔA^0 and calculated free

energies of binding (ΔG_{GBSA} and ΔG_{PBSA}) for MMB-4 and obidoxime systems are

tabulated in Table 4.2. Only the $\Delta G_{GBSA/PBSA}$ values of hBChE-obidoxime were

comparable with TI values.

Table 4.2   Comparison of free energies (kcal/mol) calculated using thermodynamic integration, GBSA, and PBSA for all systems of MMB-4 and obidoxime.

System	ΔA^0	ΔG_{GBSA}	ΔG_{PBSA}
hAChE-sarin-MMB-4	-7.0	7.7	0.3
hAChE-tabun-MMB-4	-3.6	5.7	8.9
hAChE-MMB-4	-5.4	4.3	9.9
hBChE-sarin-MMB-4	-6.1	274.1	24.9
hBChE-tabun-MMB-4	-13.3	0	6.6
hBChE-MMB-4	-4.6	10.7	2.9
hAChE-sarin-obidoxime	-3.2	0	0.1
hAChE-tabun-obidoxime	-7.4	3.5	-1.6
hAChE-obidoxime	-2.9	15.2	8.9
hBChE-sarin-obidoxime	-11.8	287.9	36.0
hBChE-tabun-obidoxime	-8.1	2.4	0.6
hBChE-obidoxime	-8.2	-7.03	-11.8

One of the major challenges with the present MD simulations is to accurately

calculate protein-ligand entropies of binding.[277] The normal mode analysis treats various

modes of a protein using the harmonic oscillator approximation. Usually, the low

frequency modes correspond to large motions of a biological system, and these motions

are not well described using the harmonic oscillator approximation. Hence, the entropy

contribution with respect to these modes must be approximately calculated. The entropy

of vibration is calculated using Eq. 2.56. The second term in the summation plays an

important role in estimating the S_{vib} value. As υ approaches zero, *i.e.* low frequency, the

exponential term becomes unity, the logarithm term goes to negative infinity, and S_{vib}

becomes positive infinity. On the other hand as $\upsilon \rightarrow 0$, the first term goes to 1. So, there

exists a fundamental problem for calculating the vibrational entropy for low frequency modes.

While performing the normal mode analysis, in all the snapshots of inhibited or uninihibited systems of 2-PAM, obidoxime, HI-6, and MMB-4 the vibrational frequencies less than 10 cm^{-1} were observed. For example in one of the snapshot of hAChE-sarin-MMB-4 a few low frequencies, *i.e.* 1.826 cm^{-1}, 2.222 cm^{-1}, 3.337 cm^{-1}, 3.480 cm^{-1}, 3.613 cm^{-1}, *etc*. were observed. If the algorithm makes a slight error in calculating the vibrational entropies with respect to these low frequencies, the S_{vib} term blows up due to reason explained earlier. Therefore, we believe that the present algorithms cannot effectively estimate the vibrational entropies due to this reason. As a result, the calculated $T\Delta S$ values are lower than or equal in magnitude to the ΔH values in our systems. In general, the normal mode analysis is performed to explore the large motions or conformational changes of a biomolecule.[278]

The reactivators MMB-4, HI-6, and obidoxime are structurally similar. Hence, we have assumed that these oximes can have a similar change in a binding entropy value ($T\varDelta S$) when they bind to hAChE or hBChE. So, using the presumably accurate TI ΔA^0 results and the binding ΔH values calculated with MM-GBSA and MM-PBSA, the $T\Delta S$ values were estimated for the MMB-4 and obidoxime systems. The hBChE-sarin-MMB-4 and hBChE-sarin-obidoxime systems were excluded, as their ΔH values were positive. The $T\Delta S$ values were estimated using Eq. 4.3 and the corresponding ΔS values are tabulated in Table 4.3,

$$T\Delta S_{GBSA/PBSA} = \Delta H_{GBSA/PBSA} - \Delta A^o. \qquad (4.3)$$

Table 4.3 ΔS values of MMB-4 and obidoxime systems (cal mol^{-1} K^{-1})

System	ΔS_{GBSA}	ΔS_{PBSA}
hAChE-sarin-MMB-4	- 16.0	- 40.7
hAChE-tabun-MMB-4	- 37.0	- 26.3
hAChE-MMB-4	- 29.0	- 10.3
hBChE-tabun-MMB-4	- 26.3	- 4.3
hBChE-MMB-4	- 23.7	- 50.0
hAChE-sarin-obidoxime	- 55.7	- 55.3
hAChE-tabun-obidoxime	- 26.7	- 43.7
hAChE-obidoxime	- 2.0	- 23.0
hBChE-tabun-obidoxime	- 50.3	- 56.3
hBChE-obidoxime	- 41.3	- 57.0

The average ΔS value calculated using ΔS_{GBSA} values was –30.8 cal mol^{-1}K^{-1}. The ΔS_{PBSA} value was -36.7 cal mol^{-1} K^{-1}. The average ΔS values were used to estimate free energies ($\Delta G_{GBSA/PBSA}$) using Eq. 4.4 for MMB-4 and obidoxime systems (except hBChE-sarin-MMB-4 and hBChE-sarin-obidoxime). ΔA^0 and estimated ΔG_{GBSA} and ΔG_{PBSA} values for MMB-4 and obidoxime systems are tabulated in Table 4.4,

$$\Delta G_{estimated} = \Delta H_{GBSA/PBSA} - T\Delta S_{average}. \qquad (4.4)$$

The estimated ΔG_{GBSA} and ΔG_{PBSA} for hAChE-obidoxime and ΔG_{PBSA} of hAChE-MMB-4 were positive. The ΔG_{GBSA} values for all MMB-4 systems were higher than their corresponding ΔA^0, and ΔG_{PBSA} were also higher except for hBChE-MMB-4. On the other hand, ΔG_{GBSA} and ΔG_{PBSA} of hBChE-tabun-obidoxime and hBChE-obidoxime, and ΔG_{GBSA} of hAChE-sarin-obidoxime were lower than ΔA^0.

Table 4.4 A comparison of free energies of binding (kcal/mol) calculated using ΔA^0 and estimated free energies ($\Delta G_{GBSA/PBSA}$) for MMB-4 and obidoxime systems (kcal/mol).

System	ΔA^0	ΔG_{GBSA}	ΔG_{PBSA}
hAChE-sarin-MMB-4	-9.2	-2.6	-8.3
hAChE-tabun-MMB-4	-5.8	-5.5	-0.5
hAChE-MMB-4	-7.6	-4.9	2.4
hBChE-tabun-MMB-4	-15.5	-12.0	-3.7
hBChE-MMB-4	-6.8	-2.5	-8.5
hAChE-sarin-obidoxime	-5.4	-10.7	-8.8
hAChE-tabun-obidoxime	-9.6	-6.2	-9.5
hAChE-obidoxime	-5.1	5.7	1.2
hBChE-tabun-obidoxime	-10.3	-14.0	-13.9
hBChE-obidoxime	-10.4	-11.4	-14.3

ΔG_{GBSA} and ΔG_{PBSA} are the estimated free energies using Eq. 4.4.

The free energies for all HI-6 systems were estimated using Eq. 4.4 and are tabulated in Table 4.5. The estimated free energies ($\Delta G_{GBSA/PBSA}$) were negative for all the inhibited and uninhibited systems of HI-6. The estimated $\Delta G_{GBSA/PBSA}$ values for hAChE-sarin-HI-6 were higher than ΔG_{exp}. Whereas, the estimated free energies (GBSA/PBSA) for hBChE-sarin-HI-6 were lower than their corresponding experimental values.

Further, $\Delta G_{GBSA/PBSA}$ was also estimated for all 2-PAM systems as shown in Table 4.5. The $\Delta G_{GBSA/PBSA}$ values for hAChE-sarin-2-PAM and hBChE-sarin-2-PAM were negative. For the remaining 2-PAM systems the estimated free energies were positive. The estimated $\Delta G_{GBSA/PBSA}$ values for hAChE-sarin-2-PAM and ΔG_{PBSA} for hBChE-sarin-2-PAM were higher than the experimental free energies. 2-PAM is not structurally similar to MMB-4, HI-6, and obidoxime. However, the free energies determined using Eq. 4.4 for all 2-PAM systems are our best estimates, better than the ones that were previously calculated using Eq. 4.2.

Table 4.5   A comparison of estimated free energies $\Delta G_{GBSA/PBSA}$ (kcal/mol) with the experimental free energies (kcal/mol) for HI-6 and 2-PAM systems.

System	GBSA $\Delta G_{estimated}$	PBSA $\Delta G_{estimated}$	ΔG_{exp}
hAChE-sarin-HI-6	-2.0	-4.4	-5.9[a]
hAChE-tabun-HI-6	-0.3	-2.9	--
hAChE-HI-6	-13.1	-13.2	--
hBChE-sarin-HI-6	-8.8	-9.9	-3.6[b]
hBChE-tabun-HI-6	-6.1	-2.5	--
hBChE-HI-6	-6.2	-3.8	--
hAChE-sarin-2-PAM	-4.9	-2.5	-6.3[a]
hAChE-tabun-2-PAM	6.4	6.7	-4.4[c]
hAChE-2-PAM	0.8	0.9	--
hBChE-sarin-2-PAM	-8.3	-2.7	-4.5[b]
hBChE-tabun-2-PAM	0.5	5.6	--
hBChE-2-PAM	0.8	0.4	--

a = Ref. 264, b = Ref. 265, and c = Ref. 84

The root mean square (RMS) error of ΔA^0_{TI}, $\Delta G_{calculated}$ (using Eq. 4.2), and $\Delta G_{estimated}$ for the inhibited systems of MMB-4, obidoxime, HI-6, and 2-PAM were calculated with respect to the experimental free energies and are tabulated in Table 4.6. ΔA^0_{TI} RMS error for MMB-4 systems was lower than that of the obidoxime's. The RMS error of estimated ΔG_{GBSA} was lower than the ΔG_{PBSA} value the for MMB-4 systems. On the other hand, the RMS errors of estimated $\Delta G_{GBSA/PBSA}$ were equal for the obidoxime and HI-6 systems. In the case of the HI-6 and 2-PAM systems, the RMS errors for $\Delta G_{estimated}$ were lower than for $\Delta G_{calculated}$.

Table 4.6   Root mean square error of ΔA^0_{TI}, $\Delta G_{calculated}$, and $\Delta G_{estimated}$ values for the inhibited systems of MMB-4, obidoxime, HI-6 and 2-PAM (kcal/mol).

Reactivator	ΔA^0_{TI}	$\Delta G_{calculated}$		$\Delta G_{estimated}$	
		GBSA	PBSA	GBSA	PBSA
MMB-4	2.1	160.9	18.4	1.6	3.8
Obidoxime	4.8	146.1	20.5	6.4	6.4
HI-6		7.6	4.7	4.6	4.6
2-PAM		9.2	8.9	6.7	6.9

$\Delta G_{calculated}$ values are calculated using Eq. 4.2

4.2.3   MM-GBSA per-residue contribution

One of the advantages of the MM-GBSA calculation is that the binding enthalpy can be decomposed into per-residue contributions. The decomposition analysis can be used to identify the residues that display favorable or unfavorable interactions with the reactivators. The per-residue decomposition analyses for 2-PAM, MMB-4, HI-6, and obidoxime inhibited and uninhibited systems are tabulated in Table 4.7. The decomposition analysis was not performed for hBChE-sarin-MMB-4 and hBChE-sarin-obidoxime systems, as their corresponding ΔH_{GBSA} values were unphysical.

Table 4.7   Per-residue decomposition analyses of inhibited and uninhibited systems of 2PAM, MMB-4, HI-6, and obidoxime.

System	Favorable residues	Unfavorable residues
hAChE-sarin-2PAM	Tyr73, Tyr333	
hAChE-tabun-2PAM	Trp282	
hAChE-2PAM	Glu448	
hBChE-sarin-2PAM	Trp231, Phe398	
hBChE-tabun-2PAM	Trp430	
hBChE-2PAM	Glu197, Met81	
hAChE-sarin-MMB-4	Glu80, Met81, Glu198	Arg459
hAChE-tabun-MMB-4	Glu448	Arg429
hAChE-MMB-4	Glu448	Arg459
hBChE-tabun-MMB-4	Met81, Trp82, Glu198	Lys131
hBChE-MMB-4	Glu197, Met81, Glu80	Arg424, Lys427
hAChE-sarin-HI-6	Met81	Arg429
hAChE-tabun-HI-6	Met81	Arg459
hAChE-HI-6	Glu448, His443, Ser199	Arg459
hBChE-sarin-HI-6	Tyr332, His438, Thr120, Tyr440	Lys427
hBChE-tabun-HI-6	Met81, Trp82	Lys323
hBChE-HI-6	Met81	Arg424, Lys427
hAChE-sarin-obidoxime	Tyr129, Glu198	Arg459
hAChE-tabun-obidoxime	Glu448, Met81	Arg459, Arg429
hAChE-obidoxime	Glu80	Arg459
hBChE-tabun-obidoxime	Glu443, Trp82, Met81	Lys131
hBChE-obidoxime	Glu197	Arg424, Lys427

The residues whose enthalpy values are greater than 0.3 kcal/mol are listed under the unfavorable category and those less than -1.5 kcal/mol as favorable interactions. In

the case of 2-PAM systems, the residues which have displayed unfavorable interactions with the reactivator did not fall within the considered range. Therefore, only residues which have displayed favorable interactions are reported in Table 4.7.

In all the systems a lysine or arginine displayed an unfavorable interaction with the oxime. The reactivators, lysine, and arginine are all positively charged and therefore repel each other. The residues under the favorable interactions category interacted with the reactivators in the form of hydrogen bonds, van der Waals interactions, or π-π interactions. Hence, these residues are within the vicinity of the active site. The residues which have shown unfavorable interactions can be from any part of the protein. The residues which have exhibited favorable and unfavorable interactions with the reactivator in hAChE-sarin-2-PAM, hAChE-sarin-MMB-4, hAChE-sarin-HI-6, and hAChE-sarin-obidoxime are shown in Figures 4.1, 4.2, 4.3, and 4.4.

It was observed that 2-PAM, MMB-4, HI-6, and obidoxime have commonly exhibited favorable interactions with Met81 and unfavorable interaction with Arg459. A strong electrostatic interaction between Met81 and the reactivator was observed in many systems. The S of the Met81 and one of the pyridinium rings of the reactivator had strong electrostatic interactions, as shown in Figure 4.5.

Figure 4.1   2-PAM displaying favorable and unfavorable interactions with various residues of hAChE-sarin-2-PAM

Figure 4.2   MMB-4 displaying favorable and unfavorable interactions with various residues of hAChE-sarin-MMB-4
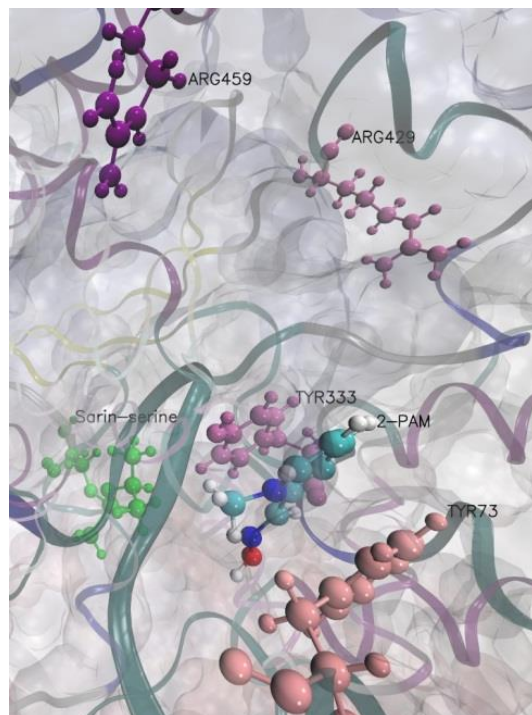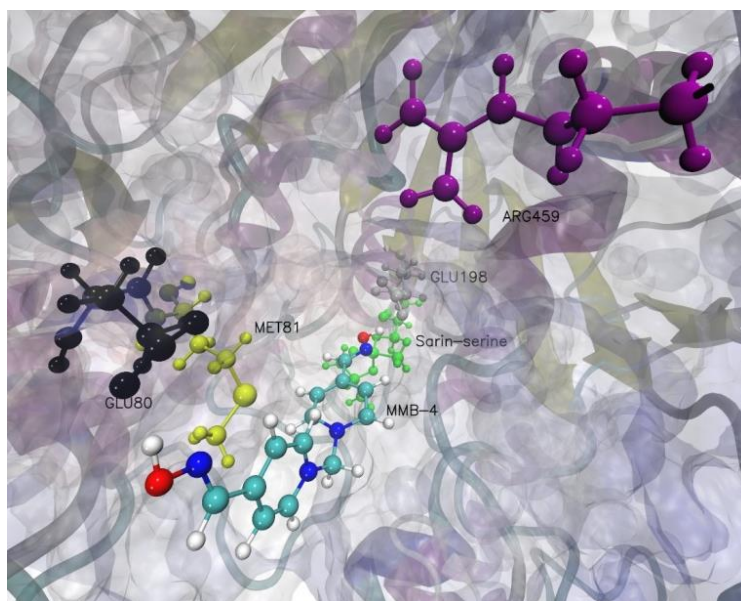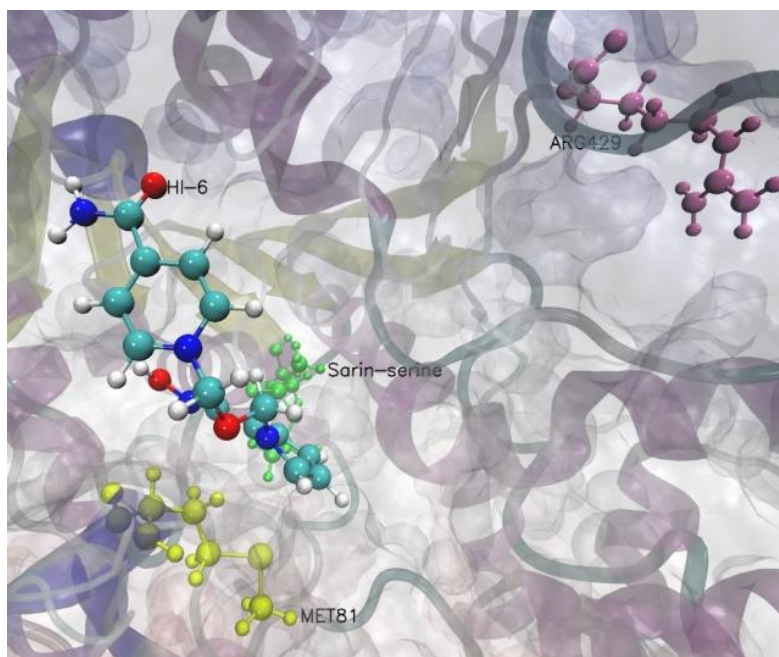
Figure 4.3   HI-6 displaying favorable and unfavorable interactions with various residues of hAChE-sarin-HI-6
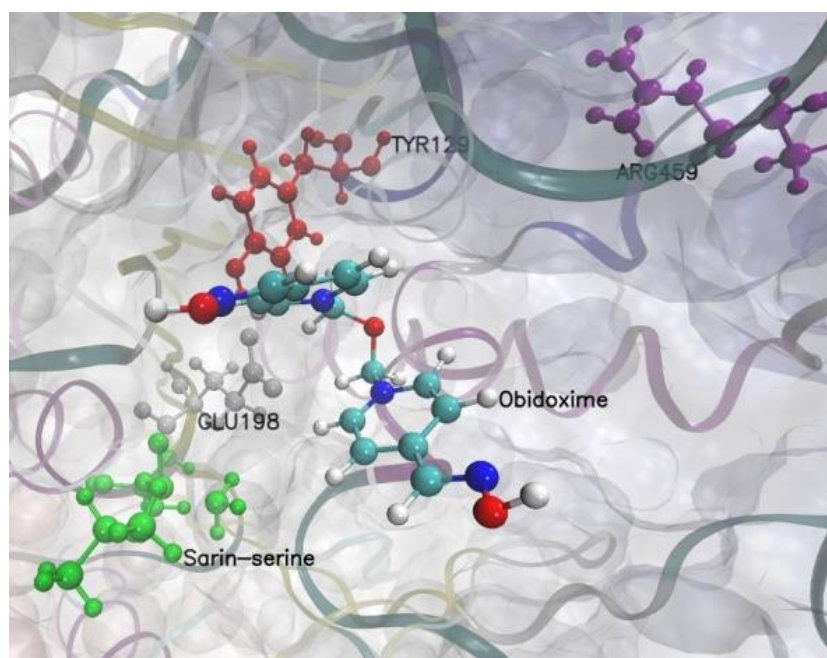
Figure 4.4   Obidoxime displaying favorable and unfavorable interactions with various residues of hAChE-sarin-obidoxime
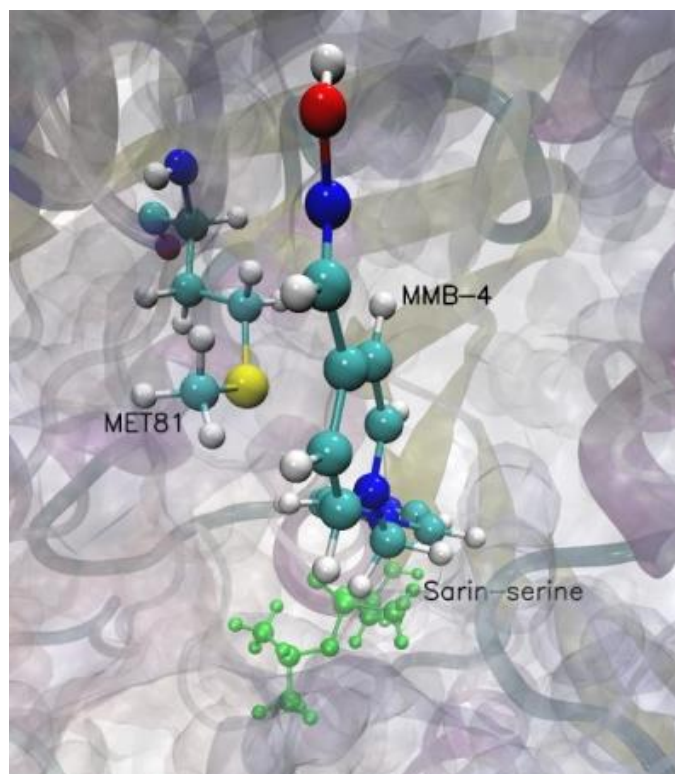
Figure 4.5   The electrostatic interaction between the S atom of Met81 and the pyridinium ring of MMB-4 in hAChE-sarin-MMB-4

CHAPTER V

DOCKING STUDIES OF HUMAN PARAOXONASE1

Some research groups have recently analyzed (experimentally and computationally) the mechanism by which an organophosphate gets hydrolyzed in the active site of PON1.[123,128,137] These studies were done using the crystal structure of rePON1. A hydroxide ion (formed from a water molecule) was taken as the nucleophile to explore various organophosphate hydrolysis mechanisms. The main goal of this project was to identify a stronger nucleophile than water to enhance the hydrolysis of organophosphates present in the active site of human PON1 (hPON1). This work was done in collaboration with Dr. Janice Chambers' group (Department of Basic Science, College of Veterinary Medicine at Mississippi State University) and Dr. Howard W. Chambers' group (Department of Biochemistry, Molecular Biology, Entomology, and Plant Pathology at Mississippi State University).

Dr. Howard Chambers' group has synthesized surrogates of sarin (3, 5, 6-trichloro-2-pyrindinyl isopropyl methylphosphonate (TIMP) and 4-nitrophenyl isopropyl methylphosphonate (NIMP)) and VX (3, 5, 6-trichloro-2-pyridinyl ethyl methylphosphonate (TEMP) and 4-nitrophenyl ethyl methylphosphonate (NEMP)) as shown in Figure 5.1. The experimentally synthesized compounds and chloropyrifos-oxon (Cpo) are structurally similar and since Cpo is a known good substrate for hPON1, we were interested in exploring the binding affinities and interactions of Cpo with various

oximes. This analysis will be helpful to understand the interactions between an organophosphate and an oxime present in the active site of hPON1.
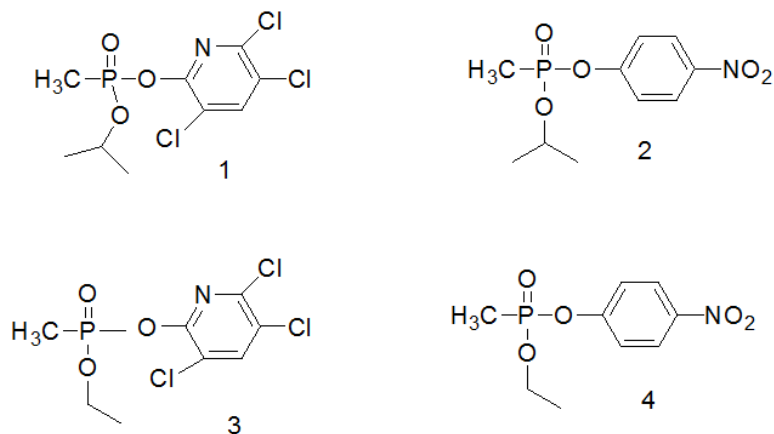
Figure 5.1   Structures of 1) TIMP, 2) NIMP, 3) TEMP, and 4) NEMP

Since the crystal structure of hPON1 was unavailable, we have built 3D structures of Q192 and R192 forms of hPON1. The docking studies were performed using the modeled hPON1 structures, Cpo, and various oximes.

5.2   Computational details

The primary sequence of hPON1 was taken from the UniportKB/Swiss-Port server[279] and was submitted to the SWISS-MODEL online server.[280,281] The tertiary structure of (Q192) hPON1 was generated by SWISS-MODEL using PDB ID: 3SRG (rePON1), as a reference template.[128] The H1 loop (residues 1-18) was missing in the crystal structure. Therefore, the H1 loop was generated using MODELLER[282] and was placed at its appropriate position in the modeled hPON1 structure. The glutamine at

position 192 of the Q192 form of hPON1 was replaced by arginine to obtain the R192 polymorphism.

The modeled structures were initially minimized for 2500 steps. Then they were heated (10-300 K) for 50 ps using Amber12[283] and the ff99SB[274] forcefield with a 12 Å cutoff. They were further equilibrated for 1 ns using an implicit solvent model. The equilibrated structures were then cooled to 0 K, by decreasing the temperature by 100 K for every 25 ps. The resultant structures were submitted to the H++ server[250,251] to obtain the protonation states of the titratable residues and total charge of the protein.

5.2.1 Explicit solvent model simulations

Explicit solvent model simulations were performed using Amber12 and the ff99SB forcefield. Using *tleap,* hPON1 (Q192/R192) was placed in a rectangular box and solvated with TIP3P[257] water molecules. The Q192 form of hPON1 was neutralized by adding 10 Na^+ ions and the R192 form with 9 Na^+ ions. Both the systems were initially minimized for 2500 steps by restraining the protein with a force constant of 500 kcal/mol·$Å^2$. The whole systems were minimized for another 2500 steps without any restraints. Then, the systems were heated for 50 ps from 10K to 300 K under NVT conditions with a force constant of 10 kcal/mol·$Å^2$ on the protein. Next, they were equilibrated for 450 ps at 300 K under NPT conditions. Finally, both systems were sampled for 30 ns under NVT conditions. During the equilibration and sampling process, hydrogens were constrained using the SHAKE algorithm,[258,259] and a constant temperature was maintained using Langevin dynamics with a collision frequency of 1.0 ps^{-1}.[181] The electrostatic interactions were handled using Particle Mesh Ewald[260-262]

under periodic boundary conditions with a 12 Å cutoff. All the dynamics were performed with a time step of 1 fs.

5.2.2 Docking studies of chloropyrifos-oxon (Cpo)

Using the last 2 ns of the sampling process of (Q192/R192) hPON1, 20 snapshots were generated (1 snapshot for every 100 ps) with the *mmpbsa.pl* script of Amber12. The water molecules and counter ions were removed from the generated snapshots. Also, a conformational analysis of Cpo was performed using the MMFFaq[284] forcefield in Spartan'10. The lowest energy conformer was chosen and was then optimized using HF and the 6-31G* basis set with Q-Chem 3.2.[151] The partial atomic charges were generated using the restrained electrostatic potential approach.[253] The optimized ligand was docked into the active site of the generated snapshots. All the docking studies were performed using Autodock Vina.[285]

During the docking studies, the surface loop (residues 72-79) of hPON1 was made flexible, while rest of the protein was treated as rigid. The orientation of Cpo and its interaction with the catalytic Ca^{2+} ion (Ca1) and with the active site residues were visualized using VMD.[255] In the Q192 form of hPON1, the O on P=O of Cpo was facing towards or away from Ca1. The distance between O (P=O) atom of Cpo and Ca1 was more than 10 Å when the O on P=O of Cpo was facing away from Ca1. In 11 snapshots of the Q192 system, the Cpo was found close to Ca1, and the O of P=O was facing towards Ca1. Out of those snapshots, the system in which the distance between O on P=O of Cpo and Ca1 was the minimum was chosen as **Case 1**. In the remaining Q192 systems (9 snapshots), the structure in which the distance between O (P=O) atom of Cpo and Ca1 was the maximum was selected as **Case 2**.

In the case of the R192 docking studies, in all the snapshots Cpo was interacting with Ca1 or with the structural Ca^{2+} ion (Ca2). The Ca2 is located in the top portion of the central tunnel, and Ca1 is situated in the bottom part. The Cpo conformer in which the distance between O (P=O) and Ca1 was the minimum was chosen as **Case 3**. Similarly, the conformer where the distance between O (P=O) of Cpo and Ca2 was the minimum was selected as **Case 4**. Hence, in both hPON1 systems two unique Cpo conformers were considered.

The chosen structures (Q192/R192 + Cpo) were again placed in a rectangular box and solvated with TIP3P water molecules. The counter ions were added to neutralize the systems. The Amber *gaff* forcefield[256] was used to describe Cpo. The systems were minimized, heated, equilibrated, and sampled (25 ns) using a similar procedure to that mentioned earlier.

5.2.3   Docking studies of neutral and monopyridinium oximes

Out of the four explicitly sampled systems, Cpo was closely interacting with Ca1 only in **Case 1** and **Case 3**. Therefore, these equilibrated systems were considered for further docking studies. Again, using the last 2 ns of the sampling process, four snapshots were generated for each system.

Meanwhile, Dr. Janice Chambers' group had tested 26 neutral oximes and various monopyridinium oximes to analyze the hydrolysis of TIMP, NIMP, TEMP, and NEMP bound to hPON1 using an *in vitro* human serum model. Among the neutral oximes only pinacolone oxime showed any increase in hydrolysis activity, and this increase was only 5%. However, some of the monopyridinium oximes showed larger increases in hydrolysis rates. A detailed explanation is provided in the next section.

All the oximes were modeled using Spartan'10 and the conformational analyses were performed using the MMFFaq.[284] For each system, a lowest energy conformer was chosen. Then, the selected conformers were individually docked to the generated snapshots of **Case 1** and **Case 3** systems. During the docking studies, only the Cpo was made flexible; rest of the system was rigid. Gasteiger charges were used as the partial atomic charges for all ligands.[286] The ligand alignment, its orientation, and its interactions with Cpo, Ca1 or Ca2, and also with the active site residues were visually inspected using VMD.

5.3 Results and discussion

5.3.1 Explicit solvent simulations of hPON1

The generated Q192 and R192 forms of hPON1 were equilibrated using an explicit solvent model for 30 ns. Using an explicit solvent model, rePON1 was also minimized, heated, equilibrated, and sampled (30 ns) using a similar procedure as described earlier. The rePON1 crystal structure (PDB ID: 3SRG) was taken as the starting structure, and the phosphate ion and 2-hydroxyquinoline were removed from the active site. RMSd vs. time graphs were plotted for rePON1 and the Q192 and R192 forms of hPON1 and are shown in Figure 5.2. Since rePON1 does not have the H1 loop, these residues were not included in the RMSd calculations for the sampled hPON1 systems. The RMSd values of the sampled hPON1 (Q192 and R192) and rePON1 were calculated with respect to the crystal structure of rePON1 using VMD at 10, 20, and 30 ns and are tabulated in Table 5.1. The RMSd values of Q192 hPON1 at 10, 20, and 30 ns were higher than the corresponding values of R192 hPON1 and equilibrated rePON1.
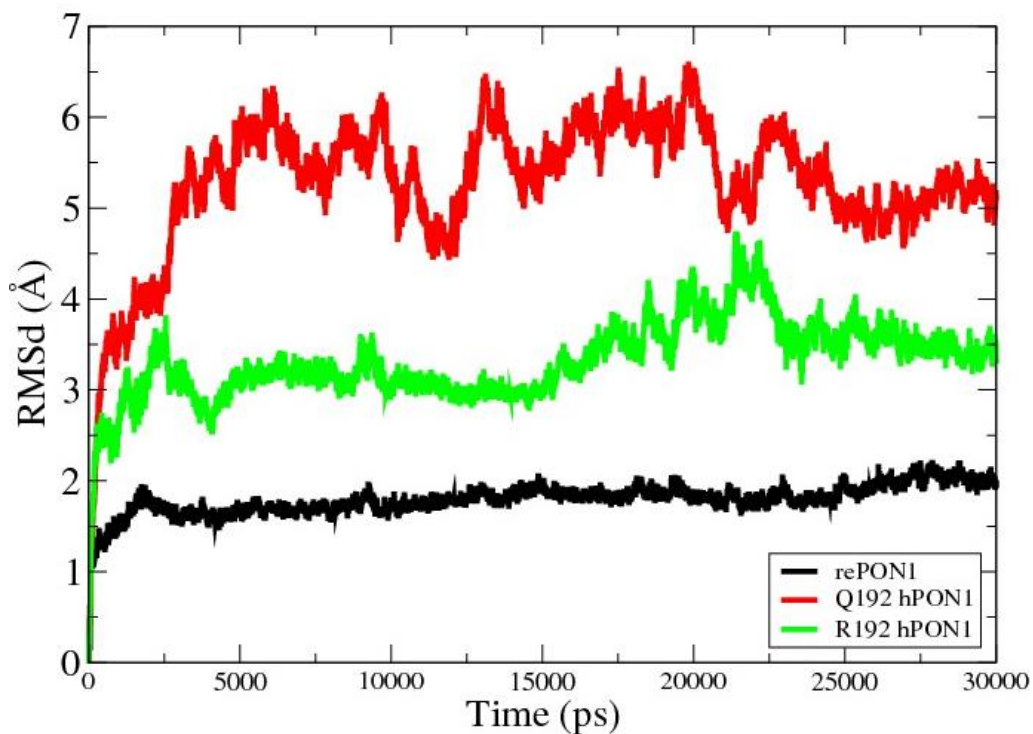
Figure 5.2   RMSd vs. time plot of rePON1 and the Q192 and R192 forms of hPON1

Table 5.1   RMSd values of rePON1 and (Q192/R192) hPON1 equilibrated structures
calculated with respect to crystal structure of rePON1.

System	10 ns	20 ns	30 ns
Q192	1.72	1.95	1.95
R192	1.47	1.72	1.64
rePON1 equilibrated	1.35	1.26	1.47
rePON1 crystal structure	0	0	0

In the Q192 polymorph, Ca1 was in coordination with Glu53, Asp54, His115,

Asn168, and Asp169, as shown in Figure 5.3. Ca1 was closely interacting with Glu53,

Asp54, and Asp269 in the R192 system, as shown in Figure 5.4. Similarly, Ca2 was

close to Glu53, Asp269, Asn270, and Thr332 in the Q192 form of hPON1, and Asp169

and Asn270 in R192. The distance between Ca1 or Ca2 and the O atoms located at the δ

and ε positions of these residues of Q192 and R192 hPON1 are tabulated in Tables 5.2

and 5.3, respectively. The distance between Ca1 and Ca2 in the Q192 system was about

4.5 Å and about 6.5 Å in R192. In both of the structures, Ca1 was located at the bottom

of the active site. Since the H1 loop was not in contact with the lipid bilayer, the loop has

taken a closed conformation to minimize contacts with the solvent molecules in the

(Q192/R192) hPON1 models.
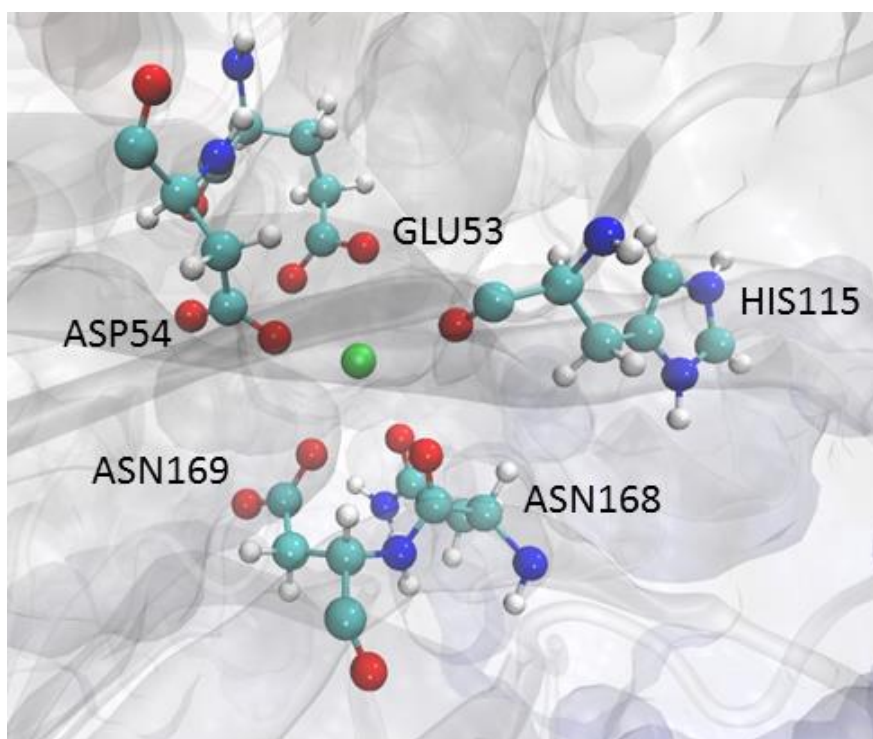
Figure 5.3   The interaction of catalytic Ca^{2+} ion (Ca1) with various active site residues
in the Q192 hPON1
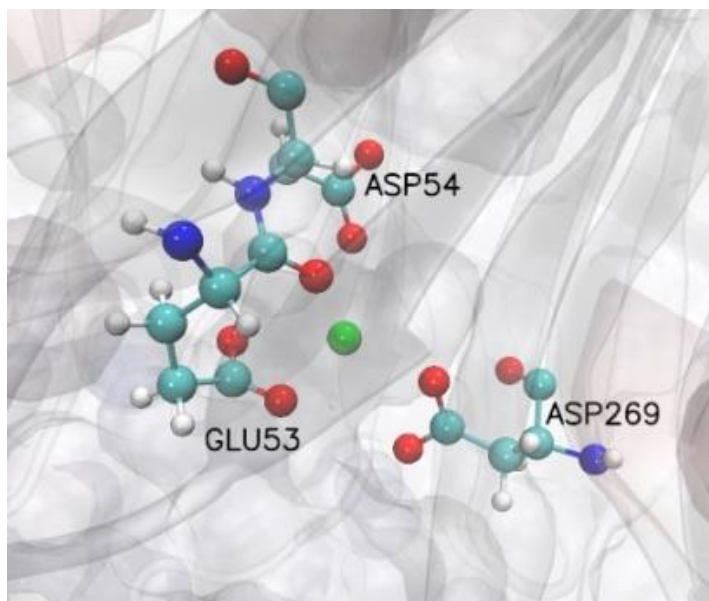
Figure 5.4   The interaction of catalytic Ca^{2+} ion (Ca1) with various active site residues in the R192 hPON1

Table 5.2   Distance between Ca1 or Ca2 and various O atom of active site residues in the Q192 system.

Ca^{2+} ion	Residue	Distance (Å)
Ca1	Glu53@OE	2.68
Ca1	Glu53@OE'	2.78
Ca1	Asp54@OD	2.52
Ca1	His115@O	2.66
Ca1	Asn168@OD	2.70
Ca1	Asp169@OD	2.49
Ca2	Glu53@OE	2.62
Ca2	Asp269@OD	2.84
Ca2	Asn270@OD	2.69
Ca2	Thr332@O	2.82

OD = oxygen at the δ position, OE = OE' = oxygen at the ε position, and O = oxygen on the carbonyl group

Table 5.3   Distance between Ca1 or Ca2 and various O atom of active site residues in the R192 system.

Ca^{2+} ion	Residue	Distance (Å)
Ca1	Glu53@OE	2.70
Ca1	Glu53@OE'	2.53
Ca1	Asp54@OD	2.54
Ca1	Asp269@OD	2.53
Ca2	Asp54@OD	2.59
Ca2	Asp169@OD	2.75
Ca2	Asp169@OD	2.56
Ca2	Asn270@OD	2.68

OD = oxygen at the δ position and OE = OE' = oxygen at the ε position.

5.3.2   Docking studies of Cpo

In all the generated snapshots of the Q192 system, the Cpo was found close to Tyr71 and Ile74 or only to Ile74. For the snapshots in which the O (P=O) atom was facing towards Ca1, the Cpo was closely interacting with Tyr71 and Ile74. When the O (P=O) atom of Cpo was facing away from Ca1, the Cpo was adjacent to Ile74. Nine Cpo conformers were found close to the active site entrance. Therefore, we have chosen a conformer (**Case 2**) to examine whether the Cpo will block the active site entrance during MD simulations. Similarly, in certain R192 snapshots, the Cpo was near Tyr71 and Ile74 when it was interacting with Ca1. In other cases, Cpo was close to Ca2. Hence, we have considered a Cpo conformer which was close to Ca2 for MD simulations to analyze whether this interaction is stable or not.

5.3.3   Explicit solvent simulations of (Q192/R192) hPON1 + Cpo

The selected complex (Q192/R192 + Cpo) systems were equilibrated for 25 ns using an explicit solvent model. RMSd vs. time graphs were plotted for all systems and are shown in Figure 5.5. During the entire simulation, Cpo did not block the active site entrance in **Case 2**. In **Case 4**, the Cpo was in contact with Ca2. This suggests that in

91

the R192 system, the Cpo can potentially bind to Ca1 or Ca2. In **Case 1** and **Case 3**, the Cpo was bound to Ca1; therefore, the distance between O on P=O of Cpo and Ca1 were measured as a function of time. On average, the distance between the O (P=O) atom of Cpo and Ca1 in **Case 1** was about 6 Å and in **Case 3** was 2.8 Å. Hence, the Cpo was more tightly bound to Ca1 in the R192 system when compared to Q192.

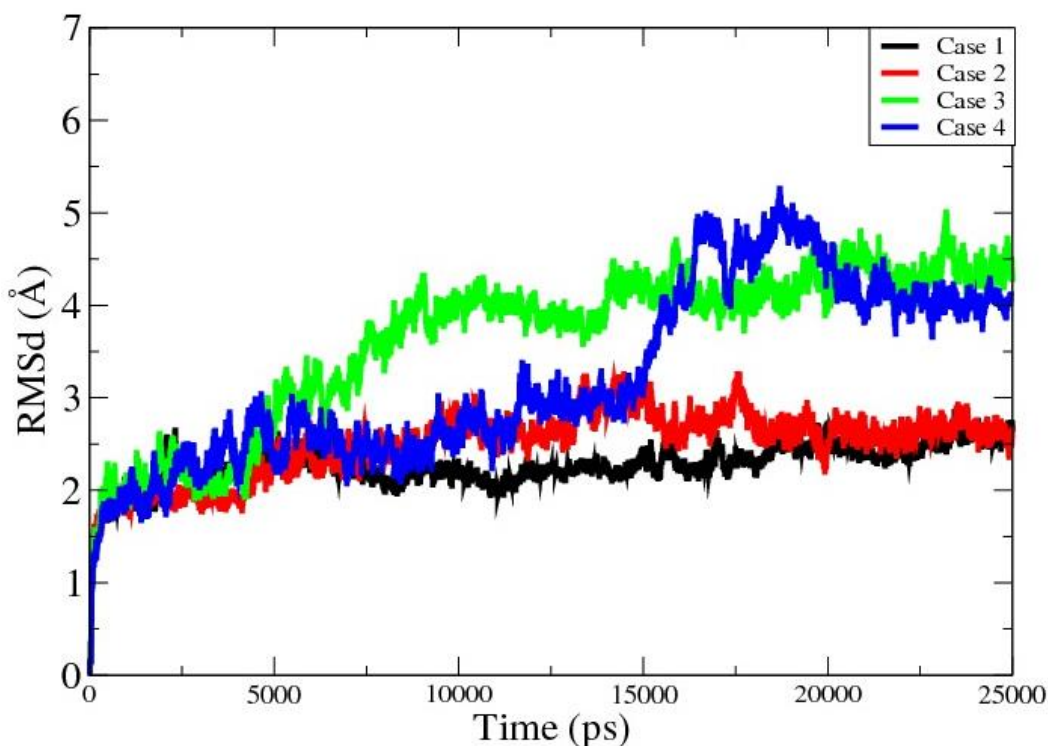Figure 5.5   RMSd vs. time plots of various (Q192/R192) hPON1 and Cpo systems

The binding enthalpies (ΔH) for all the systems were calculated using MM-GBSA and MM-PBSA methods and are shown in Table 5.4. The ΔH values (MM-GBSA and MM-PBSA) were lower when the Cpo was far away from Ca1 in the (Q192) hPON1 systems (*i.e.* **Case 2** versus **Case 1**). In the R192 system the MM-PBSA binding

enthalpy value was lower when Cpo was bound to Ca1 when compared to Ca2. The opposite result was observed using MM-GBSA.

Table 5.4   Binding enthalpies of four different (Q192/R192) hPON1 + Cpo systems.

System	Case	MM-GBSA (kcal/mol)	MM-PBSA (kcal/mol)
Q192 hPON1 + Cpo, near Ca1	1	-24.3±2.9	-21.3±4.4
Q192 hPON1 + Cpo, away from Ca1	2	-32.7±2.3	-28.0±2.6
R192 hPON1 + Cpo, near Ca1	3	-19.3±3.2	-25.8±3.6
R192 hPON1 + Cpo, near Ca2	4	-22.2±2.6	-20.9±3.2

The hydrolysis of Cpo bound to hPON1 mainly occurs at the catalytic Ca^{2+} ion (Ca1). Therefore, to analyze the interactions between various oximes with Cpo, **Case 1** and **Case 3** were considered for further docking studies.
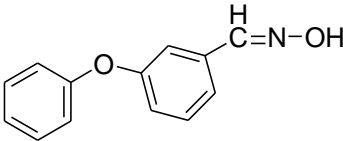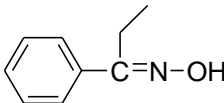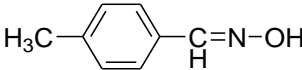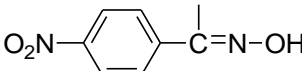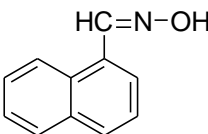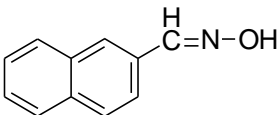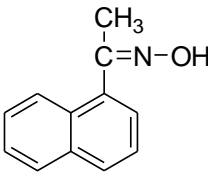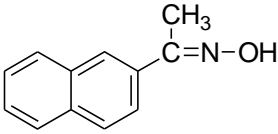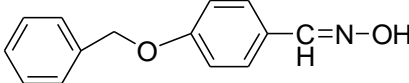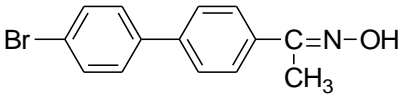
5.3.4   Neutral oximes

The experimentally tested neutral oximes are tabulated in Table 5.5. Each ligand was individually docked to four generated snapshots of the **Case 1** and **Case 3** systems. The three lowest energy conformers of each neutral oxime were chosen. The interactions between various conformers of all ligands and Cpo were carefully inspected. In the Q192 + Cpo system (**Case 1**), the ligands **1**, **2**, **3**, **7**, and **12** (Refer Table 5.5) did not exhibit interactions with Cpo in any of the four snapshots. Similarly, in the R192 + Cpo system (**Case 3**), the neutral oximes **6**, **9**, **10**, **12**, **18**, **21**, **22**, **23**, **24**, **25**, and **26** did not interact with Cpo in any snapshot. None of the chosen conformers of 4-nitrobenzaldehyde oxime (**12**) interacted with Cpo in either system. Overall the majority of ligands have exhibited more favorable interactions with **Case 1** than **Case 3**.

Table 5.5   Structures of neutral oximes

L.No	Name	Structure
1	Acetaldehyde oxime	$CH_3CH=N-OH$
2	Acetone oxime	
3	2-butanone oxime	
4	Cyclohexanone oxime	
5	Benzaldehyde oxime	
6	2-indanone oxime	
7	Benzamide oxime	
8	Acetophenone oxime	
9	2-chlorobenzaldehyde oxime	
10	Pinacolone oxime	
11	α-isonitrosopropiophenone	
12	4-nitrobenzaldehyde oxime	
13	Benzoquinone dioxime	
14	Pyruvicaldehyde-1-oxime	
15	4'-chloroacetophenone oxime	
16	2-chloroacetophenone oxime	

Table 5.5 continued

17	3-phenoxybenzaldehyde oxime	
18	Propionaldehyde oxime	
19	4-methylbenzaldehyde oxime	
20	4-nitroacetophenone oxime	
21	1-naphthaldehyde oxime	
22	2-naphthaldehyde oxime	
23	1-acetonaphthone oxime	
24	2-acetonaphthone oxime	
25	4-benzyloxybenzaldehyde oxime	
26	4-(4-bromophenyl)acetophenone oxime	

L.no = ligand number

The conformers of various ligands which were closely interacting with Cpo in **Case1** and **Case3** were identified. Then, the distance between the P on P=O of Cpo and the O of C=N-OH on the neutral oximes was measured. For every oxime the conformer with the shortest distance between the oxime O atom and the Cpo P was selected. For all the systems, the selected distance and corresponding binding enthalpies (*ΔH's*) are tabulated in Table 5.6. Again, the *ΔH* values calculated using docking studies is a sum of the internal energy of the system, electrostatic, van der Waals, hydrogen bonding interactions, and the desolvation energy in a protein-ligand system. Hence, the estimated *ΔH* is not an absolute binding enthalpy term. The binding enthalpies for all the neutral oximes and monopyridinium oximes (discussed in the next section) are not yet experimentally determined. However, the predicted binding enthalpies can be correlated to the binding affinities of various neutral oximes. The binding enthalpies of various aromatic neutral oximes in **Case 1** and **Case 3** were lower than the enthalpic values of the aliphatic ones. Therefore, we predict that an aromatic neutral oxime is likely to bind with a higher binding affinitiy to Cpo than an aliphatic ligand.

The distance between the oxime O atom and Ca1 or Ca2 are measured using a similar criterion as mentioned above. In Q192 + Cpo docking studies, the distance between the oxime O of the 4-methylbenzaldehyde oxime and the P atom of Cpo was shortest (3.9 Å) among the ligands studied. This interaction is shown in Figure 5.6. Pinacolone oxime has the next shortest distance (4.5 Å). Similarly, benzoquinone dioxime was the closest to Cpo (4.1 Å) in **Case 3**, as shown in Figure 5.7.

Table 5.6 Distance between the O atom on the oxime group of a neutral oxime and the P atom of Cpo in various **Case 1** and **Case 3** systems along with their binding enthalpy values.

Ligand	System	Distance (Å)	ΔH (kcal/mol)
Cyclohexanone oxime	**Case 1**	5.1	-4.9
Benzaldehyde oxime	**Case 1**	8.9	-5.1
2-indanone oxime	**Case 1**	8.1	-6.2
Acetophenone oxime	**Case 1**	7.4	-5.3
2-chlorobenzaldehyde oxime	**Case 1**	9.7	-5.7
Pinacolone oxime	**Case 1**	4.5	-4.8
α-isonitropropiophenone oxime	**Case 1**	8.9	-6.1
4'-chloroacetophenone oxime	**Case 1**	8.1	-5.7
2-chloroacetophenone oxime	**Case 1**	8.0	-5.7
3-phenoxybenzaldehyde oxime	**Case 1**	8.8	-6.9
Propionaldehyde oxime	**Case 1**	4.6	-5.6
4-methylbenzaldehyde oxime	**Case 1**	3.9	-5.5
4-nitroacetophenone oxime	**Case 1**	6.9	-6.6
1-naphthaldehyde oxime	**Case 1**	9.4	-6.9
2-naphthaldehyde oxime	**Case 1**	8.2	-6.8
1-acetonaphthone oxime	**Case 1**	8.9	-7.3
2-acetonaphthone oxime	**Case 1**	9.4	-6.9
4-benzyloxybenzaldehyde oxime	**Case 1**	8.8	-7.1
4-(4-bromophenyl)-acetophenone oxime	**Case 1**	8.2	-8.1
Acetaldehyde oxime	**Case 3**	9.5	-3.2
Acetone oxime	**Case 3**	8.3	-3.8
2-butanone oxime	**Case 3**	9.8	-4.0
Cyclohexanone oxime	**Case 3**	9.6	-4.9
Benzaldehyde oxime	**Case 3**	8.8	-5.1
Benzamide oxime	**Case 3**	7.5	-5.9
Acetophenone oxime	**Case 3**	9.1	-5.5
α-isonitropropiophenone oxime	**Case 3**	9.6	-6.2
Benzoquinone dioxime	**Case 3**	4.1	-5.5
Pyruvicaldehyde oxime	**Case 3**	8.9	-3.8
4'-chloroacetophenone oxime	**Case 3**	11.3	-5.4
2-chloroacetophenone oxime	**Case 3**	9.7	-5.6
3-phenoxybenzaldehyde oxime	**Case 3**	11.2	-6.5
4-methylbenzaldehyde oxime	**Case 3**	11.3	-5.1
4-nitroacetophenone oxime	**Case 3**	12.0	-5.8
4-(4-bromophenyl)-acetophenone oxime	**Case 3**	8.3	-6.9
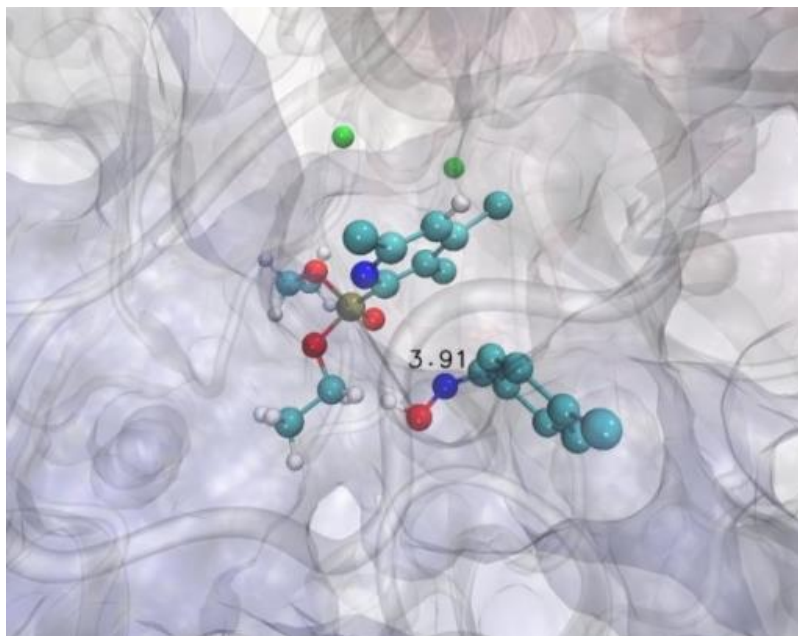
Figure 5.6   Interaction between Cpo and 4-methylbenzaldehyde oxime in (Q192) hPON1 + Cpo system
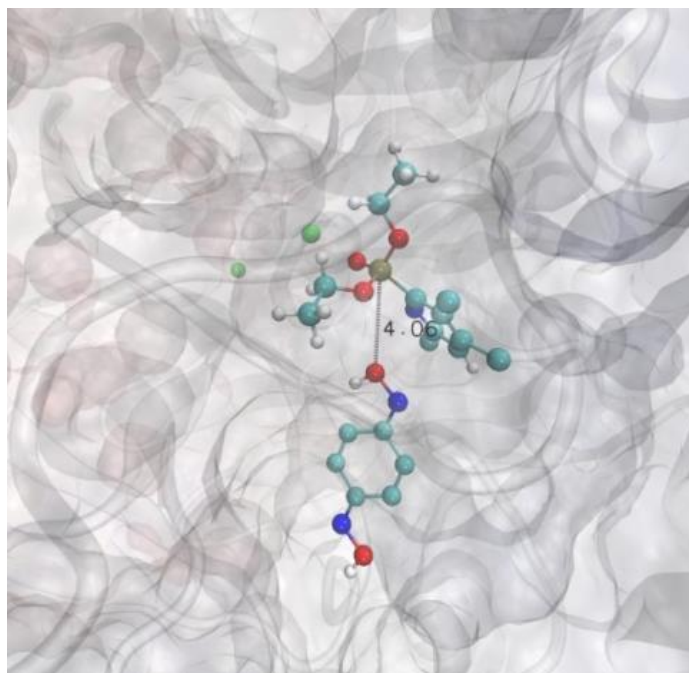
Figure 5.7   Interaction between Cpo and benzoquinone dioxime in (R192) hPON1 + Cpo system

In **Case 1** and **Case 3** systems, 4-(4-bromophenyl)-acetophenone oxime has exhibited the highest binding affinity (lowest binding enthalpy). In the Q192 + Cpo and R192 + Cpo systems, the bulky aromatic ligands, such as **17**, **21**, **23**, **25**, etc., have shown more favorable interactions with Cpo than the aliphatic oximes.

Apart from interacting with Cpo, the neutral oximes have also shown interactions with Ca1 and Ca2. In **Case 1** docking studies, certain conformers of various ligands were exclusively bound to Ca1. Therefore, the distance between the O of C=N-OH of the ligand and Ca1 were measured and tabulated in Table 5.7. Similarly, in R192 + Cpo systems, the ligands were preferentially bound to Ca2 in all cases. Hence, the distance between Ca2 and the O (C=N-OH) atom of the ligand were measured and shown in Table 5.8.

As mentioned earlier, the Ca2 is located in the top portion of the central tunnel, and hence the incoming neutral oximes may have entered through the upper part of the central tunnel and interacted with Ca2 in the R192 hPON1 + Cpo system. The interaction between benzamide oxime (**7**) and Ca2 in **Case 3** is shown in Figure 5.8. However, the ligand should enter through the bottom part of the central tunnel (active site) to hydrolyze the organophosphate. Hence, a snapshot in which a conformer of benzamide oxime has interacted with Cpo (by entering through the active site) in the R192 hPON1 + Cpo system is shown in Figure 5.9.

Table 5.7   The distance between the O atom on the oxime group of a neutral oxime and Ca1 of various **Case 1** systems and their corresponding binding enthalpies.

Ligand	Distance (Å)	ΔH (kcal/mol)
Acetaldehyde oxime	4.7	-3.5
Acetone oxime	5.3	-3.9
2-butanone oxime	4.7	-4.2
Benzaldehyde oxime	5.9	-5.6
2-indanone oxime	4.6	-6.4
Benzamide oxime	4.7	-6.1
2-chlorobenzaldehyde oxime	5.2	-5.4
4-nitrobenzaldehyde oxime	5.7	-6.4
Benzoquinone dioxime	4.7	-6.2
Pyruvicaldehyde oxime	4.5	-4.2
4'-chloroacetophenone oxime	6.9	-6.0
2-chloroacetophenone oxime	4.7	-5.2
4-nitroacetophenone oxime	5.0	-6.7
2-acetonaphthone oxime	5.2	-7.4
4-benzyloxybenzaldehyde oxime	4.8	-7.9
4-(4-bromophenyl)-acetophenone oxime	5.3	-6.9

Table 5.8   The distance between the O atom on the oxime group of a neutral oxime and Ca2 of various **Case 3** systems and their corresponding binding enthalpies.

Ligand	Distance (Å)	ΔH (kcal/mol)
Cyclohexanone oxime	7.1	-4.7
Benzaldehyde oxime	7.1	-5.0
2-indanone oxime	7.0	-6.0
Benzamide oxime	6.6	-5.6
Acetophenone oxime	7.1	-5.4
2-chlorobenzaldehyde oxime	6.6	-5.4
Pinacolone oxime	7.2	-4.4
α-isonitropropiophenone oxime	7.1	-5.8
4-nitrobenzaldehyde oxime	7.0	-5.7
Pyruvicaldehyde oxime	7.1	-3.6
4'-chloroacetophenone oxime	6.8	-5.4
2-chloroacetophenone oxime	6.9	-5.2
3-phenoxybenzaldehyde oxime	6.9	-7.2
Propionaldehyde oxime	7.1	-5.3
4-methylbenzaldehyde oxime	7.2	-5.4
4-nitroacetophenone oxime	8.2	-6.0
1-naphthaldehyde oxime	7.9	-6.2
2-naphthaldehyde oxime	6.8	-6.7
1-acetonaphthone oxime	7.1	-7.1
2-acetonaphthone oxime	6.6	-6.8
4-benzyloxybenzaldehyde oxime	8.1	-7.1
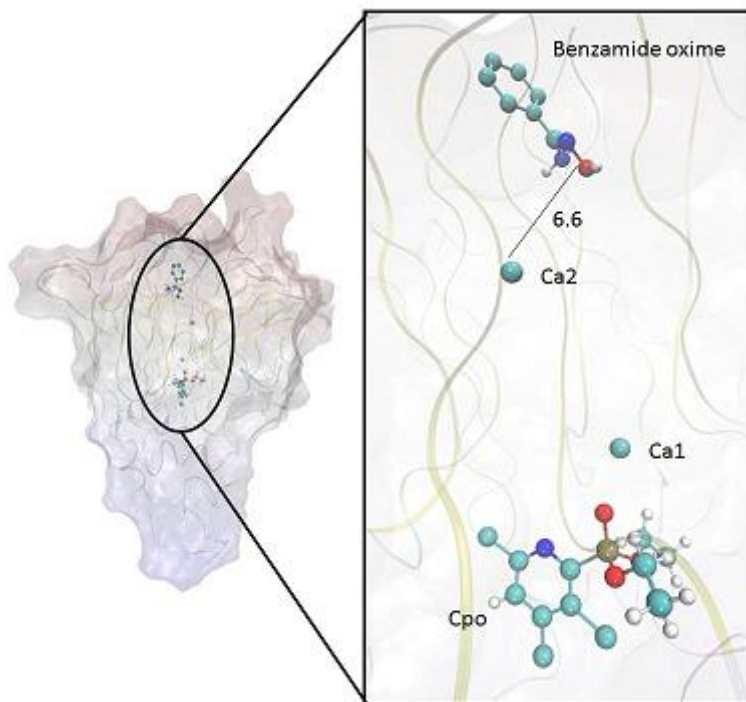
Figure 5.8   Interaction between benzamide oxime and Ca2 in the R192 hPON1 + Cpo
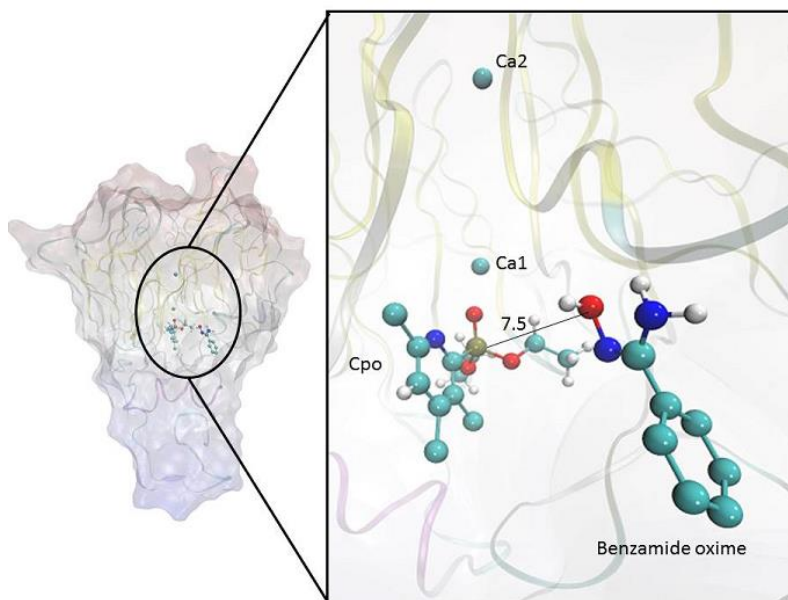
Figure 5.9   Interactions between benzamide oxime and Cpo in the R192 hPON1 + Cpo

Various conformers of the ligands **5**, **6**, **7**, **9**, **15**, **16**, **20**, **24**, and **25** have exhibited interactions with Cpo, Ca1, and Ca2 in both **Case 1** and **Case 3** systems. Therefore, the experimentally tested neutral oximes can potentially interact with Ca1 or Ca2 along with Cpo. On the other hand, in some of the Cpo conformers, the aromatic ring of Cpo was blocking the O atom (C=N-OH) of the ligand during the nucleophilic attack. In other words, the aromatic ring on Cpo and the oxime group of the ligand were aligning on the same axis. This alignment was inhibiting the O atom from attacking the P atom of Cpo. The interaction of neutral oximes with Ca1 or Ca2 and the hindrance of the Cpo aromatic ring may influence the hydrolysis process.

The docking studies performed with 26 neutral ligands have shown that the aromatic ligands exhibited higher binding affinities towards Cpo than the aliphatic ligands in both the Q192 and R192 hPON1 systems. However, the molecular framework attached to the oxime group was not flexible enough. As a result, the neutral oximes were unable to orient properly while interacting with Cpo.

5.3.5   Monopyridinium oximes

Based on the above analysis and conclusions, our experimental collaborators have synthesized and tested a series of monopyridinium oximes while varying the linker length using a reference template as shown in Figure 5.10.
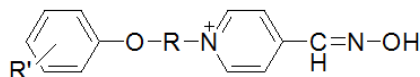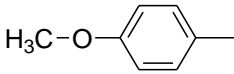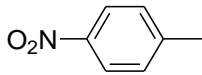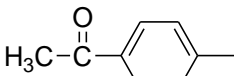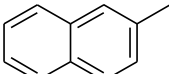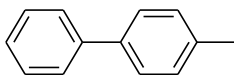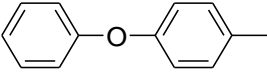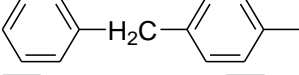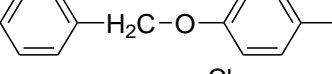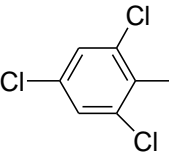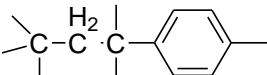
Figure 5.10   Reference template for monopyridinium oxime

where R is the linker length = $(CH_2)_n$ and n = 1- 6

The hydrolysis rate tremendously increased when the linker length was 6 (*i.e.*, R = $(CH_2)_6$). The monopyridinium oximes which have efficiently hydrolyzed the surrogates of sarin (TIMP and NIMP) and VX (TEMP and NEMP) are shown in Table 5.9. The ligands 46.15 and 46.16 have shown the highest hydrolysis rates.

Table 5.9   Structures of experimentally tested monopyridinium oximes

$$R-O-(H_2C)_6-N^+ \diagdown C=N-OH$$
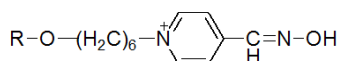
Ligand number	R
46.06	
46.10	
46.12	
46.15	
46.16	
46.23	
46.24	
46.25	
46.28	
46.43	

All 10 monopyridinium oximes were docked to the generated snapshots of **Case 1** and **Case 3** using a similar procedure to that described earlier. In **Case 1** systems the

ligands 46.10, 46.15, and 46.25 did not interact with Cpo in any of the snapshots,

whereas in **Case 3** all the ligands, except 46.10, interacted with Cpo in at least one out of

the four generated snapshots. In the Q192 + Cpo systems, most of the ligands were

closer to Ca1 than to Cpo. In the R192 + Cpo system, some of the conformers of all the

ligands were found close to Ca2. The ligands 46.15, 46.28, and 46.43 have interacted

with Cpo in a majority of the snapshots. Again, the distance between the oxime O of the

ligand and the Cpo P was measured for all systems and is shown in Table 5.10.

Similarly, the distance between the oxime O and Ca1 was measured in all **Case 1** systems

and tabulated in Table 5.11. The distance between the oxime O of the ligand and Ca2

was measured in all **Case 3** systems and is shown in Table 5.12. The monopyridinium

oximes were closer to Ca1 in Q192 + Cpo than to Ca2 in R192 + Cpo.

Table 5.10   Distance between the O atom on the oxime group of monopyridinium oxime
and the P atom of Cpo in various **Case 1** and **Case 3** systems along with
their binding enthalpies.

Ligand number	System	Distance (Å)	ΔH (kcal/mol)
46.06	**Case 1**	8.9	-6.8
46.12	**Case 1**	9.4	-7.8
46.16	**Case 1**	9.5	-7.7
46.23	**Case 1**	8.4	-6.9
46.24	**Case 1**	9.5	-6.8
46.28	**Case 1**	5.6	-8.0
46.43	**Case 1**	8.4	-7.1
46.06	**Case 3**	10.2	-7.3
46.12	**Case 3**	10.2	-6.3
46.15	**Case 3**	7.5	-8.0
46.16	**Case 3**	7.5	-6.4
46.23	**Case 3**	9.2	-7.0
46.24	**Case 3**	9.6	-7.2
46.25	**Case 3**	7.6	-6.8
46.28	**Case 3**	7.6	-7.5
46.43	**Case 3**	9.9	-6.0

Table 5.11 Distance between the O atom on the oxime group of a monopyridinium oxime and Ca1 of various **Case 1** systems and their corresponding binding enthalpies.

Ligand	Distance (Å)	ΔH (kcal/mol)
46.06	5.0	-7.5
46.10	5.5	-7.9
46.12	4.8	-7.8
46.15	5.7	-8.4
46.16	5.5	-8.5
46.23	4.6	-8.1
46.24	4.6	-8.3
46.25	5.6	-8.5
46.28	5.5	-6.9
46.43	5.4	-8.3

Table 5.12 Distance between the O atom on the oxime group of a monopyridinium oxime and Ca2 of various **Case 3** systems and their corresponding binding enthalpies.

Ligand number	Distance (Å)	ΔH (kcal/mol)
46.06	6.6	-6.7
46.10	6.7	-6.3
46.12	6.3	-6.7
46.15	7.2	-7.2
46.16	8.2	-8.3
46.23	7.2	-6.9
46.24	7.1	-6.7
46.25	7.4	-7.1
46.28	7.1	-6.6

Out of all the monopyridinium oximes, 46.28 was found closest to Cpo (5.6 Å) and also exhibited the lowest binding energy in **Case 1**. 46.15 and 46.16 were found closest to Cpo (7.5 Å), and the binding energy of 46.16 was lowest in **Case 3**. Most of the monopyridinium oximes conformers have more effectively interacted with Cpo in R192 + Cpo than in Q192 + Cpo. On the other hand, many of the neutral oximes have shown favorable interactions with Cpo in Q192 + Cpo systems. This suggests that the

105

hydrolysis of an organophosphate bound to Q192 or R192 hPON1 may depend on the nature of the oxime.

We were interested to study a new set of oximes based on a reference template, as shown in Figure 5.11. Based on this template, tertiary and quaternary amine oximes can be designed. Further, we estimated the relative deprotonation energy for deprotonating the H atom present on the oxime group in tertiary, quaternary, and monopyridinium oximes compared to a neutral oxime. All the molecules are shown in Figure 5.12. The oximes and their corresponding anions were modeled using Spartan'10. The conformational analyses were performed using MMFFaq. The lowest energy conformer was chosen and optimized with M06-2X/aug-cc-pVDZ[287] using 150 radial points and the 302 point Lebedev[288,289] angular grid using Q-Chem 4.0.1.[151] The polarized continuum solvent model[290] with a dielectric constant of 78.39 Debye was also included.
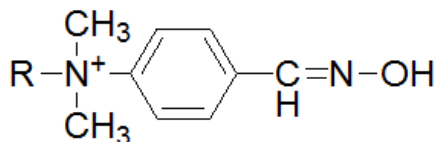
Figure 5.11   Reference template for tertiary or quaternary amine oximes

CH₃ structures...

$H_3C-C(CH_3)(CH_3)$—⬡—$C=N-OH$ (H)   1

$H_3C-N(CH_3)$—⬡—$C=N-OH$ (H)   2

$H_3C-N^+(CH_3)(CH_3)$—⬡—$C=N-OH$ (H)   3

$H_3C-C(CH_3)(CH_3)-N^+$⬡—$C=N-OH$ (H)   4
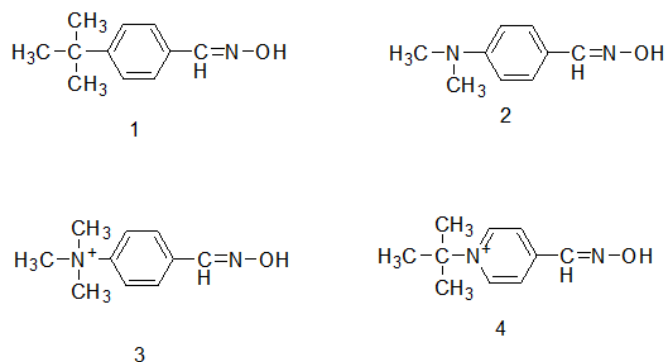
Figure 5.12   1) Neutral oxime, 2) oxime with tertiary amine, 3) oxime with quaternary amine, and 4) monopyridinium oxime

In each system the energy difference between a deprotonated oxime and the oxime which has an H atom on its oxime group was calculated. Then, the resultant energies for oximes containing tertiary amine and quaternary amine, and monopyridinium oxime were subtracted from the neutral oxime's deprotonation energy to obtain relative deprotonation energies and are shown in Table 5.13. The relative deprotonation energy of monopyridinium oxime was lowest, and the oxime containing tertiary amine was highest. In other words, more energy is required to deprotonate the H atom on the oxime group of the tertiary amine oxime compared to the neutral oxime.

Table 5.13   Deprotonation energies (kcal/mol) and relative deprotonation energies (kcal/mol) of oximes containing a tertiary amine and quaternary amine, and monopyridinium oxime calculated with respect to a neutral oxime.

Molecule	Deprotonation energy	Relative deprotonation energy
1	305.3	0
2	307.6	2.3
3	301.6	-3.7
4	293.4	-11.9

107

Similarly, less energy is required to deprotonate the H on the oxime group of the monopyridinium oxime and the oxime containing quaternary amine compared to the neutral oxime in the solvent medium. The H atom (on the oxime group) in the monopyridinium oxime is more acidic than one present on the oxime-containing quaternary amine. Hence, the hydrolysis rate of monopyridinium oximes might be higher than the oximes containing quaternary amine. Further, the monopyridinium oximes may hydrolyze organophosphates more efficiently than neutral oximes.

CHAPTER VI

CONCLUSIONS

This chapter is divided into two sections: oximes as reactivators and oximes as hydrolyzing agents.

6.1   Oximes as reactivators

All the inhibited and uninhibited systems of 2-PAM, MMB-4, HI-6, and obidoxime were sampled using explicit solvent simulations. 2-PAM displayed hydrogen bonding interactions with a few active site residues in all the systems except hAChE-sarin-2-PAM. MMB-4 did not exhibit hydrogen bonding in hBChE-sarin-MMB-4 and hBChE-tabun-MMB-4. Similarly, obidoxime did not display hydrogen bonding with the active site residues in hAChE-sarin-obidoxime and hBChE-sarin-obidoxime. HI-6 did not exhibit hydrogen bonding in hAChE-HI-6. Glu80 has shown favorable interactions with MMB-4, HI-6, and obidoxime. 2-PAM, MMB-4, and HI-6 displayed π-π interactions with various Tyr or Trp residues in some of the inhibited and uninhibited systems.

The calculated TI values can be considered to be accurate values at the ff99 forcefield limit. ΔA^0 values of MMB-4 and obidoxime systems were lower than the experimental values except for hAChE-sarin-obidoxime (3 kcal/mol). The RMS error of ΔA^0 for the inhibited systems of MMB-4 was 2.1 kcal/mol and for obidoxime systems was 4.8 kcal/mol. Usually, the binding free energies calculated using TI are closer to the

experimental values (within 1-2 kcal/mol).[270-273] However, in our systems, the calculated

ΔA^o values were lower than experimental values. This may due to the forcefield

limitations of the ff99 forcefield.

The calculated binding enthalpies using MM-GBSA and MM-PBSA for all the

inhibited and uninhibited systems of 2-PAM, MMB-4, HI-6, and obidoxime were

negative except for hBChE-sarin-MMB-4 and hBChE-sarin-obidoxime. The ΔH_{GBSA} and

ΔH_{PBSA} for these two systems were also calculated using a three trajectory method.

Again, positive binding enthalpies were obtained, suggesting that these systems might be

problematical for MM-GBSA and MM-PBSA calculations. The calculated ΔH values for

all the inhibited and uninhibited systems of MMB-4 and obidoxime were lower than

corresponding TI values except for the two systems mentioned above.

For all the systems the $T\Delta S$ values estimated using normal mode analyses were

equal to or lower in magnitude than their corresponding binding enthalpies. As a result,

the calculated free energies of binding, $i.e.,$ ΔG_{GBSA} and $\Delta G_{PBSA,}$ for most of the systems

were positive. The calculated ΔG_{GBSA} and ΔG_{PBSA} values of all the inhibited and

uninhibited systems of MMB-4 and obidoxime were compared with the TI values.

Among all the systems of MMB-4 and obidoxime, only the ΔG_{GBSA} and ΔG_{PBSA} values of

hBChE-obidoxime were comparable with the corresponding TI numbers.

The normal mode analysis treats various modes of a protein using the harmonic

oscillator approximation. However, the low frequency modes are not well described by

the harmonic oscillator approximation. Hence, the present algorithms cannot effectively

estimate the vibrational entropies for the low frequency modes. Therefore, the calculated

$T\Delta S$ values are lower than or equal in magnitude to the ΔH values in our systems.

110

Hence, the ΔS values were estimated using ΔA^0 and $\Delta H_{GBSA/PBSA}$ values for all MMB-4 and obidoxime systems except for hBChE-sarin-MMB-4 and hBChE-sarin-obidoxime. Then, average ΔS values (ΔS_{GBSA} and ΔS_{PBSA}) were calculated using the estimated binding entropies. Further, the binding free energies were estimated for HI-6 and 2-PAM systems using $\Delta H_{GBSA/PBSA}$ and average ΔS values. For all HI-6 systems $\Delta G_{GBSA/PBSA}$ was negative. For the 2-PAM systems, only the $\Delta G_{GBSA/PBSA}$ values for hAChE-sarin-2-PAM and hBChE-sarin-2-PAM were negative. However, the estimated free energies for the 2-PAM systems are still likely better estimates than the earlier free energies calculated using binding enthalpies and binding entropies ($T\Delta S$) obtained using normal mode analyses.

MM-GBSA per-residue decomposition analyses were performed for all the inhibited and uninhibited systems of 2-PAM, MMB-4, HI-6, and obidoxime. Met81 has commonly shown favorable interactions with the reactivator in most of the systems. The S atom on the Met81 and one of the pyridinium rings of the reactivator had strong electrostatic interactions. Further, lysine or arginine displayed unfavorable interactions with the reactivators in all the systems. The reactivator, lysine, and arginine are all positively charged and therefore repel each other.

Overall, we have used a variety of computational methods (TI, MM-GBSA, MM-PBSA, and normal mode analysis) to calculate binding free energies of various reactivators bound to inhibited systems: hAChE-sarin, hAChE-tabun, hBChE-sarin, hBChE-tabun, and uninhibited systems: hAChE and hBChE. The free energies calculated using TI were more accurate than the one estimated using other alternative

methods. We have also identified various active site residues participating in hydrogen bond, electrostatic, or π-π interactions with the reactivator.

6.2 Oximes as hydrolyzing agents

Ca1 and Ca2 were in coordination with O atom located at δ and ε positions on various active site residues in the Q192 and R192 polymorphs of hPON1. In Q192 + Cpo and R192 + Cpo systems, various conformers of Cpo were closely interacting with Tyr71 and Ile74. The O atom (P=O) of the Cpo was facing either towards or away from Ca1, in case of Q192 hPON1 + Cpo. In R192 + Cpo, various conformers of Cpo were interacting with either Ca1 or Ca2. Overall, Cpo was more tightly bound to Ca1 in R192 hPON1 than in Q192 hPON1.

Out of all the neutral oximes, 4-methylbenzaldehyde oxime and pinacolone oxime were found closest to Cpo in Q192 + Cpo system. The distance between the P atom of Cpo and the oxime O of 4-methylbenzaldehyde was 3.9 Å and in pinacolone oxime the distance was 4.5 Å. Similarly, in R192 + Cpo benzoquinone dioxime was closest to Cpo (4.1 Å). The neutral oximes containing aromatic rings have shown more favorable interactions with Cpo than the aliphatic ones. The neutral oximes have displayed more favorable interactions with Cpo in Q192 than with Cpo in R192.

Most of the monopyridinium oximes were found close to Ca1 in Q192 + Cpo. The ligands have interacted with Cpo or Ca2 in R192 + Cpo. All the monopyridinium oximes have shown more favorable interactions with Cpo in R192 + Cpo than in Q192 + Cpo. Various conformers of neutral oximes and monopyridinium oximes have exhibited interactions with Ca1 or Ca2 next to Cpo.

The relative deprotonation energies of the monopyridinium oxime and the oxime containing a quaternary ammonium were less than the corresponding value of the neutral oxime. Hence, the hydrolysis rate of monopyridinium oximes may be higher than the oximes containing quaternary amine and neutral oxime. This suggests that monopyridinium oximes can more effectively hydrolyze organophosphates than the neutral oximes. Finally, this study was useful to understand the binding interactions between the organophosphates and a variety of neutral and monopyridinium oximes bound to Q192 or R192 hPON1.

REFERENCES

1. Santos, C.S.A.; Monteiro, M.S.; Soares, M.V.M.; Loureiro, S. *PLoS ONE* **2012**, 7, 1-8.

2. Mahley, R.W. *Science* **1988**, 240, 622-630

3. Taylor, P.; Radic, Z.; Hosca, N.A.; Camp, S.; Marchot, P.; Berman, H.A. *Toxicol. Lett.* **1995**, 82-83, 453-458

4. Bajgar, J.; *Adv. Clin. Chem.* **2004**, 38, 151-216

5. Suzuki, T.; Morita, H.; Ono, K.; Maekawa, K.; Nagai, R.; Yazaki, Y. *Lancet* **1995**, 345, 980-980.

6. Nozaki, H.; Aikawa, N.; Fujishima, S.; Suzuki, M.; Shinozawa, Y.; Hori, S.; Nogawa, S. *Lancet* **1995**, 346, 698-699.

7. Okumura, T.; Takusa, N.; Ishimatsu, S.; Miyanoki, S.; Mitsuhashi, A.; Kumada, K.; Tanaka, K.; Hinohara, S. *Ann. Emerg. Med.* **1996**, 28, 129-135.

8. Strittmatter, W.J.; Saunders, A.M.; Schmechel, D.E.; Pericak-Vance, M.A.; Enghild, J.; Salvesen, G.S.; Roses, A.D. *Proc. Natl. Acad. Sci.* **1993**, 90, 1977-1981.

9. Corder, E.H.; Saunders, A.M.; Strittmatter, W.J.; Schmechel, D.E.; Gaskell, P.C.; Small, G.W.; Roses, A.D.; Haines, J.L.; Pericak-Vance, M.A. *Science* **1993**, 261, 921-923.

10. Sussman, J.L.; Harel, M.; Frolow, F.; Oefner, C.; Goldman, A.; Toker, L.; Silman, I. *Science* **1991**, 253, 955-979.

11. Harel, M.; Kleywetg, G.J.; Ravelli, R.B.; Silman, I.; Sussman, J.L. *Structure (Lond.)* **1995**, 3, 1355-1366.

12. Bourne, Y.; Taylor, P.; Marchot, P. *Cell.* **1995**, 83, 503-512.

13. Bourne, Y.; Taylor, P.; Bougis, P.E.; Marchot, P. *J. Biol. Chem.* **1999**, 274, 2963-2970.

14. Kryger, G.; Harel, M.; Giles, K.; Toker, L.; Velan, B.; Lazar, A.; Kronman, C.; Barak, D.; Ariel, N.; Shafferman, A.; Silman, I.; Sussman, J.L. *Acta Crystallogr. Sect. D. Biol. Crystallogr*. **2000**, 56, 1385-1394.

15. Nicolet, Y.; Lockridge, O.; Masson, P.; Fontecilla-Camps, J.C.; Nachon, F. *J. Biol. Chem.* **2003**, 278, 41141-41147.

16. Massoulié, J.; Sussman, J.; Bon, S.; Silman, I. *Prog. Brain Res.* **1993**, 98, 139-146.

17. Dale, H.H. *J. Pharmacol. Exp. Ther.* **1914**, 6, 147-190.

18. Rosenberry, T.L. *Adv. Enzymol., Relat. Areas Mol. Biol.* **1975**, 43, 103-218.

19. Lockridge, O.; Masson, P. *Neurotoxicology* **2000**, 21, 113-126.

20. Chatonnet, A.; Lockridge, O. *Biochem. J.* **1989**, 260, 625-634.

21. Lenz, D.E.; Maxwell, D.M.; Koplovitz, I.; Clark, C.R.; Capacio, B.R.; Cerasoli, D.M.; Federko, J.M.; Luo, C.; Saxena, A.; Doctor, B.P.; Olson, C. *Chem. Biol. Interact.* **2005**, 157C-158C, 205-210.

22. Fuchs, S.; Gurari, D.; Silman, I. *Arch. Biochem. Biophys.* **1974**, 165, 90-97.

23. Blumberg, S.; Silman, I. *Biochemistry* **1978**, 17, 1125-1130.

24. Goeldner, M.P., Hirth, C.G. *Proc. Natl. Acad. Sci. USA.* **1980**, 77, 6439-6442.

25. Page, J.D.; Wilson, I.B. *J. Biol. Chem.* **1985**, 260, 1475-1478.

26. Steitz, T.A.; Shulman, R.G. *Annu. Rev. Biophys. Bioeng.* **1982**, 11, 419-444.

27. Changeux, J.P. *Mol. Pharmacol.* **1966**, 2, 369-392.

28. Taylor, P.; Lappi, S. *Biochemistry* **1975**, 14, 1989-1997.

29. Bergmann, F.; Wilson, I.B.; Nachmansohn, D. *Biochim, Biophys. Acta.* **1950**, 6, 217-224.

30. Blow, D.M.; Birktoft, J.J.; Hartley, B.S. *Nature* **1969**, 221, 337-340.

31. Bachovchin, W.W.; Roberts, J.D. *J. Am. Chem. Soc.* **1978**, 100, 8041-8047.

32. Warshel, A.; Narayszabo, G.; Sussman, F.; Hwang, J.K. *Biochemistry* **1989**, 28, 3629-3637.

33. Fuxreiter, M.; Warshel, A. *J. Am. Chem. Soc.* **1998**, 120, 183-194.

34. Massiah, M.A.; Viragh, C.; Reddy, P.M.; Kovach, I.M.; Johnson, J.; Rosenberry, T.L.; Mildvan, A.S. *Biochemistry* **2001**, 40, 5682-5690.

35. Taylor, P.; Radic, Z. *Annu. Rev. Pharmacol. Toxicol.* **1994**, 34, 281-320.

36. Eyer, P. *Toxicol. Rev.* **2003**, 22, 165-190.

37. Bajgar, J.; Fusek, J.; Kassa, J.; Kuca, K.; Jun, D. *Curr. Med. Chem.* **2009**, 16, 2977-2986.

38. Tang, S.Y.H.; Chan, J.T.S. *Hong Kong J. Emerg. Med.* **2002**, 9, 83-89.

39. Antonijevic, B.; Stojiljkovic, M. *Clin. Med. Res.* **2006**, 5, 71-82

40. Robison, J.P., The Rise of CB Weapons, Vol. 1, Problem of Chemical and Biological Warfare, *Almqvist & Wiksell* **1971**.

41. Harris, R.; Paxman, J., A Higher Form of Killing: The Secret Story of Chemical and Biological Warfare, New York, NY: *Hill and Wang* **1982**.

42. Karczmar, A.G.; Usdin, E.; Wills, J.H., Anticholinesterase agents,1st edition Oxford, *Pergamon Press* **1970**.

43. MacPhee-Quigley, K.; Taylor, S. *J. Biol. Chem.* **1985**, 260, 12185-12189.

44. MaciIwain, C.; *Nature* **1993**, 363, 3.

45. Nagao, M.; Takatori, T.; Matsuda, Y.; Nakajima, M.; Iwase, H.; Iwadate, K. *Toxicol. Appl. Pharmacol.* **1997**, 144, 198-203.

46. Bakshi, K.S.; Pang, S.N.J.; Snyder, R. *J. Toxicol. Environ. Health A* **2000**, 59, 282-283.

47. Bismuth, C.; Inns, R.H.; Marris, T.C., Efficacy, toxicity and clinical use of oximes in anticholinesterase poisoning. In: Ballantyne B., Marrs, T.C., editors. Clinical and experimental toxicology of organophosphates and carbmates. Oxford: *Butterworth-Heinemann, Ltd.* **1992**.

48. Ngo, M.A.; O'Malley, M.; Maibach, H.I. *J. Appl. Toxicol.* **2010**, 30, 91-114.

49. Soukup, O.; Tobin, G.; Kumar, U.K.; Binder, J.; Jun, D.; Fusek, J.; Kuca, K. *Curr. Med. Chem.* **2010**, 17, 1708-1718.

50. Cohen, J.A.; Oosterbaan, R.A., The active site of acetylcholinesterase and related esterases and its reactivity towards substrates and inhibitors, Cholinesterases and Anticholinesterase Agents, G.B. Koelle, *Springer, Berlin* **1963**.

51. Karasova, J.Z.; Bajgar, J.; Novotny, L.; Kuca, K. *J. Appl. Biomed.* **2009**, 7, 93-99.

52. Delfino, R.T.; Riberio, T.S.; Figueroa,-Villar, J.D. *J. Braz. Chem. Soc.* **2009**, 20, 407-428.

53. Benschop, H.P.; Keijer, J.H. *Biochim. Biophys. Acta*. **1966**, 128, 586-588.

54. Viragh, C.; Kovach, I.M.; Pannell, L. *Biochemistry* **1999**, 38, 9557-9561.

55. Wong, L.; Radic, Z.; Bruggemann, R.J.M.; Hosea, N.; Berman, H.A.; Taylor, P. *Biochemistry* **2000**, 39, 5750-5757.

56. Bartling, A.; Worek, F.; Szinicz, L.; Theirmann, H. *Toxicology* **2007**, 233, 166-172.

57. Kuca, K.; Jun, D.; Musilek, K. *Mini Rev. Med. Chem.* **2006**, 6, 269-277.

58. Karasova, J.Z.; Kassa, J.; Jung, Y.S.; Musilek, K.; Pohanka, M.; Kuca, K. *Intl. J. Mol. Sci*. **2008**, 9, 2243-2252.

59. Aebersold, R.; Mann, M. *Nature* **2003**, 422, 198-207.

60. Childs, A.F.; Davies, D.R.; Green, A.L.; Rutland, I.P. *Br. J. Pharmacol*. **1955**, 10, 462-465.

61. Wilson, I.B.; Ginsburg, S.; Meislich, E.K. *J. Am. Chem. Assoc.* **1955**, 77, 4286-4291.

62. Worek, F.; Kirchner, T.; Backer, M.; Szinicz, L. *Arch. Toxicol.* **1996**, 70, 497-503.

63. Worek, F.; Eyer, P.; Kiderlen, D.; Thiermann, H.; Szinicz, L. *Arch. Toxicol.* **2000**, 71, 21-26.

64. Worek, F.; Reiter, G.; Eyer, P.; Szinicz, L. *Arch. Toxicol.* **2002**, 76, 523-529.

65. Kuca, K.; Kassa, J. *J. Enzyme Inhibition and Med. Chem.* **2003**, 18, 529-535.

66. Poziomek, E.J.; Hackley, B.E. Jr; Streinberg, G.M. *J. Org. Chem.* **1958**, 23, 714-717.

67. Paddle, B.M.; Dowling, M.H. *J. Chromatogr.* **1993**, 648, 373-380.

68.   Rousseaux, C.G.; Dua, A.K. *J. Physio. Pharm.* **1989**, 67, 1183-1189.

69.   Koplovitz, I.; Stewart, J.R. *Toxicol. Lett.* **1994**, 70, 269-279.

70.   Eyer, P. *Arch. of Toxicol.* **1992**, 66, 603-621.

71.   Romano Jr., J.A.; Lukey, B.J.; Salem, H., Chemical Warfare Agents, Chemistry, Pharmacology, Toxicology, and Therapeutics, 2nd edition, *CRC Press, New York* **2007**.

72.   Bajgar, J.; Kuca, K.; Fusek, J.; Jun, D.; Bartosova, L. *Curr. Bioactive Comp.* **2010**, 6, 2-8.

73.   Lundy, P.M.; Hamilton, M.G.; Sawyer, T.W.; Mikler, J. *Toxicology* **2011**, 285, 90-96.

74.   Dawson, R.M. *J. Appl. Toxicol.* **1994**, 14, 317-331.

75.   Wang, J.; Gu, J.; Leszczynski, J.; Feliks, M.; Sokalski, W.A. *J. Phys. Chem. B.* **2007**, 111, 2404-2408.

76.   Li, Y.; Sun, X.; Du, L.; Zhang, Q.; Wang, W. *Comp. Theo. Chem.* **2012**, 980, 108-114.

77.   Worek, F.; Szinicz, L. *Pharma. Toxicol.* **1993**, 72, 13-21.

78.   Kassa, J. *Toxicology* **1995**, 101, 167-174.

79.   Maxwell, D.M.; Brecht, K.M.; Koplovitz, I. *J. Am. College Toxicol.* **1996**, 15(Suppl.2), S78-S88.

80.   Kuca, K.; Kassa, J. *Hum. Expt. Toxicol.* **2004**, 23, 167-171.

81.   Kunesova, G.K.; Bartosova, L.; Kuca, K. *Toxicology* **2005**, 216, 32-40.

82.   Worek, F.; Szinicz, L.; Thiermann, H. *Chem. Bio. Inter.* **2005**, 157-158, 349-352.

83.   Luo, C.; Tong, M.; Chilukuri, N.; Brecht, K.; Maxwell, D.M.; Saxena, A. *Biochemistry* **2007**, 46, 11771-11779.

84.   Worek, F.; Thiermann, H.; Szinicz, L.; Eyer, P. *Biochem. Pharmacol.* **2004**, 68, 2237-2248.

85.   Wilson, I.B.; Sondheimer, F. *Arch. Biochem. Biophys.* **1957**, 69, 468-474.

86. Kuca, K.; Jun, D.; Bajgar, J. *Drug Chem. Toxicol.* **2007**, 30, 31-40.

87. Kovarik, Z.; Katalinic, M.; Bosak, A.; Sinko, G. *Curr. Bioactive Comp.* **2010**, 6, 9-15.

88. Worek, F.; Wildmann, R.; Knoff, O.; Szinicz, L. *Arch. Toxicol.* **1998**, 72, 237-243.

89. Eyer, P.; Hell W.; Kawan, A.; Klehr, H. *Arch. Toxicol.* **1986**, 59, 266-271.

90. Eyer, P.; Ladstetter, B.; Schaffer, W.; Sonnenbichler, J. *Arch. Toxicol.* **1989**, 63, 59-67.

91. Luo, C.; Chambers, C.; Tong, Y.; Saxena, A. *Chem. Biol. Interact.* **2010**, 187, 185-190.

92. Luo, C.; Chambers, C.; Pattabiraman, N.; Tong, M.; Tipparaju, P.; Saxena, A. *Biochem. Pharmacol*. **2010**, 80, 1427-1436.

93. Luo, C.; Tong, M.; Maxwell, D.M.; Saxena, A. *Chemico-Biological Interactions* **2008**, 175, 261-266.

94. Worek, F.; Wille, T.; Aurbek, N.; Eyer, P.; Therimann, H. *Toxicol. Appl. Pharma.* **2010**, 249, 231-237.

95. Worek, F.; Aurbek, N.; Wille, T.; Eyer, P.; Thiermann, H. *Toxicol. Lett.* **2011**, 200, 19-23.

96. Sakurada, K.; Matsubara, K.; Shimizu, K.; Shiono, H.; Seto, Y.; Tsuge, K.; Yoshino, M.; Sakai, I.; Mukoyama, H.; Takatori, T. *Neurochem. Res.* **2003**, 28, 1401-1407.

97. Kassa, J.; Cabal, J. *J. Pharm. Toxicol*. **1999**, 84, 41-45.

98. Kassa, J.; Cabal, J. *Hum. Exp. Toxicol.* **1999**, 18, 560-565.

99. Worek, F.; Diepold, C.; Eyer, P. *Arch. Toxicol.* **1999**, 73, 7-14.

100. Kuca, K.; Patocka, J. *J. Enzyme Inhib. Med. Chem.* **2004**, 19, 39-43.

101. Primo-Parmo, S.L.; Sorenson, R.C.; Teiber, J.; La Du, B.N. *Genomics* **1996**, 3, 498-507.

102. Zielaskowska, J.; Olszewska-Slonina, D. *Adv. Clin. Exp. Medicine* **2006**, 15, 1073-1078.

103. Hassett, C.; Richter, R.J.; Humbert, R.; Chapline, C.; Crabb, J.W.; Omiecinski, C.J.; Furlong, C.E. *Biochemistry* **1991**, 30, 10141-10149.

104. Harel, M.; Aharoni, A.; Leonid, G.; Brumshtein, B.; Khersonsky, O.; Meged, R.; Dvir, H.; Ravelli, R.B.G.; McCarthy, A.; Toker, L.; Silman, I.; Sussman, J.L.; Tawik, D.S. *Nature Stru. Mol. Bio*. **2004**, 11, 412-419.

105. Furlong, C.E.; Richter, R.J.; Seidel, S.J.; Costa, L.G.; Motulsky, A.G. *Anal. Biochem.* **1989**, 180, 242-247.

106. Smolen, A.; Eckerson, H.W.; Gan, K.N.; Hailat, N.; La Du, B.N. *Drug Metab. Dispos.* **1991**, 19, 107-112.

107. Davies, H.; Richter, R.J.; Keifer, M.; Broomfield, C.; Sowalla, J.; Furlong, C.E. *Nature Genet.* **1996**, 14, 334-336.

108. Kitchen, B.J.; Masters, C.J.; Winzor, D.J. *Biochem. J.* **1973**, 135, 93-99.

109. Don, M.M.; Masters, C.J.; Winzor, D.J. *Biochem. J.* **1975**, 151, 625-630.

110. Mackness, M.I.; Walker, C.H. *Biochem. J.* **1988**, 250, 539-545.

111. Gadiukov, L.; Tawfik, D.S. *Biochemistry* **2005**, 44, 11843-11854.

112. Gadiukov, L.; Rosenblat, M.; Aviram, M.; Tawfik, D.S. *J. Lipid Res.* **2006**, 47, 2492-2502.

113. Mackness, M.I.; Abbott, C.A.; Arrol, S.; Durrington, P.N. *Biochem. J.* **1993**, 294, 829-834.

114. Mackness, M.I.; Arrol, S.; Abbott, C.A.; Durrington, P.N. *Atherosclerosis* **1993**, 104, 129-135.

115. Rosenblat, M.; Gaidukov, L.; Khersonsky, O.; Vaya, J.; Tawfik, D.S.; Aviram, M. *J. Biol. Chem.* **2006**, 281, 7657-7665.

116. Gupta, N.; Singh, S.; Matura, V.N.; Sharma, Y.P.; Gill, K.D. *PLoS ONE* **2011**, 6, 1-9.

117. Aldridge, W.N. *Biochem. J.* **1953**, 53, 110-117.

118. Aldridge, W.N. *Biochem. J.* **1953**, 53, 117-124.
119. Uriel, J. *Ann. Inst. Pasteur (Paris)* **1961**, 101, 104-119.

120. Khersonsky, O.; Tawfik, D.S. *Biochemistry* **2005**, 44, 6371-6382.

121. Draganov, D.I.; Telber, J.F.; Speelman, A.; Osawa, Y.; Sunahara, R.; La Du, B.N. *J. Lipid Res.* **2005**, 46, 1239-1247.

122. Otto, T.C.; Harsch, C.K.; Yeung, D.T.; Magliery, T.J.; Cerasoli, D.M.; Lenz, D.E. *Biochemistry* **2009**, 48, 10416-10422.

123. Muthukrishnan, S.; Shete, V.S.; Sanan, T.T.; Vyas, S.; Oottikal, S.; Porter, L.M.; Magliery, T.J.; Hadad, C.M. *J. Phys. Org. Chem.* **2012**, 25, 1247-1260.

124. Brophy, V.H.; Jarvik, G.P.; Richter, R.J.; Rozek, L.S.; Schellenberg, G.D.; Furlong, C.E. *Pharmacogenetics* **2000**, 10, 453-460.

125. Balcerzyk, A.; Zak, I.; Krauze, J. *Arch. Med. Res.* **2007**, 38, 545-550.

126. Jansen, K.L.; Cole, T.B.; Park, S.S.; Furlong, C.E.; Costa, L.G. *Toxixol. Appl. Pharma.* **2009**, 236, 142-153.

127. Gencer, N.; Arslan, O. *Fresenius Envir. Bull.* **2011**, 20, 590-596.

128. David, M.B.; Eilas, M.; Filippi, J.J.; Dunach, E.; Silman, I.; Sussman, J.L.; Tawfik, D.S. *J. Mol. Biol.* **2012**, 418, 181-196.

129. Nguyen, S.D.; Sok, D.E. *Biochem. J.* **2003**, 375, 275-285.

130. Adkins, S.; Gan, K.N.; Mody, M.; La Du, B.N. *Am. J. Hum. Genet.* **1993**, 52, 598-608.

131. Josse, D.; Lockridge, O.; Xie, W.; Bartels, C.F.; Schopfer, L.M.; Masson, P. *J. Appl. Toxicol.* **2001**, 21, S7-S11.

132. Lawlor, D.A.; Day, I.N.M.; Gaunt, T.R.; Hinks, L.J.; Timpson, N.; Ebrahim, S.; Smith, G.D. *J. Epidemiol. Community Health* **2007**, 61, 85-87.

133. Blum, M.; Koglin, A.; Ruterjans, H.; Schoenborn, P.; Langan, P.; Chen, J.C.H. *Acta. Cryst.* **2007**, F46, 42-44.

134. Blum, M.; Timperley, C.M.; Williams, G.R.; Thiermann, H.; Worek, F. *Biochemistry* **2008**, 47, 5216-5224.

135. Blum, M.; Mustyakimov, M.; Ruterjans, H.; Kehe, K.; Schoenborn, B.P.; Langan, P.; Chen, J.C.H. *Proc. Natl. Acad. Sci. USA* **2009**, 106, 713-718.

136. Worek, F.; Eyer, P.; Szinicz, L. *Arch. Toxicol.* **1998**, 72, 996-998.

137. Sanan, T.T.; Muthukrishnan, S.; Beck, J.M.; Tao, P.; Hayes, C.J.; Otto, T.; Cerasoli, D.M.; Lenz, D.; Hadad, C.M. *J. Phys. Org. Chem.* **2010**, 23, 357-369.

138.   Wang, W.; Kollman, P.A. *PNAS* **2001**, 98, 14937-14942.

139.   Muller-Plathe, F. *Chem. Phys. Chem.* **2002**, 3, 754-769.

140.   Paolini, G.V.; Shapland, R.H.B.; Van Hoorn, W.P.; Mason, J.S.; Hopkins, A.L. *Nature Biotech.* **2006**, 24, 805-815.

141.   Samanta, A.; Appelo, D.; Colonius, T.; Nott, J.; Hall, J. *AIAA Journal* **2010**, 48, 1007-1016.

142.   Oyanagi, Y. *J. Comp. Appl. Math.* **2002**, 149, 147-153.

143.   Strohmaier, E.; Dongarra, J.J.; Meuer, H.W.; Simon, H.D. *Parallel Comp.* **2005**, 31, 261-273.

144.   Mackerell Jr., A.D.; Bashford, D.; Bellott, M.; Dunbrack Jr., R.L.; Evanseck, J.D.; Field, M.J.; Fischer, S.; Gao, J.; Guo, H.; Ha, S.; Joseph-MacCarthy, D.; Kuchnir, L.; Kuczera, K.; Lau, F.T.K.; Mattos, C.; Michnick, S.; Ngo, T.; Ngygen, D.T.; Prodhom, B.; Reiher III, W.E.; Roux, B.; Schlenkrich, M.; Smith, J.C.; Stote, R.; Straub, J.; Watanbe, M.; Wiorkiewicz-Kuczera, J.; Yin, D.; Karplus, M. *J. Phys. Chem.* **1998**, 102, 3586-3616.

145.   Lindahl, E.; Hess, B.; van der Spoel, D. *J. Mol. Modeling* **2001**, 7, 306-317.

146.   Bursulaya, B.D.; Totrov, M.; Abagyan, R.; Brooks III, C.L. *J. Computer-Aided Mol. Design* **2003**, 17, 755-763.

147.   Dunning Jr. T.H. *J. Chem. Phys*. **1970**, 53, 2823-2833.

148.   Rienstra-Kiracofe, J.C.; Tschumper, G.S.; Schaefer III, H.F.; Nandi, S.; Eillson, G.B. *Chem. Rev.* **2002**, 102, 231-282

149.   Snow, C.D.; Nguyen, H.; Pande, V.S.; Gruebele, M. *Nature* **2002**, 420, 102-106.

150.   Feng, Y.; Liu, L.; Wang, J.T.; Huang, H.; Guo, Q.X. *J. Chem. Info. Comp. Sci.* **2003**, 43, 2005-2013.

151. "Advances in quantum chemical methods and algorithms in the Q-Chem 3.0 program package", Shao, Y.; Molnar, L.F.; Jung, Y.; Kussmann, J.; Ochsenfeld, C.; Brown, S.T.; Gilbert, A.T.B.; Slipchenko, L.V.; Levchenko, S.V.; O'Neill, D.P.; DiStasio Jr., R.A.; Lochan, R.C.; Wang, T.; Beran, G.J.O.; Besley, N.A.; Herbert, J.M.; Lin, C.H.; Voorhis, T.V.; Chien, S.H.; Sodt, A.; Steele, R.P.; Rassolov, V.A.; Maslen, P.E.; Korambath, P.P.; Adamson, R.D.; Austin, B.; Baker, J.; Byrd, E.F.C.; Daschel, H.; Doerksen, R.J.; Dreuw, A.; Dunietz, B.D.; Dutoi, A.D.; Furlani, T.R.; Gwaltney, S.R.; Heyden, A.; Hirata, S.; Hsu, C.P.; Kedziora, G.; Khaliullin, R.Z.; Klunzinger, P.; Lee, A.M.; Lee, M.S.; Liang, W.; Lotan, I.; Nair, N.; Peters, B.; Proynov, E.I.; Pieniazek, P.A.; Rhee, Y.M.; Ritchie, J.; Rosta, E.; Sherrill, C.D.; Simmonett, A.C.; Subotnik, J.E.; Woodcock III, H.E.; Zhang, W.; Bell, A.T.; Chakraborty, A.K.; Chipman, D.M.; Keil, F.J.; Warshel, A.; Hehre, W.J.; Schaefer III, H.F.; Kong, J.; Krylov, A.I.; Gill, P.M.W.; Head-Gordon, M. *Phys. Chem. Chem. Phys.* **2006**, 8, 3172-3191.

152. Wang, J.; Morin, P.; Wang, W.; Kollman, P.A. *J. Am. Chem. Soc*. **2001**, 123, 5221-5230.

153. Mongan, J.; Case, D.A.; Mccammon, J.A. *J. Comp. Chem.* **2004**, 25, 2038-2048.

154. Van Der Ploeg, P.; Berendsen, H.J.C. *J. Chem. Phys.* **1982**, 76, 3271-3276.

155. Breneche, S.; Roux, B. *Biophys. J.* **2000**, 78, 2900-2917.

156. Wang, W.; Donini, O.; Reyes, C.M.; Kollman, P.A. *Annual Reviews of Biophys. Biomol. Struct.* **2001**, 30, 211-243.

157. Roux, B.; Allen, T.; Berneche, S.; Im, W. *Quarterly Reviews of Biophy.* **2004**, 37, 15-103.

158. Beck, D.A.C.; Jonsson, A.L.; Schaeffer, R.D.; Scott, K.A.; Day, R.; Toofanny, R.D.; Alonso, D.O.V.; Daggett, V. *Protein Engg. Design and Selection* **2008**, 21, 353-368.

159. Cordomi, A.; Caltabiano, G.; Pardo, L. *J. Chem. Theory Comput.*, **2012**, 8, 948-958.

160. Alder, B.J.; Wainwright, T.E. *J. Chem. Phys*. **1957**, 27, 1208-1209.

161. Alder, B.J.; Wainwright, T.E. *J. Chem. Phys.* **1959**, 31, 459-467.

162. McCammon, J.A.; Gelin, B.R.; Karplus, M. *Nature* **1977**, 267, 585-590.

163. Lim, T.C. *J. Math. Chem.* **2007**, 41, 381-391.

164. Wu, M.Y.; Dai, D.Q.; Yan, H. *Prot. Struct. Function and Bioinf.* **2012**, 80, 2137-2153.

165. Lim, T.C. *Zeitschrift fur Naturforschung-Section A J. Phys. Sci.* **2003**, 58, 615-617.

166. Gonzalez, C.; Bernhard Schlegel, H. *J. Chem. Phys.* **1989**, 90, 2154-2161.

167. Kresse, G.; Furthmuller, J. *Comp. Material Sci.* **1996**, 6, 15-50.

168. Celani, P.; Robb, M.A.; Garavelli, M.; Bernardi, F.; Olvucci, M. *Chem. Phys. Lett.* **1995**, 243, 1-8.

169. Leach, A.R., Molecular Modelling: Principles and Applications, 2nd edition, *Pearson* **2010**.

170. Tironi, I.G.; Sperb, R.; Smith, P.E.; Van Gunsteren, W.F. *J. Chem. Phys.* **1995**, 102, 5451-5459.

171. Anezo, C.; De Vries, A.H.; Holtje, H.D.; Tieleman, D.P.; Marrink, S.J. *J. Phys. Chem. B* **2003**, 107, 9424-9433.

172. Schnieders, M.J.; Fenn, T.D.; Pande, V.S. *J. Chem. Theory and Comput.* **2011**, 7, 1141-1156.

173. Norberg, J.; Nilsson, L. *Biophysical J.* **2000**, 79, 1537-1553.

174. Darden, T.; York, D.; Pedersen, L. *J. Chem. Phys.* **1993**, 98, 10089-10092.

175. Essmann, U.; Perera, L.; Berkowitz, M.L.; Darden, T.; Lee, H.; Pedersen, L.G. *J. Chem. Phys.* **1995**, 103, 8577-8593.

176. Verlet, L. *Phys. Rev.* **1967**, 159, 98-103.

177. Hockney, R.W. *Methods in Comp. Phys.* **1970**, 9, 136-211.

178. Swope, W.C.; Anderson, H.C.; Berens, P.H.; Wilson, K.R. *J. Chem. Phys.* **1982**, 76, 637-649.

179. Beeman, D. *J. Comp. Phys.* **1976**, 20, 130-139.

180. Berendsen, H.J.C.; Postma, J.P.M.; Van Gunsteren, W.F.; DiNola, A.; Haak, J.R. *J. Chem. Phys.* **1984**, 81, 3684-3690.

181. Feller, S.E.; Zhang, Y.; Pastor, R.W.; Brooks, B.R. *J. Chem. Phys.* **1995**, 103, 4613-4621.

182. Evans, D.J.; Holian, B.L. *J. Chem. Phys.* **1985**, 83, 4069-4074.

183. Zwanzig, R.W. *J. Chem. Phys.* **1954**, 22, 1420-1426.

184. Hummer, G.; Szabo, A.J. *J. Chem. Phys.* **1996**, 105, 2004-2010.

185. Simonoson, T.; Free energy calculations. In Computational Biochemistry and Biophysics, Becker, O., MacKereell, A.D., Roux, B., Watanabe, M., New York, *Marcel Dekker* **2001**.

186. Singh, N.; Warshel, A. *Proteins* **2010**, 15, 1705-1723.

187. Simonson, T. *Rep. Prog. Phys.* **2003**, 66, 737-787.

188. Cortis, C.; Friesner, R.A. *J. Comput. Chem.* **1997**, 18, 1570-1590.

189. Fogolari, F.; Brigo, A.; Molinari, H. *J. Mol. Recognit.* **2002**, 15, 377-392.

190. Zhang, L.Y.; Gallicchio, E.; Friesner, R.A.; Levy, R.M. *J. Comp. Chem.* **2001**, 22, 591-607.

191. Born, M. *Zeitschrift Für Physik* **1920**, 1, 45-48.

192. Constanciel, R.; Contreras, R. *Theor. Chim. Acta.* **1984**, 65, 1-11.

193. Huo, T.; Wang, J.; Li, Y.; Wang, W. *J. Chem. Info. Modeling* **2011**, 51, 69-82.

194. Simonson, T. *Rep. Prog. Phys.* **2003**, 66, 737-787.

195. Lee, M.S; Feig, M.; Salsbury Jr., F.R.; Brooks III, C.L. *J. Comp. Chem.* **2003**, 24, 1358-1356.

196. Sitkoff, D.; Sharp, K.A.; Honig, B. *J. Phys. Chem.* **1994**, 98, 1978-1988.

197. Tan, C.H.; Tan, Y.H.; Luo, R. *J. Phys. Chem. B.* **2007**, 111, 12263-12274.

198. Zaccai, G. *Science* **2000**, 288, 1604-1607.

199. Goh, C.S.; Milburn, D.; Gerstein, M. *Cuur. Opin. Struc. Biol.* **2004**, 14, 1-6.

200. Amemiya, T.; Koike, R.; Kidera, A.; Ota, M. *Nucleic Acids Res.* **2012**, 40, D554-D558.

201. Pierce, L.C.T.; Salomon-Ferrer, R.; De Oliveira, C.A.F.; McCammon, J.A.; Walker, R.C. *J. Chem. Theory and Comp*. **2012**, 8, 2997-3002.

202. Tomic, A.; Gonzalez, M.; Tomic, S. *J. Chem. Info. Model*. **2012**, 52, 1583-1594.

203. Spirko, V.; Sponer, J.; Hobza, P. *J. Chem. Phys.* **1997**, 106, 1472-1479.

204. Cui, Q.; Li, G.; Ma, J.; Karplus, M. *J. Mol. Biol.* **2004**, 340, 345-372.

205. Chu, J.W.; Voth, G.A. *Biophys. J.* **2006**, 90, 1572-1582.

206. Dominguez, C.; Boelens, R.; Bonvin, A.M.J.J. *J. Am. Chem. Soc.* **2003**, 125, 1731-1737.

207. Laurie, A.T.R.; Jackson, R.M. *Bioinformatics* **2005**, 21, 1908-1916.

208. Viji, S.N.; Balaji, N.; Gautham, N. *J. Mol. Mod.* **2012**, 18, 3705-3722.

209. Taylor, R.D.; Jewsbury, P.J.; Essex, J.W. *J. Comput. Aided Mol. Des.* **2002**, 16, 151-166.

210. Wang, R.; Lai, L.; Wang, S. *J. Comp. Aided Mol. Design* **2002**, 16, 11-26.

211. Clark, R.D.; Strizhev, A.; Leonard, J.M.; Blake, J.F.; Mathhew, J.B. *J. Mol. Grap. Mod.* **2002**, 20, 281-295.

212. Verdonk, M.L.; Cole, J.C.; Hartshorn, M.J.; Murray, C.W.; Taylor, R.D. *Proteins: Struc. Func. Gene.* **2003**, 52, 609-623.

213. Warren, G.L.; Andrews, C.W.; Capelli, A.M.; Clarke, B.; LaLonde, J.; Lambert, M.H.; Lindvall. M.; Nevins, N.; Semus, S.F.; Senger, S.; Tedesco, G.; Wall, I.D.; Woolven, J.M.; Peishoff, C.E.; Head, M.S. *J. Med. Chem.* **2006**, 49, 5912-5931.

214. Trott, O. Olson, A.J. *J. Comput. Chem.* **2010**, 31, 455-461.

215. Pierce, B.G.; Hourai, Y.; Weng, Z. *PLoS ONE* **2011**, 6, e24657.

216. Chowdhury, R.; Rasheed, M.; Keidel, D.; Moussalem, M.; Olson, A.; Sanner, M.; Bajaj, C. *PLoS ONE* **2013**, 8, e51307.

217. Kang, L.; Li, H.; Jiang, H.; Wang, X. *J. Comp. Aided Mol. Design* **2009**, 23, 1-12.

218. Cavasotto, C.N.; Abagyan, R.A. *J. Mol. Biol.* **2004**, 337, 209-225.

219. Charifson, P.S.; Corkey, J.J.; Murcko, M.A.; Walters, W.P. *J. Med. Chem.* **1999**, 42, 5100-5109.

220. Gray, J.J.; Moughon, S.; Wang, C.; Schueler-Furman, O.; Kuhlman, B.; Rohl, C.A.; Baker, D. *J. Mol. Biol.* **2003**, 331, 281-299.

221. Jiang, F.; Kim, S.H. *J. Mol. Biol.* **1991**, 219, 79-102.

222. Ferrari, A.M.; Wei, B.Q.; Costantino, L.; Shoichet, B.K. *J. Med. Chem.* **2004**, 47, 5076-5084.

223. Halperin, I.; Ma, B.; Wolfson, H.; Nussinov, R. *Proteins: Struct. Func. Gene*. **2002**, 47, 409-443.

224. Sherman, W.; Day, T.; Jacobson, M.P.; Friesner, R.A.; Farid, R. *J. Med. Chem.* **2006**, 49, 534-553.

225. Leach, A.R. *J. Mol. Biol.* **1994**, 235, 245-356.

226. Desmet, J.; Maeyer, M.D.; Hazes, B.; Lasters, I. *Nature* **1994**, 356, 539-542.

227. Carlson, H.A.; McCammon, J.A. *Mol. Pharmacol.* **2000**, 57, 213-218.

228. Carlson, H.A. *Curr. Pharm. Des.* **2002**, 8, 1571-1578.

229. Teodoro, M.L.; Kavraki, L.E. *Curr. Pharm. Des.* **2003**, 9, 1635-1648.

230. Claussen, H.; Buning, C.; Rarey, M.; Lengauer, T. *J. Mol. Biol.* **2001**, 308, 377-395.

231. Wei, B.Q.; Weaver, L.H.; Ferrari, A.M.; Matthews, B.W.; Shoichet, B.K. *J. Mol. Biol.* **2004**, 337, 1161-1182.

232. Kroemer, R.T. *Curr. Prot. Peptide Sci.* **2007**, 8, 312-328.

233. McMartin, C.; Bohacek, R.S. *J. Comput. Aided Mol. Des.* **1997**, 11, 333-344.

234. Ventakachalam, C.M.; Jiang, X.; Oldfield, T.; Waldman, M. *J. Mol. Grap. Mod.* **2003**, 21, 289-307.

235. Dixon, J.S.; Oshiro, C.M. *J. Comput. Aided Mol. Des.* **1995**, 9, 113-130.

236. Morris, G.M.; Goodsell, D.S.; Halliday, R.S.; Huey, R.; Hart, W.E.; Belew, R.K.; Olson, A.J. *J. Comp. Chem.* **1998**, 19, 1639-1662.

237. Kitchen, D.B.; Decornez, H.; Furr, J.R.; Bajorath, J. *Nature Rev.* **2004**, 3, 935-949.

238. Meng, E.C. Shoichet, B.K. Kuntz, I.D. *J. Comput. Chem.* **1992**, 13, 504-524.

239. Huang, N.; Kalyanaraman, C.; Irwin, J.J.; Jacobson, M.P. *J. Chem. Inf. Model.* **2006**, 46, 243-253.

240. Bohm, H.J. *J. Comput. Aided Mol. Des.* **1992**, 6, 593-606.

241. Tanaka, S.; Scheraga, H.A. *Macromolecules* **1976**, 9, 945-950.

242. Miyazawa, S.; Jernigan, R.L. *Macromolecules* **1985**, 18, 534-552.

243. Sippl, M.J. *J. Mol. Biol.* **1990**, 213, 859-883.

244. Huang, S.Y.; Zou, X. *Annu. Rep. Comput. Chem.* **2010**, 6, 281-296.

245. Kryger, G.; Harel, M.; Giles, K.; Toker, L.; Velan, B.; Lazar, A.; Kronman, C.; Barak, D.; Ariel, N.; Shafferman, A.; Silman, I.; Sussman, J.L. *Acta Cryst. Sec. D.* **2000**, 56, 1385-1394.

246. Nicolet, Y.; Lockridge, O.; Masson, P.; Fontecilla-Camps, J.C.; Nachon, F. *J. Biol. Chem.* **2003**, 278, 41141-41147.

247. www.pdb.org

248. Case, D.A.; Darden, T.A.; Cheatham, III, T.E.; Simmerling, C.L.; Wang, J.; Duke, R.E.; Luo, R.; Merz, K.M.; Wang, B.; Pearlman, D.A.; Crowley, M.; Brozell, S.; Tsui, V.; Gohlke, H.; Mongan, J.; Hornak, V.; Cui, G.; Beroza, P.; Schafmesiter, C.; Caldwell, J.W.; Ross, W.S.; Kollman, P.A. **2004**, AMBER 8, University of California, San Francisco.

249. Wang, J.M.; Cieplak, P.; Kollman, P.A. *J. Comp. Chem.* **2000**, 21, 1049-1074.

250. Anandkrishnan, R.; Aguilar, B.; Onufriev, A.V. *Nuc. Acids Res.* **2012**, 40, 537-541.

251. Myers, J.; Grothaus, G.; Narayanan, S.; Onufriev, A. *Proteins* **2006**, 63, 928-938.

252. Dewar, M. J. S.; Zoebisch, Z.; Healy, E. F.; Stewart, J. J. P. *J. Am. Chem. Soc.*, **1985**, 107, 3902-3909.

253. Bayly, C.I.; Cieplak, P.; Cornell, W.D.; Kollman, P.A. *J. Phys. Chem.* **1993**, 97, 10269-10280.

254. Morris, G.M.; Huey, R.; Lindstrom, W.; Sanner, M.F.; Belew, R.K.; Goodsell, D.S.; Olson, A.J. *J. Comp. Chem.* **2009**, 30, 2785-2791.

255. Humphrey, W.; Dalke, A.; Schulten, A. *J. Molec. Graphics* **1996**, 14, 33-38.

256. Wang, J.M.; Wolf, R.M.; Caldwell, J.W.; Kollman, P.A.; Case, D.A. *J. Comput. Chem.* **2004**, 25, 1157-1174.

257. Jorgensen, W.L.; Chandrasekhar, J.; Madura, J.D.; Impey, R.W.; Klein, M.L. *J. Chem. Phys.* **1983**, 79, 926-935.

258. Miyamoto, S.; Kollman, P.A. *J. Comput. Chem.* **1992**, 13, 952-962.

259. Rychaert, J.P.; Ciccotti, G.; Berendsen, H.J.C. *J. Comput. Phys.* **1977**, 23, 327-341.

260. Darden, T.; York, D.; Pedersen, L. *J. Chem. Phys.* **1993**, 98, 10089-10092.

261. Essmann, U.; Perera, L.; Berkowitz, M.L.; Darden, T.; Lee, H.; Pedersen, L.G. *J. Chem. Phys.* **1995**, 103, 8577-8593.

262. Crowley, M.F.; Darden, T.A.; Cheatham, T.E. III; Deerfield, D.W. II *J. Supercomput.* **1997**, 11, 255-278.

263. http://ambermd.org/tutorials/advanced/tutorial6

264. Bartling, A., Worek, F., Szinicz, L., Thiermann, H. *Toxicology* **2007**, 233, 166-172.

265. Aurbek, A., Thiermann, H., Eyer, F., Eyer, P., Worek, F. *Toxicology* **2009**, 259, 133-139.

266. Worek, F., Wille, T., Aurbek, N., Eyer, P., Thiermann, H. *Toxicol. Appl. Pharm.* **2010**, 249, 231-237.

267. Worek, F., Wille, T., Koller, M., Thiermann, H. *Biochem. Pharm.* **2012**, 83, 1700-1706.

268. Gilson, M.K., Given, J.A., Bush, B.L., McCammon, J.A. *J. Biophys.* **1997**, 72, 1047-1069.

269. General, I.G. *J. Chem. Theory Comput*. **2010**, 6, 2520-2524.

270. Dang, L.X., Merz Jr., K.M., Kollman, P.A. *J. Am. Chem. Soc.* **1989**, 111, 8505-8508.

271. Singh, S.B., Ajay, Wemmer, D.E., Kollman, P.A. *PNAS* **1994**, 91, 7673-7677.

272. Helms, V. and Wade, R.C. *J. Comp. Chem.* **1997**, 18, 449-462.

273. Yildirim, I., Kennedy, S.D., Stern, H.A., Hart, J.M., Kierzek, R., Turner, D.H. *J. Chem. Theory and Comp.* **2012**, 8, 172-181.

274. Hornak, V., Abel, R., Okur, A., Strockbine, B., Roitberg, A., Simmerling, C. *Proteins* **2006**, 65, 712-725.

275. Case, D.A., Cheatham III, T.E., Darden, T., Gohlke, H., Luo, R., Merz Jr., K.M., Onufriev, A., Simmerling, B., Wang, B., Woods, R. *J. Comput. Chem.* **2005**, 26, 1668-1688.

276. Sitkoff, D., Sharp, K.A., Honig, B. *J. Phys. Chem.* **1994**, 98, 1978-1988.

277. Meirovitch, H., Cheluvaraja, S., White, R.P. *Curr. Protein and Peptide Sci.* **2009**, 10, 229-243.

278. Ma, J. *Structure* **2005**, 13, 373-380.

279. The Uniprot Consortium *Nucleic Acids Res.* **2012**, 40, D71-D75.

280. Schwede, T., Kopp, J., Guex, N., Peitsch, M.C., Nucleic Acids Res.*,* 2003, 31, 3381-3385.

281. Arnold, K., Bordoli, L., Kopp, J., Schwede, T. *Bioinformatics* **2006**, 22, 195-201.

282. Šali, A. and Blundell T.L*. J. Mol. Biol.* **1993**, 234, 779-815.

283. Case, D.A.; Darden, T.A.; Cheatham, III, T.E.; Simmerling, C.L.; Wang, J.; Duke, R.E.; Luo, R.; Walker, R.C.; Zhang, W.; Merz, K.M.; Roberts, B.; Hayik, S.; Roitberg, A.; Seabra, G.; Swails, J.; Götz, A.W.; Kolossváry, I.; Wong, K.F.; Paesani, F.; Vanicek, J.;Wolf, R.M.; Liu, J.; Wu, X.; Brozell, S.R.; Steinbrecher, T.; Gohlke, H.; Cai, Q.; Ye, X.; Wang, J.; Hsieh, M.-J.; Cui, G.; Roe, D.R.; Mathews, D.H.; Seetin, M.G.; Salomon-Ferrer, R.; Sagui, C.; Babin, V.; Luchko, T.; Gusarov, S.; Kovalenko, A.; and Kollman, P.A.; AMBER 12, **2012**, University of California, San Francisco.

284. Kim, H., Sulaimon, S., Menezes, S., Son, A., Menezes, W.J.C. *J. Chem. Edu.* **2011**, 88, 1389-1393.

285. Trott, O. and Olson, A.J. *J. Comp. Chem.* **2010**, 31, 455-461.

286. Gasteiger J. and Marsili M. *Tetrahedron* **1980**, 36, 3219–3228.

287. Zhao, Y.; Truhlar, D. G. *J. Chem. Phys.* **2006**, 125, 194101-18.

288. Lebedev, *Sibirsk. Mat. Zh.* **1977**, 18, 132.

289. Dupuis, M. and King, H.F. *J. Chem. Phys.* **1978**, 68, 3998-4004.

290. Cossi, M., Rega, N., Scalmani, G., Barone, V. *J. Comput. Chem.* **2003**, 24, 669-681.